

# Quantum information processing with superconducting circuits: a review

**G. Wendin**

Department of Microtechnology and Nanoscience - MC2,  
Chalmers University of Technology,  
SE-41296 Gothenburg, Sweden

**Abstract.**

During the last ten years, superconducting circuits and systems have passed from interesting physical devices to contenders for useful information processing in the near future. There are now advanced simulation experiments with nine qubits, and commitments to demonstrate quantum supremacy with fifty qubits within just a few years. The time is therefore ripe for providing an overview of superconducting devices and systems: to discuss the state of the art of applications to quantum information processing (QIP), and to describe recent and upcoming applications of superconducting systems to digital and analogue computing and simulation in Physics and Chemistry. On top of that, the review will try to address general questions like "What can a quantum computer do that a classical computer can't?".

**Contents**

<b>1</b>	<b>Introduction</b>	<b>5</b>
<b>2</b>	<b>Easy and hard problems</b>	<b>7</b>
2.1	Computational complexity . . . . .	8
2.2	Hard problems . . . . .	8
2.3	Quantum speedup . . . . .	9
2.4	Quantum supremacy . . . . .	10
<b>3</b>	<b>Superconducting circuits and systems</b>	<b>11</b>
3.1	The DiVincenzo criteria (DV1-DV7) . . . . .	11
3.2	Qubits (DV1) . . . . .	11
3.2.1	Phase qubit . . . . .	13
3.2.2	Cooper pair box . . . . .	13
3.2.3	Transmon . . . . .	13
3.2.4	Xmon . . . . .	13
3.2.5	Gatemon . . . . .	14
3.2.6	Fluxonium . . . . .	14
3.2.7	Flux qubit . . . . .	15
3.3	Initialisation (DV2) . . . . .	15
3.4	Universal gate operation (DV3) . . . . .	15
3.5	Readout (DV4) . . . . .	15
3.6	Coherence times (DV5) . . . . .	16
3.7	Algorithms, protocols and software . . . . .	16
<b>4</b>	<b>Transmon circuit quantum electrodynamics</b>	<b>17</b>
4.1	The Transmon qubit . . . . .	17
4.2	Multi-qubit transmon Hamiltonians . . . . .	18
4.2.1	Capacitive coupling . . . . .	19
4.2.2	Resonator coupling . . . . .	19
4.2.3	Josephson junction coupling . . . . .	20
4.2.4	Tunable coupling . . . . .	20
<b>5</b>	<b>Hybrid circuits and systems</b>	<b>21</b>
5.1	Quantum interfaces for qubit interconversion (DV6) . . . . .	21
5.1.1	Transmon-spin-cQED . . . . .	22
5.1.2	Transmon-micromechanical oscillator-cQED . . . . .	22
5.1.3	Transmon-SAW . . . . .	22
5.2	Quantum interfaces to flying qubits (DV7) . . . . .	23
5.2.1	Microwave-optical conversion: optomechanics . . . . .	23
5.2.2	Microwave-optical conversion: micromechanics . . . . .	24
5.2.3	Microwave-optical conversion: SAW . . . . .	24

<b>6</b>	<b>Quantum gates</b>	<b>26</b>
6.1	Quantum state time evolution . . . . .	26
6.2	Gate operations . . . . .	27
6.3	1q rotation gates . . . . .	27
6.4	2q resonance gates . . . . .	28
6.4.1	iSWAP . . . . .	28
6.4.2	CPHASE . . . . .	29
6.4.3	CNOT . . . . .	30
6.4.4	Controlled rotation . . . . .	30
6.4.5	2q-time evolution . . . . .	30
6.5	2q gates induced by microwave driving . . . . .	31
6.5.1	Driving qubits . . . . .	31
6.5.2	Driving a tunable bus . . . . .	32
6.6	Gate synthesis and universal sets of gates . . . . .	33
<b>7</b>	<b>Quantum state preparation and characterisation</b>	<b>35</b>
7.1	Quantum state characterisation . . . . .	35
7.2	Quantum supremacy characterisation . . . . .	36
7.3	Multi-qubit state preparation . . . . .	36
7.3.1	Bell states . . . . .	36
7.3.2	GHZ states . . . . .	38
7.3.3	W-states . . . . .	38
7.3.4	Generating Bell states by parity measurement . . . . .	38
7.4	Teleportation . . . . .	39
7.4.1	Teleportation of states . . . . .	39
7.4.2	Teleportation of entanglement . . . . .	40
7.5	Distillation of entanglement . . . . .	41
<b>8</b>	<b>Quantum state protection</b>	<b>43</b>
8.1	Quantum control . . . . .	43
8.2	Feedforward control . . . . .	43
8.3	Feedback control . . . . .	43
8.3.1	Digital feedback . . . . .	43
8.3.2	Analogue feedback . . . . .	44
8.3.3	Measurement and back-action . . . . .	44
8.4	Error correction codes and stabilisers . . . . .	44
8.5	Three qubit code . . . . .	45
8.6	Surface codes . . . . .	47
8.6.1	Basic concepts and models . . . . .	47
8.6.2	4-qubit parity measurements on a surface code plaquette . . . . .	47
8.6.3	Multi 2-qubit parity measurements on a surface code 1D chain . . . . .	48

<b>9</b>	<b>Quantum simulation of many-body systems</b>	<b>50</b>
9.1	Basics of quantum simulation . . . . .	50
9.2	Trotterisation . . . . .	51
9.3	Phase estimation . . . . .	51
9.4	Digital quantum simulation of spin models . . . . .	52
9.4.1	Two spin Ising and Heisenberg models . . . . .	52
9.4.2	Digitized adiabatic four spin transverse Ising model . . . . .	55
9.5	Digital quantum simulation of fermionic models . . . . .	56
9.6	Analogue/adiabatic quantum simulation . . . . .	59
9.7	Digital-analogue quantum simulation . . . . .	59
<b>10</b>	<b>Toward quantum chemistry simulation</b>	<b>60</b>
10.1	Hamiltonian ground-state energy estimation . . . . .	60
10.1.1	Quantum energy estimation . . . . .	61
10.1.2	Quantum variational eigensolver . . . . .	61
10.2	H-H ground-state energy curve . . . . .	62
10.3	He-H <sup>+</sup> ground-state energy curve . . . . .	63
10.4	Toward large-scale simulations . . . . .	64
10.4.1	From high-level language to hardware instructions . . . . .	64
10.4.2	Quantum computer emulation . . . . .	65
10.4.3	Electronic structure calculations - molecules . . . . .	65
10.4.4	Electronic structure of strongly correlated materials . . . . .	65
<b>11</b>	<b>Adiabatic quantum optimisation</b>	<b>67</b>
11.1	Adiabatic quantum algorithms . . . . .	67
11.2	Quantum annealing . . . . .	68
<b>12</b>	<b>Perspectives</b>	<b>70</b>
12.1	Looking back . . . . .	70
12.2	Looking around . . . . .	70
12.3	Looking ahead . . . . .	71

## 1. Introduction

Quantum Computing is the art of controlling and exploiting the time evolution of highly complex, entangled quantum states of physical hardware registers for the purpose of computation and simulation. "Quantum supremacy" is a recent term for an old ambition - to prove and demonstrate that quantum computers can outperform conventional classical computers [1].

For quite some time, since the 1980's, quantum computer science has been way ahead of experiment, driving the development of quantum information processing (QIP) at abstract and formal levels. This situation may now be changing due to serious efforts in several places to scale up and operate highly coherent and operational qubit platforms. In particular one can expect superconducting quantum hardware systems with 50-100 qubits during the next few years.

The near-term purpose is to demonstrate "Quantum" - to build and operate a physical quantum device that a classical computer cannot simulate [2]. When it comes to QIP one often wants "killer applications" for it to be of any interest, like beating classical supercomputers on problems of "real-world importance", e.g. factorisation and code breaking [3]. However, this may not be a particularly useful way to look upon the power of QIP: during the last seventy years, classical information processing has progressed via development and improvement of more or less efficient algorithms to solve specific tasks, in tune with the development of increasingly powerful hardware. The same will certainly apply also to QIP, the really useful applications arriving along the way.

This is already manifested in the broadening of the QIP field toward quantum technologies (QT) and quantum engineering (QE). Quantum device physics and quantum computing are two very different things - two different worlds. Although the original intention often was to perform quantum computing with large-scale devices and systems, much of the work naturally came to be focussed on device physics and quantum measurement. The work on improving coherence has demonstrated that qubits are extremely sensitive noise detectors, and the need to make measurements without destroying the coherence has led to the development of a range of quantum limited superconducting amplifiers. As a result, quantum sensors and quantum measurement can be said to represent "a quantum computer at the tip of a probe", greatly enhancing the sensitivity of measurement [4-6].

The potential of superconducting circuits for QIP has been recognised for more than twenty years [7-9] but the first embryonic qubit, a Josephson-junction (JJ) based Cooper-pair Box (CPB) in the charge regime, was not demonstrated until 1999 [10]. However, the coherence time was very short, only a few nanoseconds, and it took another five years to find a working concept: a CPB embedded in a superconducting coplanar microwave resonator - circuit quantum electrodynamics (cQED) [11,12]. And it took another two years to find the present basis for potentially scalable multi-qubit systems with useful long coherence times - the Transmon version of a CPB [13]. Moreover, in

2011 the invention of a Transmon embedded in a 3D-cavity suddenly increased coherence times toward  $100 \mu\text{s}$  [14]. At present there is intense development of 2D and 3D multi-qubit circuits with long-lived qubits and resonators capable of performing a large number of high-fidelity quantum gates and control and readout operations. This has opened realistic opportunities for scaling up superconducting circuits and to perform proof-of-principles demonstrations of potentially useful quantum simulation and computation with superconducting platforms.

The purpose of this review is to provide a snapshot of current progress, and to outline some expectations for the future. We will focus on hardware and protocols actually implemented on current superconducting devices, and discuss what we judge to be the most promising development to scale up superconducting circuits and systems. In fact, superconducting quantum circuits are now being scaled up to systems with several tens of qubits, to address real issues of quantum computing and simulation [15–24].

The aim is to present a self-contained discussion for a broad QIP readership. To this end, time evolution and the construction and implementation of 1q and 2q gates in superconducting devices are treated in considerable detail to make recent experimental work more easily accessible. On the other hand, the more general discussion of theory, as well as of much of the experimental work, necessarily only touches the surface and is hopefully covered by references to the most recent results. Reviews and analyses of the QIP field are given by [25–36]. For a comprehensive treatise on QIP we refer to Nielsen and Chuang [37]. Extensive technical discussions of a broad range of superconducting qubits and circuits can be found in [38, 39].

The present review also tries to look beyond the experimental state of the art, to anticipate what will be coming up in the near future in the way of applications. There is so much theoretical experience that waits to be implemented on superconducting platforms. The ambition is therefore also to outline and describe opportunities for addressing real-world problems in Chemistry and Materials science.

## 2. Easy and hard problems

Why are quantum computers and quantum simulators of such great interest? Quantum computers are certainly able to solve some problems much faster than classical computers. However, this does not say much about solving computational problems that are hard for classical computers. Hard problems are not only a question of whether they take long time - the question is whether they can be solved at all with finite resources. If one looks at the map of computational complexity (Fig. 1), classifying the hardness of computational (decision) problems, one finds that the BQP class of quantum computation only encompasses a rather limited space, basically not solving really hard problems. One may then ask what is the relation between problems of practical interest and really hard mathematical problems - what is the usefulness of quantum computing, and which problems are hard even for quantum computers?

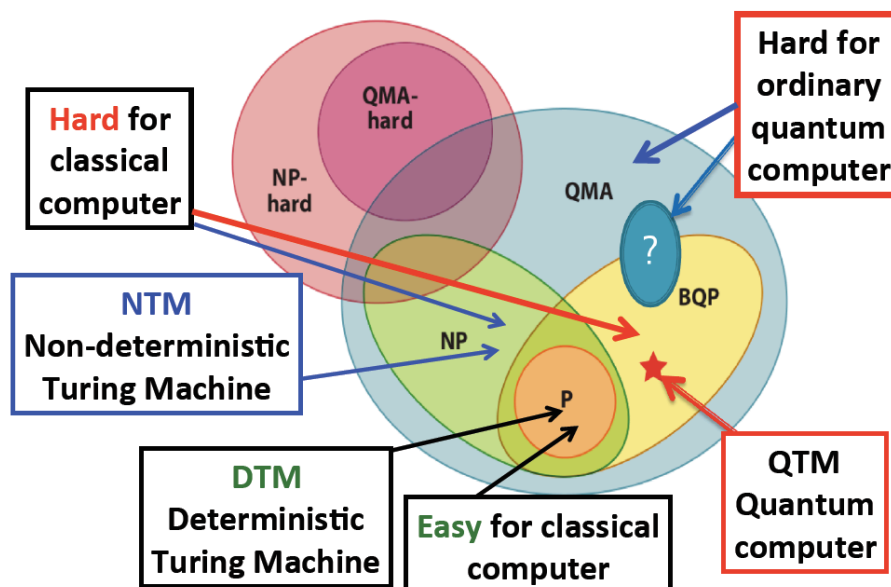


Figure 1: Computational complexity is defined by Turing machines (TM) providing digital models of computing [1, 40, 41]: deterministic TM (DTM); quantum TM (QTM); classical non-deterministic TM (NTM); quantum non-deterministic QTM). Tractable problems are defined by polynomial time execution and define complexity classes:  $P$  denotes problems that are efficiently solvable with a classical computer;  $P$  is a subset of  $NP$ , the problems efficiently checkable by a classical computer.  $QMA$  denotes the problems efficiently checkable by a quantum computer.  $NP$ -hard problems are the problems at least as hard as any  $NP$  problem, and  $QMA$ -hard problems are the problems at least as hard as any  $QMA$  problem. For a discussion of how to classify combinatorial problems, including games, see [53].

### 2.1. Computational complexity

Computational complexity [1, 40–42] is defined in terms of different kinds of Turing machines (TM) providing digital models of computing. A universal TM (UTM) can simulate any other TM (even quantum computers) and defines what is computable in principle, without caring about time and memory. Problems that can be solved by a deterministic TM (DTM) in polynomial time belong to class P (Fig. 1), and are considered to be "easy", or at least tractable. A DTM is a model for ordinary classical computers - a finite state machine (FSM) reading a writing from a finite tape.

A probabilistic TM (PTM) makes random choices of the state of the FSM upon reading from the tape, and traverses all the states in a random sequence. This defines the class BPP (bounded-error probabilistic polynomial time). A PTM may be more powerful than a DTM since it avoids getting stuck away from the solution. Nevertheless, a PTM can be simulated by a DTM with only polynomial overhead, so the relation  $BPP=P$  is believed to be true.

A quantum TM (QTM), with a quantum processor and quantum tape (quantum memory) is a model for a quantum computer. Problems that can be solved by a QTM in polynomial time belong to class BQP (Fig. 1), and there, outside P ( $P \subset BQP$ ), we find problems like Shor's algorithm [3] where a QTM provides exponential speedup. Nevertheless, Fig. 1 shows that BQP is a limited region of the complexity map, not including a large part of the NP-class containing many hard problems for a classical computer - these may be hard also for a quantum computer. The class NP (non-deterministic polynomial) is defined by a non-deterministic TM (NTM) being able to provide an answer that can be verified by a DTM in polynomial time. The NTM is not a real computer, but rather works as an oracle, providing an answer. A subclass of NP is the MA (Merlin-Arthur) class where the all-mighty Merlin provides the answer and the classical Arthur verifies in polynomial time. Some of these problems are beyond a quantum computer to calculate, but it might be used to verify solutions in polynomial time. This is the large quantum Merlin-Arthur (QMA) complexity class shown in Fig. 1. When not even a quantum computer can verify a solution in polynomial time, then that problem belongs to the NP-hard complexity class, and there a quantum computer is of no use.

### 2.2. Hard problems

Can physical processes be too hard to compute but still exist? Or just too hard for Turing machines? Or does Nature actually not solve really hard instances of hard problems? Perhaps the results of Evolution are based on optimisation and compromises?

There is a long-time notion that unconventional non-digital computing (e.g. adaptive analogue systems) can provide solutions to NP-hard problems that take exponential resources (time and/or memory) for classical digital machines to solve [43–46], and the challenge to solve NP-hard problems in polynomial time is actively explored [47–50]. Tractable ("easy") problems are those that can be solved by a DTM

in polynomial time.

The key question therefore is: Can unconventional computing provide solutions to NP-complete problems? The answer is in principle given by the Strong Church Thesis (SCT): Any finite analog computer can be simulated *efficiently* by a digital computer, in the sense that the time required by the digital computer to simulate the analog computer is bounded by a polynomial function of the resources used by the analogue machine [51]. The answer therefore seems straightforward: physical systems cannot provide solutions to NP-complete problems. NP-completeness is a worst case analysis - there is at least one case that requires exponential, rather than polynomial, resources in the form of time or memory.

Given the idea that "Nature is physical and does not solve NP-hard problems" [52–54], where does this place quantum computing? In a better position than classical, in principle, to compute the properties of physical quantum systems, but not much in general [53], e.g. for combinatorial problems. Tractable problems for quantum computers (BQP) are in principle hard for classical computers (P). In 1982 Feynman [55] introduced the concept of simulating one quantum system by another, emulating quantum physics by tailored quantum systems describing model quantum Hamiltonians - analogue quantum computers. The subsequent development went mostly in the direction of gate circuit models [56], but two decades later the analogue/adiabatic approach was formally established as an equivalent universal approach [57–60]. Nevertheless, also for quantum computers the class of tractable problems (BQP) is limited - many problems described by quantum Hamiltonians are hard for quantum computers, residing in QMA, or worse (QMA-hard, or NP-hard) [61–72]. Note however that the many-body problem is tractable for quantum spin chains [73, 74].

### 2.3. Quantum speedup

Quantum speedup is, by definition, connected with non-classical correlations [75, 76]. *Entanglement* is a fundamental manifestation of quantum superposition and non-classical correlations for pure states [77]. An elementary example of classical behavior is provided by a tensor product of independent superpositions of two 2-level systems,  $|\psi_1\rangle = \frac{1}{\sqrt{2}}(|0\rangle + |1\rangle)$  and  $|\psi_2\rangle = \frac{1}{\sqrt{2}}(|0\rangle + |1\rangle)$ . The tensor product of  $N(= 2)$  states  $|\psi\rangle = |\psi_1\rangle \otimes |\psi_2\rangle = \frac{1}{\sqrt{2}}(|0\rangle + |1\rangle) \otimes \frac{1}{\sqrt{2}}(|0\rangle + |1\rangle) = \frac{1}{2}(|00\rangle + |01\rangle + |10\rangle + |11\rangle)$  contains  $2^N (= 4)$  superposed configurations: this is the basis for creating exponentially large superpositions with only a linear amount of physical resources (qubits). It is interesting to note that one needs exponentially large  $2^N$  superpositions to create a completely disentangled quantum mechanical product state.

Highly entangled states are created by finite numbers of superpositions. In the present 2-qubit case, a maximally entangled state is the 2-qubit Bell state,  $\frac{1}{\sqrt{2}}(|00\rangle + |11\rangle)$ : it is not possible to assign a single state vector to any of the two subsystems, only to the total system. Entanglement allows us to construct maximally entangled superpositions with only a linear amount of physical resources, e.g. a large cat state:

$\frac{1}{\sqrt{2}}(|0\dots 00\rangle + |1\dots 11\rangle)$ , entangling  $N$  2-level systems. This is what allows us to perform non-classical tasks and provide speedup [75, 76].

Interestingly, just to characterise the entanglement can be a hard problem for a classical computer, because several entanglement measures are NP-hard to compute [78]. There is a large number of measures of entanglement, e.g. concurrence; entropy of entanglement (bipartite); entanglement of formation; negativity; quantum discord [76, 78–84]. Quantum discord is defined as the difference between two classically equivalent measures of information [85], and indicates the presence of correlations due to noncommutativity of quantum operators. For pure states it equals the entropy of entanglement [80]. Quantum discord determines the interferometric power of quantum states [82]. It provides a fundamental concept for computation with mixed quantum states in open systems, separable and lacking entanglement but still providing useful non-classical correlations.

Quantum speedup is achieved by definition if a quantum calculation is successful, as discussed by Dewes et al. [86] in the case of Grover search with a transmon 2-qubit system. It is then related to the expected known success probabilities of the classical and quantum systems. In general, however, speedup of a computation is an asymptotic-scaling property [87]. Nevertheless, in practice there are so many different aspects involving setting up and solving different instances of various classes of problems that the time to solution (TTS) may be the most relevant measure [88].

Polynomial or exponential speedup has not been much discussed in connection with digital QC because the systems are still small (5-10 qubits), and the limited coherence time does not allow very long calculations. In contrast, defining and detecting quantum speedup is presently a hot issue when assessing the performance of the D-Wave quantum annealing machines [87–90].

#### 2.4. Quantum supremacy

As already mentioned in the introduction, "Quantum supremacy" is a recent term for an old ambition - to provide proof that quantum computers can outperform conventional classical computers [1]. On a very practical level, Quantum Supremacy is about creating a physical quantum device that cannot be simulated by existing classical computers with available memory in any reasonable time. Currently, such a device would be a 50 qubit processor. It could model a large molecule that cannot be simulated by a classical computer. It would be an artificial physical piece of quantum matter that can be characterized by various quantum benchmarking methods in a limited time, but cannot be simulated by classical computers of today. And by scaling up by a small number of qubits it will not be simulatable even by next generation classical computers. A recent example of this given by Boixo et al. [2], discussing how to characterise quantum supremacy in near-term circuits and systems with superconducting devices.

### 3. Superconducting circuits and systems

The last twenty years have witnessed a dramatic development of coherent nano- and microsystems. When the DiVincenzo criteria were first formulated during 1996-2000 [91,92] there were essentially no useful solid-state qubit devices around. Certainly there were a number of quantum devices: Josephson-junctions, single-electron and Cooper pair boxes, SQUIDs, semiconductor quantum dots, implanted spin, etc. However, there was no technology for building coherent system that could be kept isolated from the environment and controlled at will from outside. These problems were addressed through a steady technological development during the subsequent ten years, and the most recent development is now resulting in practical approaches toward scalable systems.

#### 3.1. The DiVincenzo criteria (DV1-DV7)

The seven DiVincenzo criteria [92] formulate necessary conditions for gate-driven (digital) QIP:

1. Qubits: fabrication of registers with several (many) qubits (DV1).
2. Initialisation: the qubit register must be possible to initialise to a known state (DV2).
3. Universal gate operations: high fidelity single and 2-qubit gate operations must be available (DV3).
4. Readout: the state of the qubit register must be possible to read out, typically via readout of individual qubits (DV4).
5. Long decoherence times: a large number of single and 2-qubit gate operations must be performed within the coherence time of the qubit register,  $T_2$  (DV5).
6. Quantum interfaces for qubit interconversion: qubit interfaces must be possible for storage and on-chip communication between qubit registers (DV6).
7. Quantum interfaces to flying qubits for optical communication: qubit-photon interfaces must be available for long-distance transfer of entanglement and quantum information (DV7).

#### 3.2. Qubits (DV1)

The recent systematic development of reliable transmon-based JJ-cQED circuits is now forming a basis for serious upscaling to more than 10-20 qubits in the near future, to develop system control, error correction and quantum simulation schemes.

The qubits are based on the superconducting non-linear oscillator circuit in Fig. 2. The Hamiltonian of the LC circuit alone is given by

$$\hat{H} = E_C \hat{n}^2 + E_L \frac{\hat{\phi}^2}{2}, \quad (1)$$

where  $\hat{n}$  is the induced charge on the capacitor measured in units of  $2e$  (Cooper pair), and  $\hat{\phi}$  is the phase difference of the inductor measured in units of the flux quantum  $\Phi_0 = h/2e$ .  $E_C = (2e)^2/2C$  is the charging energy of one Cooper pair, and  $E_L = \Phi_0^2/4\pi^2L$  is the energy of one flux quantum.

Table 1: The DiVincenzo criteria [92] and the status of the main types of superconducting JJ-based qubits (September 2016). The figures in the table refer to the best published results. The coherence times in operational multi-qubit circuits are often considerably lower.

	2D Tmon [13]	3D Tmon [14]	Xmon [17, 105]	Fluxm [108]	C-shunt [121, 122]	Flux [110]	Gatemon [106]
<i>DV1, #q</i>	5 [19]	4 [192]	9 [20, 22]	1 [109]	2 [185]	4 [?]	2 [107]
<i>DV2</i>	<i>Yes</i>	<i>Yes</i>	<i>Yes</i>	<i>Yes</i>	<i>Yes</i>	<i>Yes</i>	<i>Yes</i>
<i>DV3</i>	<i>Yes</i>	<i>Yes</i>	<i>Yes</i>	<i>Yes</i>	<i>Yes</i>	<i>Yes</i>	<i>Yes</i>
$t_{1q}(ns)$	5	5	5	–	–	5	30 [107]
$n_{op,1q}$	$\sim 10^4$	$3 \cdot 10^4$	$10^3$	–	–	$\sim 10^3?$	$\sim 10^2$
$F_{1q}$	0.99... [?]	0.99.. [?]	0.99.. [?]	–	–	–	0.995 [107]
$t_{2q}(ns)$	5-10	5-10	5-30	–	–	–	30 [107]
$n_{op,2q}$	$5 \cdot 10^3$	$> 2 \cdot 10^4$	–	–	–	–	$\sim 10^2$
$F_{2q}$	0.9... [?]	0.9...x [?]	0.994 [17]	–	–	–	0.91 [107]
<i>DV4</i>	<i>Yes</i>	<i>Yes</i>	<i>Yes</i>	<i>Yes</i>	<i>Yes</i>	<i>Yes</i>	<i>Yes</i>
<i>DV5</i>	<i>Yes</i>	<i>Yes</i>	<i>Yes</i>	<i>Yes</i>	<i>Yes</i>	<i>Yes</i>	<i>Yes</i>
$T_1(\mu s)$	40	100	50	1000?	40-50	20 [120]	5 [107]
$T_2^*(\mu s)$	40	140 –	20		40	–	4 [107]
$T_2^{echo}(\mu s)$	40	140 ?	–		80	–	9.5 [107]
<i>DV6</i>	<i>Yes</i>	–	–	<i>No</i>	<i>No</i>	<i>Yes</i>	<i>No</i>
<i>DV7</i>	<i>No</i>	<i>No</i>	<i>No</i>	<i>No</i>	<i>No</i>	<i>No</i>	<i>No</i>

Note:

- The number of qubits (*DV1, #q*) refers to operational circuits with all qubits connected.
- D-Wave 2X contains around 1150 (now upgraded to 2000) connected operational flux qubits, but with very short coherence time, and does so far not qualify as a quantum computer (see Sect. 11.2).
- Table entries marked with a hyphen (-) only indicate present lack of knowledge on the part of the author, waiting to be updated.
- Uncertain (to the author) numbers are marked with (?).

For a high-Q oscillator at low temperature the discrete spectrum can be observed. However, in order to serve as a qubit, the oscillator must be anharmonic so that a specific pair of levels can be addressed.

Adding the Josephson junction (JJ), the Hamiltonian of the LCJ circuit becomes

$$\hat{H} = E_C (\hat{n} - n_g)^2 - E_J \cos(\phi) + E_L \frac{\hat{\phi}^2}{2} \quad (2)$$

where the Josephson energy  $E_J$  is given by  $E_J = \frac{\hbar}{2e} I_c$  in terms of the critical current

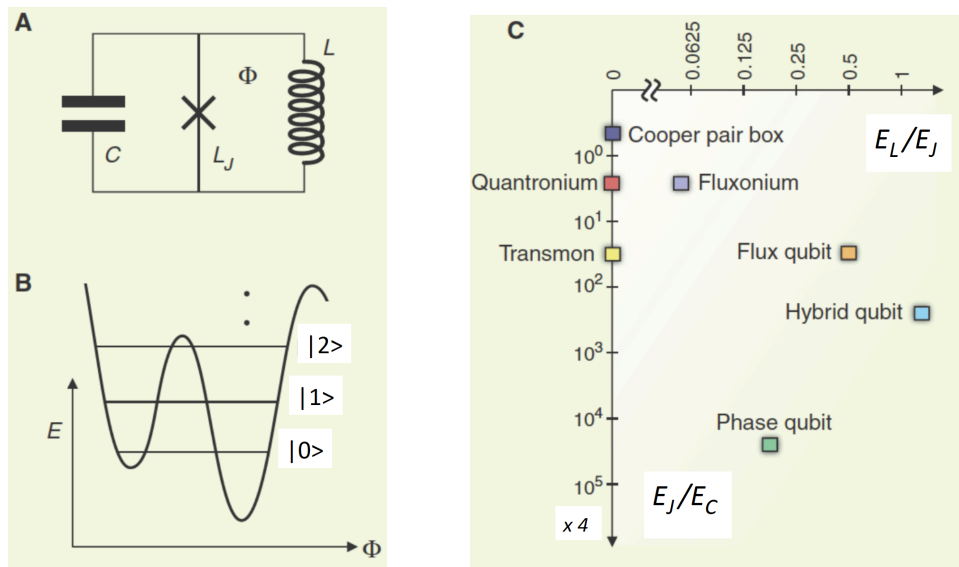


Figure 2: *JJ-based qubits: (a) Basic equivalent circuit; (b) Generic level structure; (c) Characterisation of JJ qubits in term of  $E_J/E_C$  and  $E_L/E_J$ . Adapted from [31].*

$I_c$  of the junction [38]. Typically, the JJ is of SIS type (superconductor-insulator-superconductor) with fixed critical current  $I_c$  [38]. The JJ-energy term in Eq. 2 is then tuned via the phase difference  $\phi$  (i.e. the supercurrent through the junction).

**3.2.1. Phase qubit** The phase qubit is formed by the two lowest levels in the potential wells formed by a current-biased Josephson junction. The phase qubit was the first one to be used for advanced and groundbreaking QIP applications with up to four qubits [93–99]. However, the coherence time has stayed rather short ( $< 1\mu s$ ); therefore, phase-qubit technology cannot be scaled up at the present time. See [38] for a detailed description.

**3.2.2. Cooper pair box** The Cooper pair box (CPB) has evolved from the original charge qubit (1999) [10] via the Quantronium (2002) [100–102] and CPB-cQED [11] to the Transmon (2007) [13] and the Xmon [103, 104]. See [38] for a detailed description.

**3.2.3. Transmon** The transmon [13] is a Josephson junction (JJ)/CPB shunted by a large capacitor. This keeps the charge on the CPB island constant (flattens the energy bands in the charge variable) and makes the transmon quite insensitive to charge fluctuations. The Transmon is now established as one of the major scalable platforms, with applications to a wide range of QIP problems.

**3.2.4. Xmon** The Xmon [17, 20–22, 103, 104] is a Transmon-type qubit developed for architectures with 2D arrays of nearest-neighbour capacitively coupled qubits. The Xmon is also established as one of the major scalable platforms. Circuits and systems

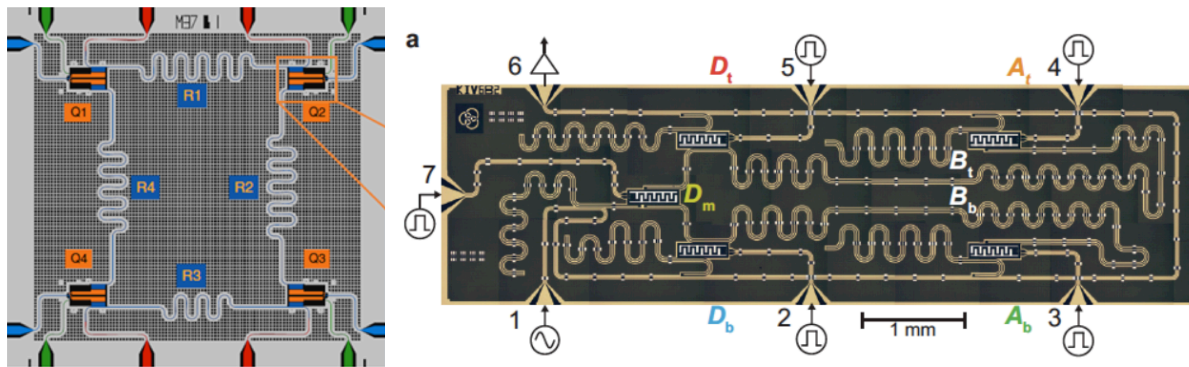


Figure 3: *Transmon-cQED multi-qubit circuits. Left: 4q circuit, adapted from [303]. Right: 5q circuit, adapted from [19]*

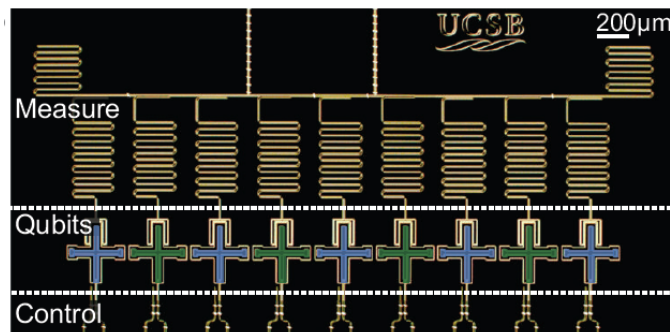


Figure 4: *Xmon with 9 qubits. Adapted from [20].*

with up to 9 Xmon qubits are presently being investigated with applications to a wide range of QIP problems. A variation is the gmon with direct tunable coupling between qubits [105].

**3.2.5. Gatemon** The Gatemon [106, 107] is a new type of transmon-like device, a semiconductor nanowire-based superconducting qubit. The gatemon is of weak-link SNS type (superconductor-normal-metal-superconductor), and the Josephson energy is controlled by an electrostatic gate that depletes carriers in a semiconducting weak link region, i.e. controls the critical current  $I_c$ , like a superconducting transistor. There is strong coupling to an on-chip microwave cavity and coherent qubit control via gate voltage pulses. Experiments with a two-qubit gatemon circuit has demonstrated coherent capacitive coupling, swap operations and a two-qubit controlled-phase gate [107].

**3.2.6. Fluxonium** Fluxonium [108] is a CPB-type qubit shunted by large inductance in the form of a Josephson array. This flattens the bands also in the flux (phase) variable and makes the fluxonium insensitive to flux fluctuations. Published value of 150 milliseconds  $T_1$  under special circumstances, due to suppression of quasiparticles [109].

*3.2.7. Flux qubit* The flux qubit [110–112] is the quantum version of the rf- and dc-SQUIDs. It has always been a major contender for scaled-up multi-qubit systems, but the coherence time has not improved much, which has limited applications to cases making use of the SQUID properties and strong flux coupling [113] for applications to microwave technology [114, 115], analog computing [116], and metamaterials [117–119]. A recent experiment has demonstrated somewhat longer coherence time of a flux qubit in a 3D cavity [120]. Moreover, there is a recent variation - the C-shunt flux qubit [121] - that experimentally shows great promise [122], with broad frequency tunability, strong anharmonicity, high reproducibility, and coherence times in excess of 40  $\mu$ s at its flux-insensitive point.

*D-Wave Systems'* approach represents a special case, building a large processor based on arrays of flux qubits with short coherence time. The technology is based on classical Nb RSFQ circuits combined with Nb rf-SQUID qubits, and forms the basis of the current D-Wave processors [123, 124]. The architecture is based on a square network of communication buses (cross-bar) allowing (limited) coupling of distant qubits. The qubits are operated by varying the dc-bias, changing the qubit energies and qubit-qubit couplings.

### *3.3. Initialisation (DV2)*

Qubit lifetimes are now so long that one cannot depend on natural relaxation time  $T_1$  for initialization to the ground state. For fast initialisation on demand, qubits can be temporarily connected to strongly dissipative circuits, or to measurement devices [125–128].

### *3.4. Universal gate operation (DV3)*

Universal high fidelity single- and two-qubit operations (Clifford + T gates; see Sect. 6.6) have been achieved for all major types of superconducting qubits. The shortest time needed for basic 1- and 2-qubit quantum operation is a few nanoseconds. Entangling gates with 99.4% fidelity have recently been demonstrated experimentally [17].

### *3.5. Readout (DV4)*

There are now well-established efficient methods for single-shot readout of individual qubits, typically performed via dispersive readout of a resonator circuit coupled to the qubit. A strong measurement "collapses" the system to a specific state, and that repeated non-destructive measurements will give the same result. Single-shot measurements require extremely sensitive quantum-limited amplifiers, and it is the recent development of such amplifiers [31, 125, 126, 129–139] that have made single-shot readout of individual qubits possible.

### 3.6. Coherence times (DV5)

JJ-qubits are manufactured and therefore sensitive to imperfections. Nevertheless, there has been a remarkable improvement of the coherence times of both qubits and resonators during the last five years [31, 104, 140, 141]. Table 1 shows the present state of the art.

### 3.7. Algorithms, protocols and software

A number of central quantum algorithms and protocols have been performed with multi-qubit circuits and platforms built from the main types of superconducting JJ-based qubits (see e.g. [21, 22, 86, 98, 142–145]), demonstrating proof of principle and allowing several transmon-type systems to be scaled up.

In practice, a quantum computer (QC) is always embedded in a classical computer (CC), surrounded by several classical shells of hardware (HW) and software (SW). Quantum computation and quantum simulation then involve a number of steps:

- (i) CC control and readout HW (shaped microwave pulses, bias voltages, bias magnetic fluxes).
- (ii) CC control and readout SW for the HW ("machine language"; including optimal control).
- (iii) CC subroutines implementing gates (gate libraries).
- (iv) High-level CC optimal control of quantum operations.
- (v) CC subroutines implementing quantum gate sequences (benchmarking, QFT, time evolution, etc.).
- (vi) High-level CC programming, compilation, and simulation of quantum algorithms and circuits [146–149].
- (vii) High-level CC programs solving problems [150, 151]

The only truly quantum part is step (v), explicitly performing quantum gates on quantum HW and quantum states. This is where quantum speedup can be achieved, in principle. Since the quantum gates have to be implemented by classical SW, it is necessary that the needed number of gates to describe a quantum circuit scales polynomially in the size of problem. For the Clifford gates there are efficient (polynomial) representations. However, to describe an arbitrary, universal quantum circuit needs T-gates and may take exponential resources [152].

If the quantum gates are executed in SW on representations of quantum states on a classical machine, then the quantum computer is emulated by the classical machine. Then to execute the gates scales exponentially, which means that a classical computer can only simulate a small quantum system. The present limit is around 50 qubits [2, 152] - beyond that is the realm of "Quantum supremacy".

#### 4. Transmon circuit quantum electrodynamics

The present development of quantum information processing with scalable Josephson Junction circuits and systems goes in the direction of coupling transmon-type qubits with quantum oscillators, for operation, readout and memory. In this section we will therefore focus on the Transmon, and describe the components in some detail.

##### 4.1. The Transmon qubit

A generic compact circuit model for the device is shown in Fig. 5a, and a hardware implementation is shown in Fig. 5b.

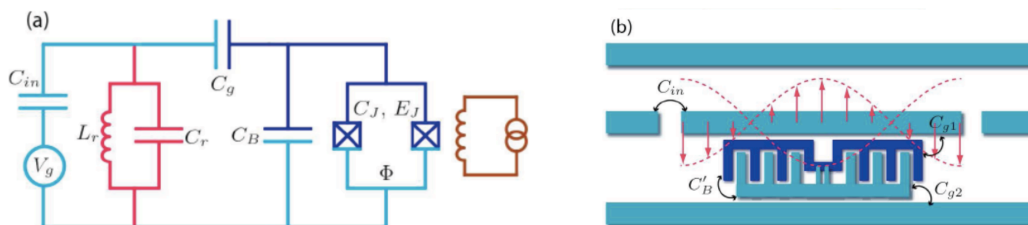


Figure 5: *Transmon-cQED: (a) Equivalent circuit; (b) Physical device. Adapted from [13].*

The transmon circuit considered consists of a number of fundamental components:

- A Cooper pair box (CPB) with one or two Josephson junctions (JJ) sitting in closed circuit with a large capacitance  $C_B$  ("anharmonic oscillator")
- An  $LC$  resonator circuit  $L_r C_r$  (harmonic oscillator)
- A capacitance  $C_g$  coupling the transmon and the resonator
- A drive circuit (right) flux-coupled to the SQUID-type JJ circuit for tuning the qubit energy
- A microwave drive circuit (left) capacitively coupled to the CPW for qubit operation

What is missing in Fig. 5a is an explicit readout resonator.

The transmon [13] is a development of the CPB toward a circuit with low sensitivity to charge noise, and therefore much longer coherence times. This is achieved by radically flattening the bands in the charge direction by increasing the  $E_J/E_C$  ratio. Figure 6 shows the progression from quantonium (top left) with  $E_J/E_C = 0.25$  [100, 101] to the transmon (bottom right) with  $E_J/E_C = 12.5$  [13]. The charge dispersion reduces exponentially in  $E_J/E_C$ , while the anharmonicity only decreases algebraically with a slow power law in  $E_J/E_C$  [101], making it still possible to individually address the transitions between level. It should be noted that the transmon is really a flat-band multilevel system (qudit), and the higher levels are often used for implementation of 2-qubit gates.

The transmon-cQED Hamiltonian takes the form

$$\hat{H} = -\frac{1}{2}\epsilon \sigma_z + g\sigma_x(a + a^\dagger) + \hbar\omega_{LC} (a^\dagger a + \frac{1}{2}) \quad (3)$$

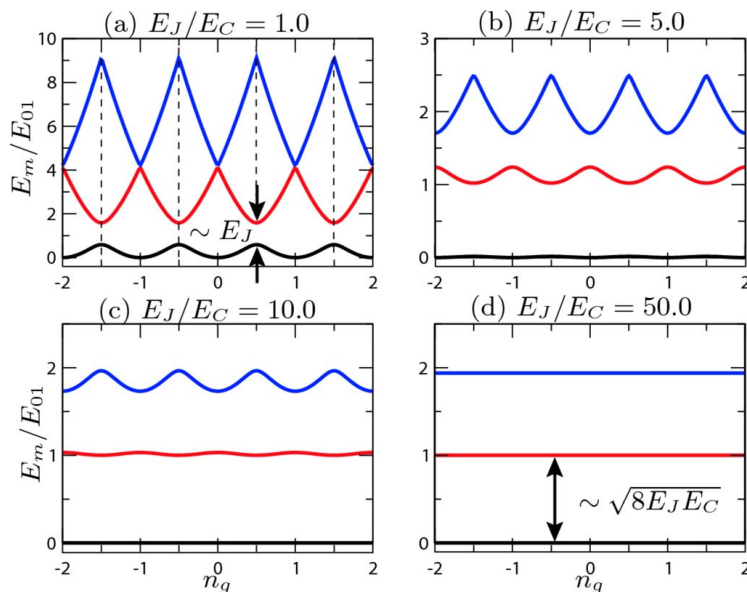


Figure 6: *Development of the CPB level spectrum when the  $E_J/E_C$  ratio is increased [13]. Note that 2-JJ transmons (Fig. 5), the energy bands oscillate with magnetic flux - providing flux-tunability of the transmon energy. However, this also leads to sensitivity to flux noise. Adapted from [13].*

Introducing the step operators  $\sigma_{\pm} = (\sigma_x \pm i \sigma_y)/2$ , one obtains

$$\hat{H} = -\frac{1}{2}\epsilon \sigma_z + g(\sigma^+ a + \sigma^- a^\dagger) + g(\sigma^+ a^\dagger + \sigma^- a) + \hbar\omega (a^\dagger a) \quad (4)$$

In the rotating-wave approximation (RWA) one only keeps the first term, which gives the canonical Jaynes-Cummings model [153, 154],

$$H \approx -\frac{1}{2}\epsilon \sigma_z + g(\sigma^+ a + \sigma^- a^\dagger) + \hbar\omega (a^\dagger a) \quad (5)$$

describing dipole coupling of a two-level "artificial atom" to a resonator cavity.

Diagonalising the Jaynes-Cummings Hamiltonian to second order by a unitary transformation gives

$$H = -\frac{1}{2}\left(\epsilon + \frac{g^2}{\delta}\right) \sigma_z + \left(\hbar\omega + \frac{g^2}{\delta} \sigma_z\right) a^\dagger a \quad (6)$$

where  $\delta = \epsilon - \hbar\omega$  is the so-called detuning. The result implies that (i) the qubit transition energy  $\epsilon$  is Stark shifted (renormalized) by the coupling to the oscillator, and (ii) the oscillator energy  $\hbar\omega$  is shifted by the qubit in different directions depending on the state of the qubit. This condition allows discriminating the two qubit states in a readout measurement.

#### 4.2. Multi-qubit transmon Hamiltonians

In the following we will focus on transmon multi-qubit systems, and then the effective basic Hamiltonian in the Jaynes-Cummings approximation takes the general form

(omitting the harmonic oscillator term):

$$\hat{H} = -\frac{1}{2} \sum_i \epsilon_i \sigma_{zi} + \sum_i g_i (\sigma_i^+ a + \sigma_i^- a^\dagger) + \frac{1}{2} \sum_{i,j;\nu} \lambda_{\nu,ij} \sigma_{\nu i} \sigma_{\nu j} \quad (7)$$

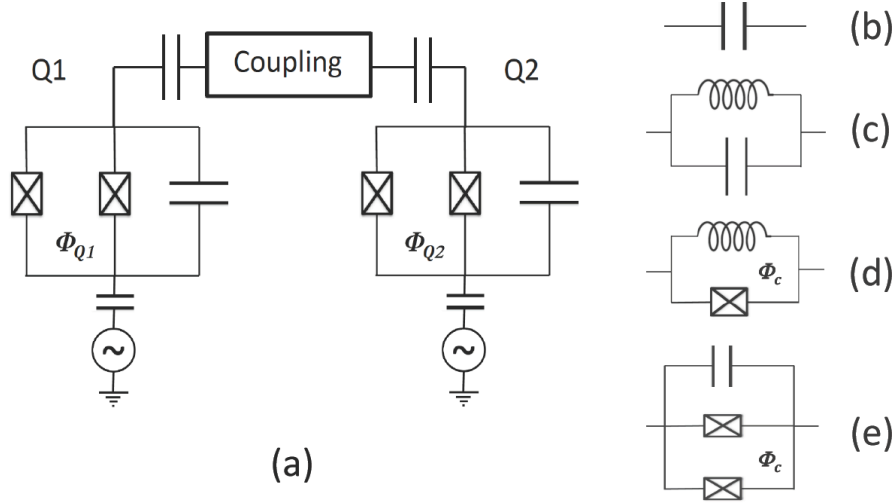


Figure 7: *Two coupled transmon qubits. (a) Generic coupling scheme; (b) Capacitive coupling; (c) Resonator coupling; (d) JJ-coupling; (e) "Transmon-bus" coupling. The transmons and the JJ-couplings can be flux tunable.*

*4.2.1. Capacitive coupling* This case (Fig. 7b) is described by an Ising-type model Hamiltonian with direct qubit-qubit charge coupling (the form is also relevant for inductively coupled flux qubits). For the transmon [38],

$$H = - \sum_{i=1,2} \frac{\epsilon_i}{2} \sigma_{zi} + \lambda_{12} \sigma_{y1} \sigma_{y2} \quad (8)$$

and in the rotating-wave approximation (RWA) one obtains the Jaynes-Cummings Hamiltonian

$$H = - \sum_{i=1,2} \frac{\epsilon_i}{2} \sigma_{zi} + \lambda_{12} (\sigma_1^+ \sigma_2^- + \sigma_1^- \sigma_2^+) \quad (9)$$

*4.2.2. Resonator coupling* In this case (Fig. 7c) the coupling is primarily indirect, via virtual excitation (polarisation) of the detuned bus resonator, and the Transmon Hamiltonian takes the form [38]:

$$\hat{H} = - \sum_i \frac{\epsilon_i}{2} \sigma_{zi} + \frac{g_1 g_2}{\delta} \sigma_{x1} \sigma_{x2} \quad (10)$$

Finally, in the rotating-wave approximation (RWA) one again obtains the Jaynes-Cummings Hamiltonian

$$H = - \sum_{i=1,2} \frac{\epsilon_i}{2} \sigma_{zi} + \frac{g_1 g_2}{\delta} (\sigma_1^+ \sigma_2^- + \sigma_1^- \sigma_2^+) \quad (11)$$

*4.2.3. Josephson junction coupling* Instead of the capacitor, the transmon qubits can be connected via a Josephson junction circuit [38, 105, 155], as illustrated in Fig. 7d. For the transmon [38],

$$H = - \sum_{i=1,2} \frac{\epsilon_i}{2} \sigma_{zi} + \lambda_{12} (\sigma_{z1} \sigma_{z2} + \sigma_{x1} \sigma_{x2}) \quad (12)$$

and in the rotating-wave approximation (RWA) one obtains the Jaynes-Cummings Hamiltonian

$$H = - \sum_{i=1,2} \frac{\epsilon_i}{2} \sigma_{zi} + \lambda_{12} \sigma_{z1} \sigma_{z2} + \lambda_{12} (\sigma_1^+ \sigma_2^- + \sigma_1^- \sigma_2^+) \quad (13)$$

*4.2.4. Tunable coupling* Tunable qubit-qubit coupling can be achieved in a number of ways, for example (i) by tuning two qubits directly into resonance with each other; (ii) by tuning the qubits (sequentially) into resonance with the resonator; (iii) by tuning the resonator sequentially into resonance with the qubits [156]; (iv) by driving the qubits with microwave radiation and coupling via sidebands; (v) by flux-tunable inductive coupling [157]. In particular, for JJ-coupling, the qubit-qubit coupling can be made tunable by current-biasing the coupling JJ [155, 158, 159].

## 5. Hybrid circuits and systems

In this section we will discuss the status of the DiVincenzo criteria DV6 and DV7 listed in Sect. 3.1.

Even if a QIP system in principle can consist of a single large coherent register of qubits, practical systems will most likely be built as hybrid systems with different types of specialized quantum components: qubits, resonators, buses, memory, interfaces. The relatively short coherence time of JJ-qubits ( $\mu s$ ) compared to spin qubits ( $ms$ ) and trapped ions ( $s$ ) has promoted visions of architectures with fast short-lived JJ-qubit processors coupled to long-lived memories and microwave-optical interfaces, as illustrated in Fig. 8.

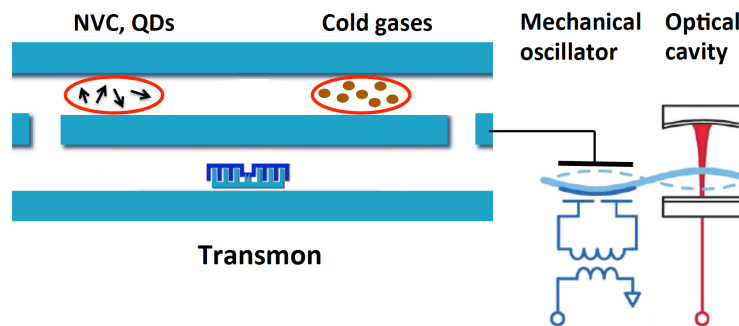


Figure 8: A conceptual view of a transmon hybrid system with "peripherals" serving as long-term memory and communication devices.

There are numerous demonstrations of coherent transfer between JJ-qubits and microwave resonators (both lumped circuits and microwave cavities, and mechanical resonators), as well as between JJ-qubits and spin ensembles. In principle, qubits coupled to microwave resonators (q-cQED) is a hybrid technology. An interesting aspect is that the development of long-lived transmon qubits and high-Q 2D and 3D resonators has changed the playground, and it is no longer clear what other kind of hybrid memory devices are needed for short-term quantum memory. Even for long-term memory, the issue is not clear: with emerging quantum error correction (QEC) techniques it may be possible to dynamically "refresh" JJ-cQED systems and prolong coherence times at will. To achieve long-term "static" quantum memory, spin ensembles are still likely candidates, but much development remains.

The current situation for hybrid systems is described in two recent excellent review articles [160, 161]. Here we will only briefly mention a few general aspects in order to connect to the DiVincenzo criteria DV6 and DV7 and refer to some of the most recent work.

### 5.1. Quantum interfaces for qubit interconversion (DV6)

The name of the game is to achieve strong coupling between the modes of two or more different components so that the mixing leads to pronounced sideband structures. This

can then be used for entangling different types of modes for information storage or conversion from localised to flying qubits.

*5.1.1. Transmon-spin-cQED* Experimentally, strong coupling between an ensemble of electronic spins and a superconducting resonator Fig. 8 has been demonstrated spectroscopically, using NV centres in diamond crystal [162–164] and  $Er^{3+}$  spins doped in a  $Y_2SiO_5$  [165].

Moreover, storage of a microwave field into multi-mode collective excitations of a spin ensemble has recently been achieved [166,167]. This involved the active reset of the nitrogen-vacancy spins into their ground state by optical pumping and their refocusing by Hahn-echo sequences. This made it possible to store multiple microwave pulses at the picowatt level and to retrieve them after up to 35  $\mu s$ , a three orders of magnitude improvement compared to previous experiments [167].

The ultimate purpose is to connect qubits to the superconducting resonator bus, and to use the spin ensemble as a long-lived memory. Such experiments have been performed, entangling a transmon with a NV spin ensemble [168] via a frequency-tunable superconducting resonator acting as a quantum bus, storing and retrieving the state of the qubit. Although these results constitute a proof of the concept of spin-ensemble-based quantum memory for superconducting qubits, the life-time, coherence and fidelity of spin ensembles are still far from what is needed. Similar results were also achieved by directly coupling a flux qubit to an ensemble of NV centers without a resonator bus [169].

*5.1.2. Transmon-micromechanical oscillator-cQED* Mechanical oscillators Fig. 8 can be designed to have resonance frequencies in the microwave GHz range and achieve strong coupling to superconducting qubits. Mechanical resonators therefore provide a new type of quantum mode - localised phonons. However, for this to be useful for quantum information processing one must be able to cool the mechanical oscillator to its ground state, to be able to create and control single phonons [170,171]. It is then possible to induce Rabi oscillations between the transmon and the oscillator by microwave driving via motional sidebands, resulting in periodic entanglement of the qubit and the micromechanical oscillator [172].

*5.1.3. Transmon-SAW* Surface acoustic waves (SAW) are propagating modes of surface vibrations - sound waves. Recently, propagating SAW phonons on the surface of a piezoelectric crystal have been coupled to a transmon in the quantum regime Fig. 9, reproducing findings from quantum optics with sound taking over the role of light [173]. The results highlight the similarities between phonons and photons but also point to new opportunities arising from the unique features of quantum mechanical sound. The low propagation speed of phonons should enable new dynamic schemes for processing quantum information, and the short wavelength allows regimes of atomic physics to be explored that cannot be reached in photonic systems [174].

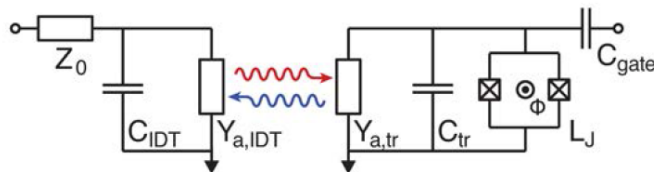


Figure 9: *Propagating surface acoustic wave (SAW) phonons coupled to an artificial atom. Semi-classical circuit model for the qubit. The interdigital transducer (IDT) converts electrical signals to SAWs and vice versa. Adapted from [173].*

### 5.2. Quantum interfaces to flying qubits (DV7)

The principle is that of good old radio technology: From the transmitter side, one achieves low-frequency ( $\omega$ ) modulation of a strong high-frequency ( $\Omega$ ) carrier (pump) beam by controlling the amplitude, frequency or phase of the carrier. The modulation is achieved by mixing the signals in a non-linear device, creating sidebands  $\Omega \pm \omega$  around the carrier frequency.

In the present case, the mixers are different types of electro-optomechanical oscillators that influence the conditions for transmitting or reflecting the optical carrier beam. Typically three different oscillators are coupled in series: a microwave resonator ( $\omega_r$ ), a micro/nanomechanical oscillator ( $\omega_m$ ), and an optical cavity ( $\Omega_c$ ), as illustrated in Fig. 8:

$$\hat{H} = \hbar\omega_r (a^\dagger a + \frac{1}{2}) + \hbar\omega_m (b^\dagger b + \frac{1}{2}) + \hbar\Omega_c (c^\dagger c + \frac{1}{2}) + g_{rm}(a + a^\dagger)(b + b^\dagger) + g_{mc} c^\dagger c (b + b^\dagger) \quad (14)$$

The mechanical oscillator changes the frequency of the optical cavity. This is the same principle as readout: the phase of the reflected carrier carries information about the state of the reflecting device. Here the phase of the reflected optical beam maps the state of the mechanical oscillator. Tuning the laser frequency  $\Omega$  so that  $\Omega_c \approx \Omega \pm \omega$ , either sideband is now in resonance with the optical cavity. If the resonance linewidth of the optical cavity is smaller than  $\omega$ , then the sideband is resolved and will show a strong resonance. Adding a (transmon) qubit coupled to the microwave resonator (Fig. 8) one then has a chain of coupled devices that, if coherent, can entangle the localised qubit with the optical beam and the flying photon qubits.

We will now briefly describe a few technical approaches to the central mechanical component: piezoelectric optomechanical oscillator [175], micromechanical membrane oscillator [176, 178, 179], and SAW [180].

#### 5.2.1. Microwave-optical conversion: optomechanics .

This approach (Fig. 10) is based on the established optomechanical devices for modulating light [160], and has been investigated experimentally [175]. A beam of piezoelectrical material is patterned to contain a nanophotonic(1D) crystal, localizing

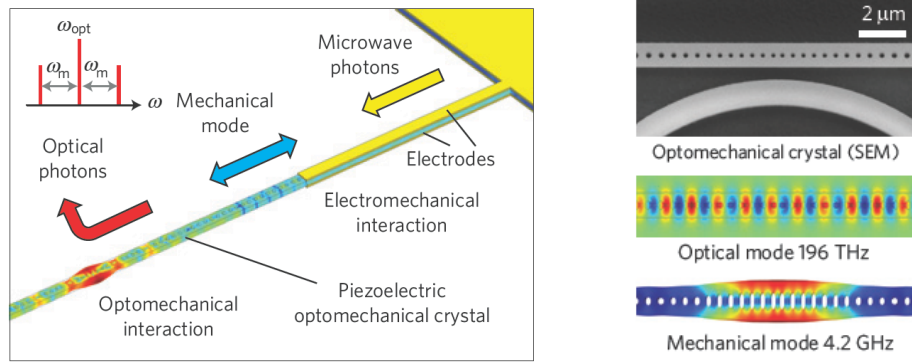


Figure 10: *Layout and operation of microwave-to-optical converter using a piezoelectric optomechanical oscillator. Adapted from [175].*

light in a region of enhanced vibrational amplitude.

### 5.2.2. Microwave-optical conversion: micromechanics .

This approach (Fig. 11) is based on the well-know technique of modulating reflected light, e.g. to determine the position of the tip of an AFM probe. The radiation pressure (light intensity) exerts a ponderomotive force on the membrane (Fig. 11), coupling the mechanical oscillator and the optical cavity. There are proof-of-concept experimental results showing coherent bi-directional efficient conversion of GHz microwave photons and THz optical photons [176]. Moreover, this technique was recently used for demonstrating optical detection of radiowaves [178].

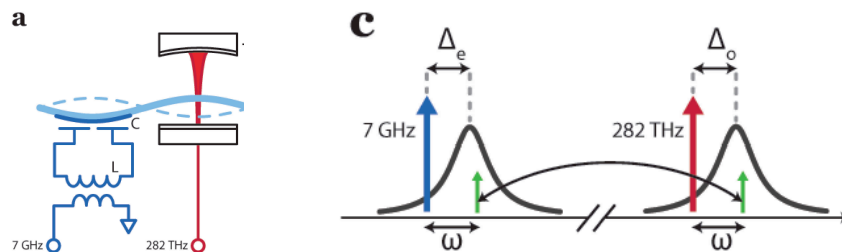


Figure 11: *Layout and operation of microwave-optical interface using an oscillating micromechanical membrane [176]. Microwave-to-optical conversion is achieved by pumping at optical frequency  $\Omega$  with detuning so as to amplify the sidebands at  $\Omega \pm \omega$  inside the optical cavity resonance line. Optical-to-microwave conversion is achieved by pumping at MW frequency  $\omega_p$  with detuning so as to amplify the sidebands at  $\omega_p \pm \omega$  inside the MW resonator resonance line. Adapted from [176]*

### 5.2.3. Microwave-optical conversion: SAW .

Shumeiko [180] presents a theory for a reversible quantum transducer (Fig. 12) connecting superconducting qubits and optical photons using acoustic waves in

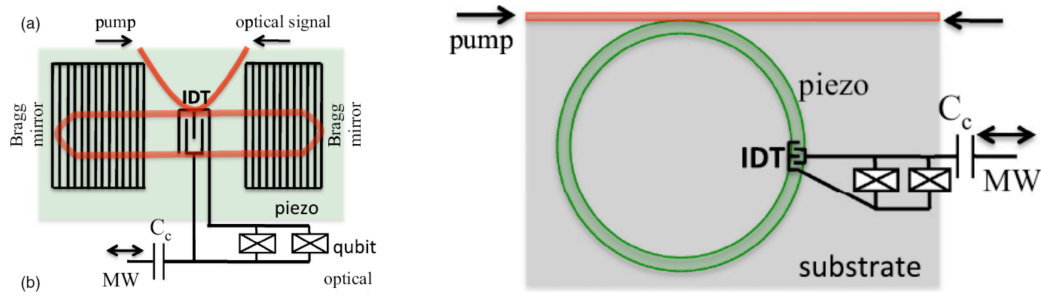


Figure 12: *Layout and operation of microwave-to-optical converter using an SAW travelling wave. Adapted from [180].*

piezoelectrics, using stimulated Brillouin scattering for phonon-photon conversion, and piezoelectric effect for coupling of phonons to qubits. It is shown that full and faithful quantum conversion is feasible with state-of-the-art integrated acousto-optics.

## 6. Quantum gates

### 6.1. Quantum state time evolution

In quantum information processing (QIP) one maps classical data on the Hilbert space of a given quantum circuit, studies the resulting time evolution of the quantum system, performs readout measurements of quantum registers, and analyses the classical output. At this level there is no difference between quantum computing (QC) and quantum simulation (QS).

*Time-evolution operator* The time evolution of a many-body system can be described by the Schrödinger equation for the state vector  $|\psi(t)\rangle$ ,

$$i\hbar\delta_t|\psi(t)\rangle = \hat{H}(t)|\psi(t)\rangle. \quad (15)$$

in terms of the time-evolution operator  $\hat{U}(t, t_0)$

$$|\psi(t)\rangle = \hat{U}(t, t_0)|\psi(t_0)\rangle. \quad (16)$$

determined by the time-dependent many-body Hamiltonian  $\hat{H}(t)$  of the system

$$\hat{H}(t) = \hat{H}_{syst} + \hat{H}_{ctrl}(t) \quad (17)$$

describing the intrinsic system and the applied control operations. In general, the perturbing noise from the environment can be regarded as additional time dependence of the control parameters.

For simplicity,  $\hat{H}_{syst}$  can be regarded as time-independent, and  $\hat{H}_{ctrl}(t)$  taken to describe DC and microwave drives controlling the parameters of the total Hamiltonian, e.g. gates tuning of qubits and resonators for coupling and readout, or setting up and evolving the Hamiltonian. For the transmon, the intrinsic Hamiltonian takes the form:

$$\hat{H}_{syst} = -\frac{1}{2} \sum_{\nu i} \Delta_i \sigma_{zi} + \sum_i g_i \sigma_{xi} (a + a^\dagger) + \hbar\omega_{LC} a^\dagger a \quad (18)$$

$$+ \frac{1}{2} \sum_{i,j;\nu} \lambda_{\nu,ij} (\sigma_i^+ \sigma_j^- + \sigma_i^- \sigma_j^+) \quad (19)$$

and the control term can be written as

$$\hat{H}_{ctrl}(t) = \sum_{i;\nu} f_{\nu i}(t) \sigma_{\nu i} + \frac{1}{2} \sum_{i,j;\nu} h_{\nu,ij}(t) \sigma_{\nu i} \sigma_{\nu j} + k(t) a^\dagger a \quad (20)$$

The time dependence allows switching on and off the various terms in the Hamiltonian, as well as introducing pulse shapes. In Eq. (18), the first term allows tuning of the qubit energies, and the other terms to switch on and off the intrinsic qubit-oscillator and qubit-qubit coupling terms. In Eq. (20), the first term provides general types of single-qubit gates while the second term describes qubit-qubit coupling explicitly introduced by external driving.

Gates are the results of applying specific control pulses to selected parts of a physical circuit. This affects the various terms in the intrinsic Hamiltonian by making them

time-dependent,  $\hat{H}(t)$ , and, in addition, can introduce new driving terms with different symmetries.

The solution of Schrödinger equation for  $\hat{U}(t, t_0)$  may be written as

$$\hat{U}(t, t_0) = \hat{U}(t_0, t_0) + \int_{t_0}^t \hat{H}(t') \hat{U}(t', t_0) dt' \quad (21)$$

and in terms of the time-ordering operator  $\hat{T}$ :

$$\hat{U}(t, t_0) = \hat{T} e^{-\frac{i}{\hbar} \int_{t_0}^t \hat{H}(t') dt'} , \quad (22)$$

describing the time evolution of the entire  $N$ -particle state in the interval  $[t_0, t]$ .  $\hat{U}(t, t_0)$  in Eq. 22 is the basis for describing all kinds of quantum information processing, from the gate model for quantum computing to adiabatic quantum simulation. If the total Hamiltonian commutes with itself at different times, the time ordering can be omitted,

$$\hat{U}(t, t_0) = e^{-\frac{i}{\hbar} \int_{t_0}^t \hat{H}(t') dt'} . \quad (23)$$

This describes the time-evolution controlled by a homogeneous time-dependent potential or electromagnetic field, e.g. dc or ac pulses with finite rise times, or more or less complicated pulse shapes, but having no space-dependence. Moreover, if the Hamiltonian is constant in the interval  $[t_0, t]$ , then the evolution operator takes the simple form

$$\hat{U}(t, t_0) = e^{-\frac{i}{\hbar} \hat{H}(t-t_0)} , \quad (24)$$

describing stepwise time-evolution.

Computation is achieved by sequentially turning on and off 1q and 2q gates, in parallel on different groups of qubits, inducing effective  $N$ -qubit gates.

## 6.2. Gate operations

The time-development will depend on how many terms are switched on in the Hamiltonian during this time interval. In the ideal case all terms are switched off except for those selected for the specific computational step. A single qubit gate operation then involves turning on a particular term in the Hamiltonian for a specific qubit, while a two-qubit gate involves turning on an interaction term between two specific qubits. In principle one can perform direct  $N$ -qubit gate operations by turning on interactions among all  $N$  qubits.

## 6.3. 1q rotation gates

1q gates are associated with the time-dependent 1q term of the control Hamiltonian:  $\hat{H}_{ctrl}(t) = \sum_{i,\nu} f_{\nu i}(t) \sigma_{\nu i}$ . Expanding the state vector  $|\psi(t)\rangle$  in a computational 1q basis, one obtains for a given single qubit,

$$|\psi(t)\rangle = \sum_m a_m \sum_k |k\rangle \langle k| e^{-\frac{i}{\hbar} \int_{t_0}^t \sum_{\nu} f_{\nu}(t') dt' \sigma_{\nu}} |m\rangle \quad (25)$$

For a general control Hamiltonian the  $\sigma_\nu$ -operators do not commute, and the exponential cannot be factorised in terms of products of  $\sigma_x$ ,  $\sigma_y$  and  $\sigma_z$  terms. To get a product we must apply the operators sequentially, acting in different time slots. In that case, for a given  $\sigma_\nu$ -operator we get

$$|\psi(t)\rangle = \sum_m a_m \sum_k |k\rangle \langle k| e^{-\theta(t)\sigma_\nu} |m\rangle \quad (26)$$

where  $\theta = \theta(t) = \frac{i}{\hbar} \int_{t_0}^t f_\nu(t') dt'$

Expanding the exponential, calculating the  $\langle k|\sigma_\nu|m\rangle$  matrix elements, and resumming, one obtains the time evolution in terms of rotation operators  $R_\nu(\theta)$ :

$$|\psi(t)\rangle = \sum_m a_m \sum_k |k\rangle \langle k| R_\nu(\theta)_{km} |m\rangle \quad (27)$$

where

$$R_x(\theta) = \begin{pmatrix} \cos(\theta/2) & -i \sin(\theta/2) \\ -i \sin(\theta/2) & \cos(\theta/2) \end{pmatrix} \quad (28)$$

$$R_y(\theta) = \begin{pmatrix} \cos(\theta/2) & -\sin(\theta/2) \\ \sin(\theta/2) & \cos(\theta/2) \end{pmatrix} \quad (29)$$

$$R_z(\theta) = \begin{pmatrix} \exp(-i\theta/2) & 0 \\ 0 & \exp(i\theta/2) \end{pmatrix} \quad (30)$$

describing single qubit rotations around the x-, y-, and z-axes.

#### 6.4. 2q resonance gates

**6.4.1. iSWAP** The 2q iSWAP gate can be implemented by using  $\hat{H}_{ctrl}$  for tuning the energy of one of the qubits onto resonance with the other qubit, thereby effectively turning on the  $\hat{H}_{12}$  qubit-qubit interaction in  $\hat{H}_{syst}$ .

Expanding the state vector  $|\psi(t)\rangle$  in a computational 2q basis, one obtains

$$|\psi(t)\rangle = \sum_{m,n} a_{mn} \sum_{k,l} |kl\rangle \langle kl| e^{-i\hat{H}_{12} t} |mn\rangle \quad (31)$$

If the qubits are in resonance ( $\Delta_1 = \Delta_2$ ), then the matrix elements of the 2-qubit interaction part of the time evolution operator take the form

$$\langle kl|\hat{H}_{12}|mn\rangle = \lambda \langle kl|\sigma_1^+ \sigma_2^- + \sigma_1^- \sigma_2^+|mn\rangle \quad (32)$$

$$= \lambda \delta_{k,m-1} \delta_{l,n+1} + \delta_{k,m+1} \delta_{l,n-1} \quad (33)$$

Expanding the exponential function, introducing the matrix elements and resumming, yields,

$$U(t) = \langle kl| e^{-\frac{i}{\hbar} \hat{H}_{12} t} |mn\rangle = \langle kl| iSWAP |mn\rangle \quad (34)$$

$$iSWAP = \begin{pmatrix} 1 & 0 & 0 & 0 \\ 0 & \cos(\lambda t) & -i \sin(\lambda t) & 0 \\ 0 & -i \sin(\lambda t) & \cos(\lambda t) & 0 \\ 0 & 0 & 0 & 1 \end{pmatrix}, \quad (35)$$

referred to as the iSWAP gate.

The iSWAP gate describes how the system oscillates between the  $|01\rangle$  and  $|10\rangle$  states. The  $\sqrt{iSWAP}$  gate is obtained by choosing  $\lambda t = \pi/2$ ,

$$\sqrt{iSWAP} = \begin{pmatrix} 1 & 0 & 0 & 0 \\ 0 & 1 & -i & 0 \\ 0 & -i & 1 & 0 \\ 0 & 0 & 0 & 1 \end{pmatrix}, \quad (36)$$

putting the system in a Bell-state type of superposition  $|\psi\rangle = \frac{1}{\sqrt{2}}(|01\rangle + i|10\rangle)$ .

**6.4.2. CPHASE** The CPHASE gate can be implemented by making use of the spectral repulsion from the third level of the transmon. In a detailed treatment one expands the state vector in an extended qutrit computational basis:

$$\begin{aligned} |\psi(0)\rangle &= \sum_{m,n} a_{mn} |mn\rangle \\ &= a_{00}|00\rangle + a_{01}|01\rangle + a_{10}|10\rangle + a_{20}|20\rangle + a_{11}|11\rangle + a_{02}|02\rangle \end{aligned} \quad (37)$$

and calculates the matrix elements of the full Hamiltonian with direct or indirect qubit-qubit interaction. The result is a repulsive shift  $\zeta$  of the energy  $\frac{\Delta_1}{2} + \frac{\Delta_2}{2}$  of the  $|11\rangle$  state, as shown in Fig. 13b.

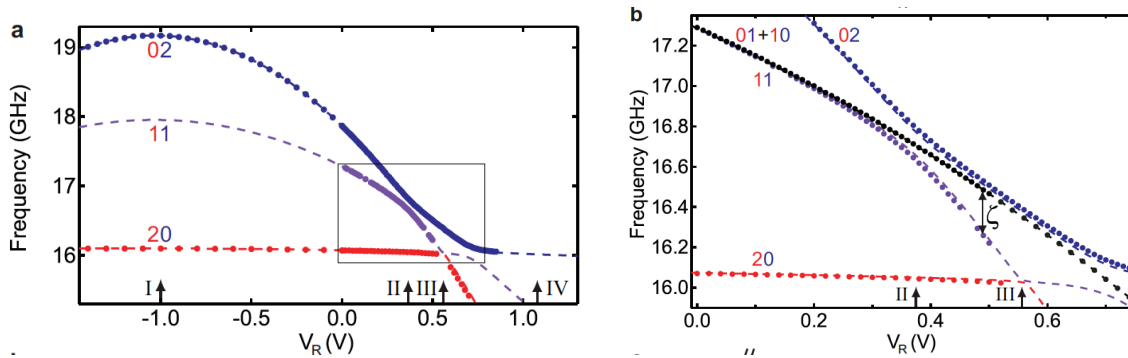


Figure 13: *CPHASE* resonance gate [142].

In this representation the evolution operator is diagonal, with the result that

$$U(t) = \begin{pmatrix} 1 & 0 & 0 & 0 \\ 0 & e^{\phi_{01}} & 0 & 0 \\ 0 & 0 & e^{\phi_{10}} & 0 \\ 0 & 0 & 0 & e^{\phi_{11}(t)} \end{pmatrix} \quad (38)$$

with

$$\phi_{01} = -\langle 01|\hat{H}|01\rangle t = -\frac{\Delta_1}{2} t; \quad \phi_{10} = -\langle 10|\hat{H}|10\rangle t = -\frac{\Delta_2}{2} t \quad (39)$$

$$\phi_{11}(t) = -\langle 11|\hat{H}|11\rangle t = -\frac{\Delta_1 + \Delta_2}{2} t + \int_0^t \zeta(t) dt \quad (40)$$

In the experiment, the 11-02 splitting is determined by the time-dependent bias tuning voltage  $V_R(t) = V_2(t)$  in Fig. 13. If  $\Delta_1 = \Delta_2$ , then

$$\phi_{01} = \phi_{10} = -\frac{\Delta}{2} t; \quad \phi_{11}(t) = -\Delta t + \int_0^t \zeta(V_R(t)) dt \quad (41)$$

After time  $t$  such that

$$\phi_{01} = \phi_{10} = -\frac{\Delta}{2} t = 2\pi \quad (42)$$

then the 11 state has rotated twice, and the phase is given by  $-4\pi + \int_0^t \zeta(V_R(t)) dt$ .

$$U(t) = \begin{pmatrix} 1 & 0 & 0 & 0 \\ 0 & 1 & 0 & 0 \\ 0 & 0 & 1 & 0 \\ 0 & 0 & 0 & e^{i\phi_{11}(t)} \end{pmatrix}; \quad \phi_{11}(t) = \int_0^t \zeta(V_R(t)) dt \quad (43)$$

At this point, the excursion of the bias voltage will decide the integrated strength needed for achieving  $\phi_{11}(t) = \pi$ , providing the CPHASE gate (Fig. 14a):

$$CPHASE = CZ = Cntrl R_z(\pi) = \begin{pmatrix} 1 & 0 & 0 & 0 \\ 0 & 1 & 0 & 0 \\ 0 & 0 & 1 & 0 \\ 0 & 0 & 0 & -1 \end{pmatrix} \quad (44)$$

*6.4.3. CNOT* The CNOT gate can be expressed in terms of CPHASE and two Hadamard gates, as commonly implemented in transmon circuits (Fig. 14b):

$$CNOT = CX = Cntrl R_y(\pi) = \begin{pmatrix} 1 & 0 & 0 & 0 \\ 0 & 1 & 0 & 0 \\ 0 & 0 & 0 & 1 \\ 0 & 0 & 1 & 0 \end{pmatrix} \quad (45)$$

The first H-gate changes from the  $z$ - to the  $x$ -basis, and the second H-gate transforms back.

*6.4.4. Controlled rotation* CPHASE is special example of the general controlled Z-rotation - Ctrl-Z( $\theta$ ) - gate in Eq. (44) and Fig. 14c, allowing one to control time evolution and (d) to map states to ancillas for phase estimation,

*6.4.5. 2q-time evolution* We now have the tools to describe the time evolution operator corresponding to 2-qubit interaction terms. The parts of the Hamiltonian with  $\sigma_z \otimes \sigma_z$  products,  $U = \exp[-i\frac{\theta}{2}\sigma_z \otimes \sigma_z]$  can be implemented by a quantum circuit of the form shown in Fig. 14e [37]. Operators like  $\exp[-i\frac{\theta}{2}\sigma_x \otimes \sigma_x]$  and  $\exp[-i\frac{\theta}{2}\sigma_z \otimes \sigma_x]$  can be generated by adding a number of 1q-rotation gates. Moreover, Fig. 14f represents a controlled version of Fig. 14e for controlled time evolution and phase estimation.

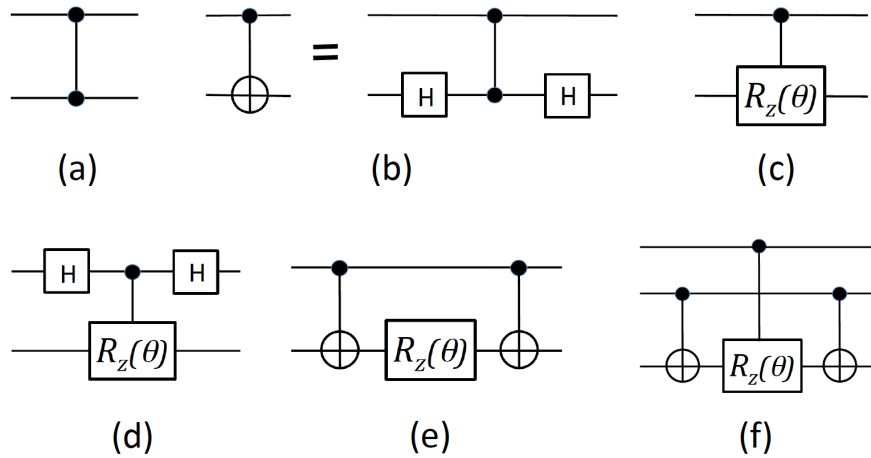


Figure 14: Circuits for implementation of (a) *CPHASE*; (b) *CNOT*; (c) *Ctrl-Z*( $\theta$ ),  $\theta$  arbitrary; (d) basic circuit for phase estimation using an ancilla (top qubit); (e) the  $U = \exp[-i\frac{\theta}{2}\sigma_z \otimes \sigma_z]$  operator; (f) a controlled version of (e) for controlled time evolution and phase estimation (top qubit).

### 6.5. $2q$ gates induced by microwave driving

The flux-tunability of transmons make them sensitive to flux noise, resulting in decoherence. One approach is therefore to use fixed-frequency transmon qubits, replacing the frequency-tuning squid by a single JJ. This is also an important design for arrays of 3D transmon qubits where direct access for tuning individual qubits may be impossible.

The generic approach for coupling non-linear oscillators is to use electromagnetic driving fields to induce parametric coupling with tunable strength by creating a spectrum of sidebands bridging frequency gaps. In this way it is possible to entangle superconducting qubits with different frequencies using (i) fixed linear couplings, (ii) only microwave control signals, and (iii) tunable effective interaction strengths. Recently these methods have been applied experimentally through a variety of schemes based on two different principles: (i) driving qubits, and (ii) driving coupling resonators, e.g. a tunable bus.

#### 6.5.1. Driving qubits

*Cross resonance (CR)  $2q$  gates* The CR scheme [181–184] exploits already present nonlinearities to achieve tunable coupling, circumventing the need for nonlinear coupling elements. The CR two-qubit gate scheme irradiates one of the qubits at the transition frequency of the other qubit. In the presence of this cross-resonant microwave drive, an effective coupling emerges between the two qubits whose strength increases linearly with the ratio (drive amplitude)/(difference frequency).

The CR coupling of two qubits, Q1 and Q2, can be understood in the dressed

state picture of quantum optics [181]. Under CR driving, the central transition at the irradiation frequency of the driven dressed Q1 system is matched to the bare transition of the undriven Q2. One thus creates a resonance between the central feature of the Mollow triplet on Q1 and the bare transition of Q2. The tunability of the effective coupling strength  $G$  results from the evolution of the dressed Q1 eigenstates as the field amplitude  $F$  is adjusted [181]:

$$\hat{H}_{eff} = g(F) \sigma_{z1} \sigma_{x2}, \quad (46)$$

which is related to the CNOT gate by one additional local  $\pi/2$  rotation of each qubit.

In addition to the CR scheme, one approach is to create a microwave-activated conditional-phase gate (MAP) [185] based on driving the  $|03\rangle$  and  $|12\rangle$  transmon states into resonance. A general problem with driving qubits is that the couplings may depend sensitively on the qubit level structure. For transmon qubits the CR scheme is limited by the weak anharmonicity of the transmon, and the MAP scheme employs specific higher excited states of the transmon. These schemes may therefore be difficult to scale up to many qubits.

*6.5.2. Driving a tunable bus* Attaching a SQUID to the end of a coplanar waveguide resonator (CPW) makes it possible to vary the boundary condition (effective length) and create a flux-tunable resonator [186,187] and to couple qubits [188,189]. In Ref. [188], fixed-frequency qubits with different frequencies were coupled by successively bringing each qubit quasi-statically in and out of resonance with the tunable CPW, effectively creating multi-qubit gates. In Ref. [186,189], the CPW was rapidly tuned (chirped) to create interference and beating of microwave emission, which in principle could dynamically couple qubits [189]. Alternatively, one can drive the resonator at high frequency to create sideband structure and dynamic parametric coupling between qubits. This is presently at the focus of extensive and promising research [190–194], potentially providing multi-qubit gate architectures for scaled-up systems. A recent proposal is based on the *Dynamical Casimir Effect* [194]: A SQUID is then connected to the midpoint of a CPW resonator that is connected to transmon qubits at both ends, varying the coupling between the two halves by flux tuning. Driving the SQUID at microwave frequencies emits pair of photons that can entangle the qubits [194].

*Resonator-induced phase gate (RIP)* In the resonator-induced phase gate (RIP) scheme [190–192] fixed-frequency transmons are statically coupled to the same bus resonator driven at the difference frequency of two qubits.

In a two 2D-transmon setup [191], parametrically oscillating a flux-tunable "bus qubit" (similar to a combination of the qubit-qubit couplings in Figs. 7b,c) at the qubit-qubit detuning enables a  $\sigma_+\sigma_- + \sigma_-\sigma_+$  resonant exchange (XX+YY) interaction. The interaction is said to implement a 183 ns two-qubit iSWAP gate between qubits separated in frequency by 854 MHz with a measured average fidelity of 0.98 from

interleaved randomized benchmarking. This gate may be an enabling technology for surface code circuits and for analog quantum simulation [191].

In a 3D-transmon-cQED setup with four superconducting qubits [192], RIP gates are experimentally implemented between pairs of qubits, demonstrating high-fidelity CZ gates between all possible pairs of qubits. The qubits are arranged within a wide range of frequency detunings, up to as large as 1.8 GHz. This setup was used to generate a four-qubit Greenberger-Horne-Zeilinger state [192].

*Mølmer-Sørensen (MS) 2q gate* In ion traps, the qubits (ions) are naturally coupled by collective vibrational modes generating a sideband structure [195]. The Mølmer-Sørensen (MS) gate [196–198] is a single-step 2-qubit entangling gate  $|00\rangle \rightarrow |11\rangle$  driven by 2-tone 2-photon excitation assisted by collective (vibrational) modes, providing resonant intermediate states with sideband structure. It looks like Rabi driving of a single qubit, coupling the  $|0, 1ph\rangle$  and  $|1, 0ph\rangle$  levels,  $|0, 1ph\rangle \pm |1, 0ph\rangle \leftrightarrow \lambda \sigma_{x1}$  extended to resonant 2-photon direct of two qubits, coupling the  $|00, 2ph\rangle$  and  $|11, 0ph\rangle$  levels,  $|00, 2ph\rangle \pm |11, 0ph\rangle$  giving rise to an effective 2-qubit interaction  $\lambda \sigma_{x1} \sigma_{x2}$ . There a recent proposal for implementing MS gates in transmon-cQED [193] by driving a SQUID to create sideband structure, as discussed above, and simultaneously driving the qubits with two microwave tones.

*Multiqubit gates* Multi-qubit gates, can be implemented in several ways: (i) sequentially, by series of 1q and 2q gates to yield CCNOT (Toffoli) or CCZ [98, 199, 200]; by (ii) a "single-shot" optimised pulse sequence [201, 202]; or by (iii) single-shot collective excitation via bus dynamics. The state of the art of (iii) is currently defined by an ion-trap experiment entangling 14 qubits via a Mølmer-Sørensen (MS) gate [195]. The MS gate can be generalised to direct Rabi-like driving of N qubits, coupling the  $|0\dots 00, Nph\rangle$  and  $|1\dots 11, 0ph\rangle$  levels, leading to an effective N-qubit interaction  $\lambda \sigma_{x1} \sigma_{x2} \dots \sigma_{xN}$ .

### 6.6. Gate synthesis and universal sets of gates

An important problem in quantum computing is how to decompose an arbitrary unitary operation in a sequence of standard elementary gates from a gate library [203]. The Clifford group can be generated by three elementary gates: a two-qubit gate, e.g. CNOT or CPHASE and two single-qubit gates: the Hadamard gate H, and the S-gate,

$$H = \frac{1}{\sqrt{2}} \begin{pmatrix} 1 & 1 \\ 1 & -1 \end{pmatrix} \quad (47)$$

$$S = \frac{1}{\sqrt{2}} \begin{pmatrix} 1 & 0 \\ 0 & i \end{pmatrix} \quad (48)$$

Adding a non-Clifford gate, such as the T gate:

$$T = \frac{1}{\sqrt{2}} \begin{pmatrix} 1 & 0 \\ 0 & e^{\pi/4} \end{pmatrix} \quad (49)$$

makes it possible to generate all quantum circuits, i.e. perform universal quantum computing.

Any quantum circuit of operations can be described by a sequence of gates from this finite universal set. For the specific case of single qubit unitaries the Solovay-Kitaev theorem [204] guarantees that this can be done efficiently, involving only a polynomial number of gates. For a general quantum circuit, to synthesize it may take an exponential number of gates. Recently Bravyi and Gosset [152] presented a new algorithm for classical simulation of quantum circuits over the universal Clifford + T gate set which is polynomial in the number of qubits and the number of Clifford gates but exponential in the number of T gates. However, the exponential scaling is sufficiently mild that it was possible to use the algorithm to simulate a medium-sized quantum circuit dominated by Clifford gates, namely a hidden-shift quantum algorithm with 40 qubits, a few hundred Clifford gates, and nearly 50 T gates.

## 7. Quantum state preparation and characterisation

### 7.1. Quantum state characterisation

Quantum state characterisation and Quantum computing are two sides of the same coin. Both involve application of long series of gates. The difference lies in the purpose of the protocol: characterisation of a quantum state, or solution of a computational problem. Tomography is all about visualisation of quantum states and processes, which means measurement and presentation of large quantities of quantum information.

In the general case, the density matrix is defined by  $(2^q)^2$  matrix elements, requiring  $2^{2q} - 1$  independent measurements for characterization, based on an ensemble of replicas of the state in question. In the 2-qubit case, 15 matrix elements have to be determined via a set of 15 measurements at different angles. In solid-stated devices the integrated detectors cannot be rotated. Therefore, measurements are typically performed by rotation gates applied to the various qubits before measurement. The data are then used to calculate the elements of the density matrix. The discussion is of course not limited to two-level systems: the transmon is a multi-level system and a single qutrit 3-level density matrix was investigated in Ref. [205].

For large-scale quantum circuits and systems to be trustworthy, it is all-important to be able to verify the functionality and performance at various levels by appropriate measurements and data analysis. Full characterisation via quantum state tomography (QST) and quantum process tomography (QPT) [206–209] scales exponentially with the number of qubits - an NP-hard problem - and is only possible for small systems. At this level, up to three qubits, QST and QPT are well-established tools for characterising quantum states, gates and processes demonstrated by a large number of recent applications involving superconducting circuits (see e.g. [200, 210–212]).

For larger systems, however, full QPT becomes impractical, and methods have to be developed for reducing the information needed, e.g. via *randomised benchmarking* (RB) (a randomised QPT procedure, applying a random sequence of gates) [213–215], compressed sensing QPT (CSQPT) (exploiting sparsity of matrices) [216–220], and adaptive Bayesian quantum tomography [221–223]

The rapid scaling up of transmon systems will make reduced-information methods indispensable, and there has already been a number of recent applications of RB and twirling protocols [224–229] and CSQPT [220] to superconducting circuits. While standard QPT provides information about a single gate, RB gives a measure of the accumulated error over a long sequence of gates. Standard QPT is limited by errors in state preparation, measurement and one-qubit gates and suffers from inefficient scaling with number of qubits. RB yields estimates of the computationally relevant errors without relying on accurate state preparation and measurement. Since it involves long sequences of randomly chosen gates, it also verifies that error behaviour is stable when used in long computations. *Interleaved* RB (IRB) is a scalable protocol for estimating the average error of individual quantum computational gates. IRB involves sequentially mixing Clifford and Pauli gates. The technique takes into account both state preparation

and measurement errors and is scalable in the number of qubits [17, 230–232]. *Twirling* provides useful partial information of a quantum channel by averaging the channel under the action of a set of unitaries [233, 234], pre-multiplying the input state by an operation, running the original process, post-multiplying by the inverse operation, and finally averaging over a set of operations. Randomly applying the Pauli operators with uniform probability to any density operator - Pauli twirling - gives the maximally mixed state. Twirling is often a part of the abovementioned RB protocols to introduce averaging.

### 7.2. Quantum supremacy characterisation

In just a few years, quantum computers without error correction are expected to be able to approximately sample the output of random quantum circuits which state-of-the-art classical computers cannot simulate [235]. In this spirit, Boixo et al. [2] study the computational task of sampling from the output distribution of pseudo-random quantum circuits composed from a universal gate set, a typical benchmarking problem, and introduce the concept of Cross Entropy (CE) to characterise Quantum Supremacy.

The Shannon entropy  $S(A) = -\sum_a P(A_a) \ln P(A_a)$  is a measure of the inherent uncertainty of a single random variable  $A$ . The Cross Entropy  $CE(A; B) = -\sum_x P(A_x) \ln P(B_x)$  is a *measure of inaccuracy* [236] and gives the average number of bits needed to identify events that occur with probability  $P(A_x)$ , if a coding scheme is used that is optimal for the probability distribution  $P(B_x)$  [237].

Boixo et al. [2] consider a 7 x 6 qubit 2D lattice with gate depth 25, close to the limit of present classical computers (7 x 7 qubits). They show how to estimate the cross entropy between the sampled output distribution  $P(A)$  of an experimental implementation of a random quantum circuit providing quantum chaos, and the ideal output distribution  $P(B)$  simulated by a supercomputer, and argue that the cross entropy is closely related to the circuit fidelity. If the experimental quantum device achieves a cross entropy surpassing the performance of the state-of-the-art classical competition, this will be a first demonstration of quantum supremacy [2, 237].

A crucial aspect of a near-term quantum supremacy proposal is that the computational task can only be performed classically through direct simulations with cost that is exponential in the number of qubits. Quantum supremacy can be claimed if the theoretical estimates are in good agreement with the experimental extrapolations.

### 7.3. Multi-qubit state preparation

**7.3.1. Bell states** Bell state preparation and characterization used to represent pioneering experiments [94, 142]. By now these experiments are "routine", and focus is on multi-qubit entangled states for QEC and QIP.

For the double-excitation Bell cat state  $|\psi\rangle = \frac{1}{\sqrt{2}}(|00\rangle + |11\rangle)$ , the density matrix

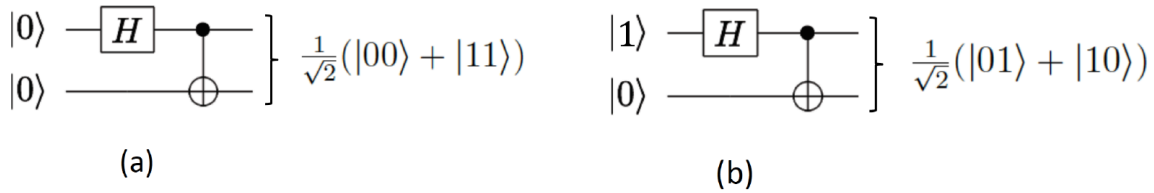


Figure 15: *Bell states. The Hadamard gate creates superposition states  $|0\rangle \rightarrow |0\rangle + |1\rangle$  and  $|1\rangle \rightarrow |0\rangle - |1\rangle$ , which allows the CNOT gate to create  $2q$ -superposition Bell states: (a)  $\frac{1}{\sqrt{2}}(|00\rangle + |11\rangle)$ ; (b)  $\frac{1}{\sqrt{2}}(|01\rangle + |10\rangle)$ .*

is given by

$$\hat{\rho} = \frac{1}{2}(|00\rangle + |11\rangle)(\langle 00| + \langle 11|) = \frac{1}{2} \begin{pmatrix} 1 & 0 & 0 & 1 \\ 0 & 0 & 0 & 0 \\ 0 & 0 & 0 & 0 \\ 1 & 0 & 0 & 1 \end{pmatrix} \quad (50)$$

Figure 16 shows characterisation of maximally entangled GHZ cat states with five capacitively coupled Xmon qubits [17] via quantum state tomography (QST). The Bell

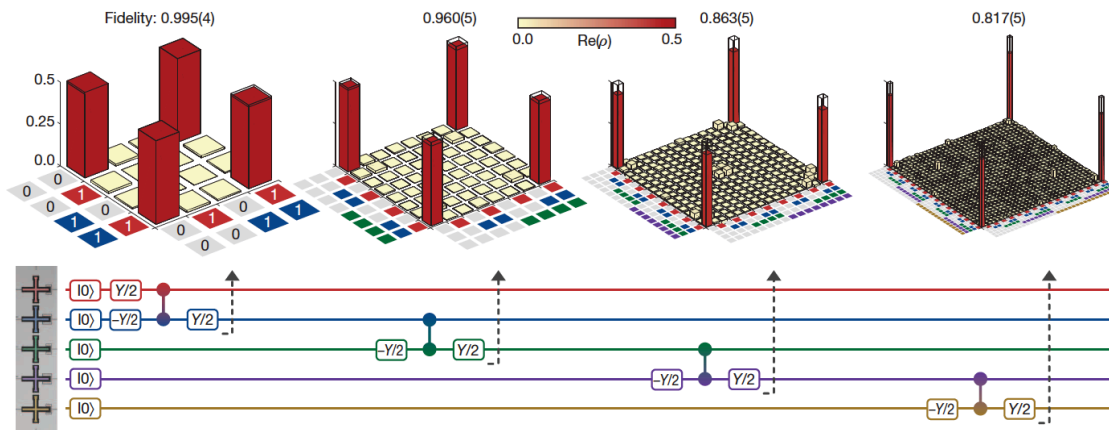


Figure 16: *Quantum state tomography (QST) and generation of GHZ type of states. Top row: Real part of the density matrix for the  $N = 2$  Bell state and the  $N = 3, 4$  and  $5$  GHZ states, measured by quantum state tomography. Ideal density matrix elements are transparent, with value  $0.5$  at the four corners. Bottom row: Algorithm used to construct the states. Adapted from [17].*

state density matrix is experimentally demonstrated in the leftmost panel of Fig. 16, showing the characteristic four corner pillars.

For the single-excitation Bell state  $|\psi\rangle = \frac{1}{\sqrt{2}}(|01\rangle + |10\rangle)$ , the density matrix is given

by

$$\hat{\rho} = \frac{1}{2}(|01\rangle + |10\rangle)(\langle 01| + \langle 10|) = \frac{1}{2} \begin{pmatrix} 0 & 0 & 0 & 0 \\ 0 & 1 & 1 & 0 \\ 0 & 1 & 1 & 0 \\ 0 & 0 & 0 & 0 \end{pmatrix} \quad (51)$$

spanning a different part of Hilbert space than the Bell cat state.

**7.3.2. GHZ states** For the triple-excitation GHZ cat state  $|\psi\rangle = \frac{1}{\sqrt{2}}(|000\rangle + |111\rangle)$ , the density matrix is given by

$$\hat{\rho} = \frac{1}{2}(|000\rangle + |111\rangle)(\langle 000| + \langle 111|) \quad (52)$$

corresponding to the corner pillars in the second panel in Fig. 16.

**7.3.3. W-states** For the 3-qubit single-excitation Werner W-state,  $|\psi\rangle = \frac{1}{\sqrt{3}}(|001\rangle + |010\rangle + |100\rangle)$ , the density matrix is given by

$$\hat{\rho} = \frac{1}{3}(|001\rangle + |010\rangle + |100\rangle)(\langle 001| + \langle 010| + \langle 100|) \quad (53)$$

The form of the density matrix is illustrated by the experimental results shown in Fig. 17 [238].

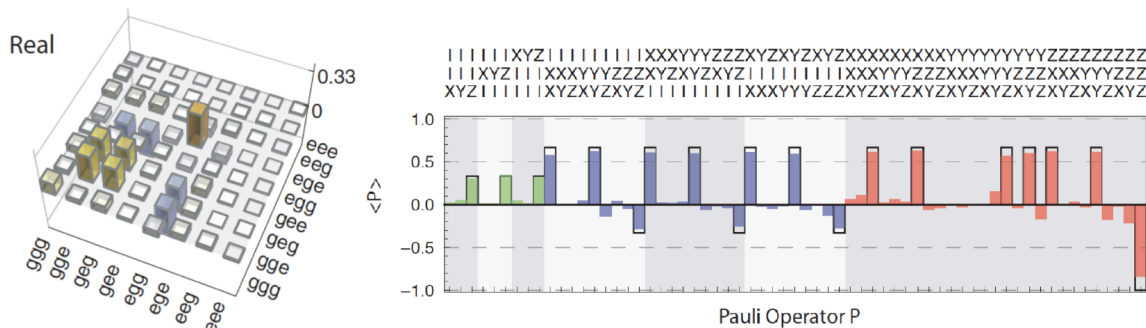


Figure 17: *Tomography of the W-state [238]. Left: Real part of the density matrix. Right: Pauli set from quantum process tomography. Adapted from [238].*

**7.3.4. Generating Bell states by parity measurement** Measurement provides an important way to prepare quantum states. Figure 18 shows a way to prepare entangled states by parity measurement [18]. The Hadamard gates generate the two-qubit product state  $|00\rangle + |01\rangle + |10\rangle + |11\rangle$ . Adding the ancilla, the three-qubit state becomes  $|000\rangle + |010\rangle + |100\rangle + |110\rangle$ , and after applying the CNOT gates the state (at the dashed line) is given by  $|000\rangle + |011\rangle + |101\rangle + |110\rangle = [|00\rangle + |11\rangle]|0\rangle + [|01\rangle + |10\rangle]|1\rangle$ , representing a sum of Bell pairs with opposite parities. Measurement of the state of the ancilla collapses the state into one of the Bell states. The entanglement process can be made deterministic by feedback control, inducing a bit flip on demand if the unwanted parity is detected, as demonstrated by Saira *et al.* [18].

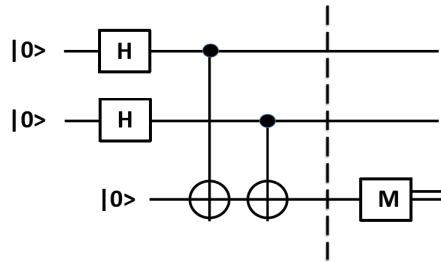


Figure 18: *Entanglement by parity measurement. The state at the dashed line is given by  $[|00\rangle + |11\rangle]|0\rangle + [|01\rangle + |10\rangle]|1\rangle$ . Projective measurement of the ancilla collapses the state into one of the Bell states [18]. The information about the state of the ancilla can be used for deterministic entanglement.*

### 7.4. Teleportation

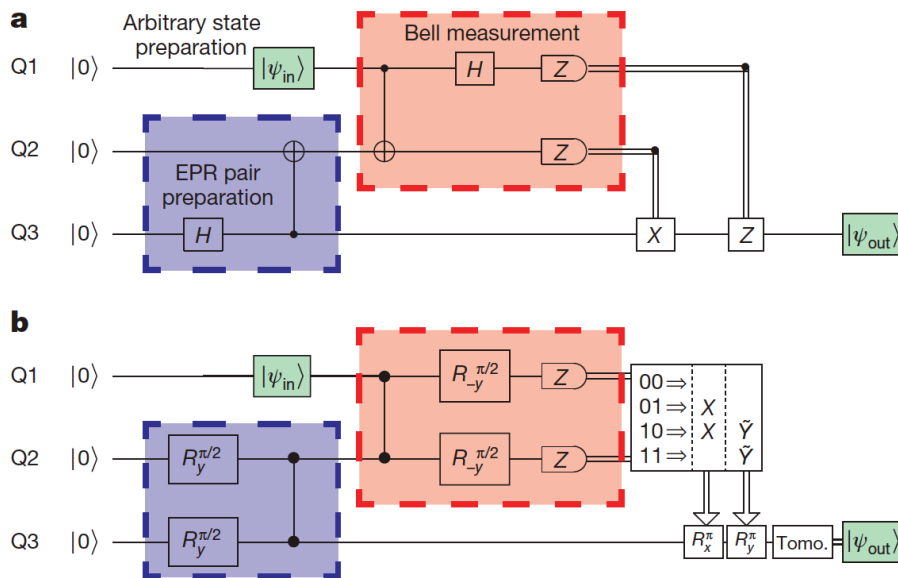


Figure 19: *Superconducting 2D transmon-cQED circuit for feedforward control of teleportation [143].*

7.4.1. *Teleportation of states* Teleportation is a fundamental QIPC protocol - it allows quantum states to be reconstructed in distant places given a coherent quantum communication channel and additional classical channels for sending control information. Teleportation is a fundamental milestone that has to be passed by any competitive technology [239, 240].

The successful demonstration of teleportation with a transmon circuit (Fig. 19) [143] therefore represents a very important step for superconducting circuits, even though it "only" involved transfer over a distance of a millimeter between two qubits on the same chip, limited by the length of the microwave bus resonator. It remains to

perform communication between distant qubits (cf. Ref. [241]), requiring long microwave transmission links, or optical links made possible by MW-optical interfaces.

*7.4.2. Teleportation of entanglement* This is an extension of the teleportation protocol - called entanglement swapping - entangling two independent qubits that never interacted in the past [242, 243].

The quantum circuit is shown in Fig. 20. The protocol first creates two independent entangled pairs, applying CNOT gates to (Q1,Q2) and (Q3,Q4), and then further applies a CNOT gate to entangle Q2 and Q3. This results in a special 4 qubit entangled state, and projective measurement of Q2 and Q3 provides classical information how to create an entangled pair (Q1,Q4) at a distant location, given that the states of qubits Q1 and Q4 are available.

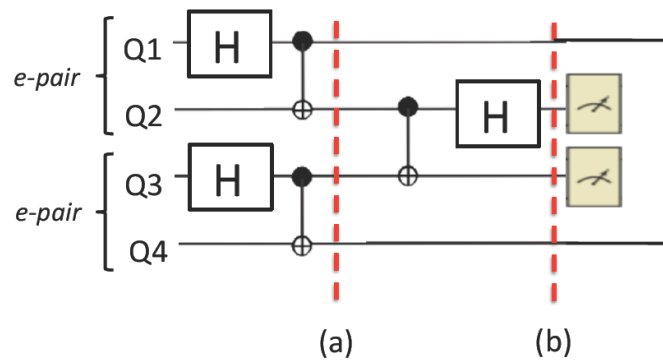


Figure 20: *Entanglement swapping.*

As a simple example, consider the input state  $|0000\rangle$ . The two first Hadamard and CNOT gates then create a product of two Bell states at (a):  $(|00\rangle + |11\rangle)(|00\rangle + |11\rangle) = |0000\rangle + |0011\rangle + |1100\rangle + |1111\rangle$ . Applying a CNOT gate to Q2, Q3 and a Hadamard gate to Q2 results in (b):  $(|0000\rangle + |1001\rangle) + (|0011\rangle + |1010\rangle) + (|0100\rangle - |1101\rangle) + (|0111\rangle - |1110\rangle)$ . Performing a Bell measurement of Q2 and Q3 then projects the state with probability 0.25 to one of the following entangled (Q1,Q4) Bell pairs:

$$00 \rightarrow |00\rangle + |11\rangle \tag{54}$$

$$01 \rightarrow |01\rangle + |10\rangle \tag{55}$$

$$10 \rightarrow |00\rangle - |11\rangle \tag{56}$$

$$11 \rightarrow |01\rangle - |10\rangle \tag{57}$$

The measurement entangles the remaining coherent qubits, and the classical 2-bit information tells exactly what Bell state was created. This at the core of a repeater protocol. Heinsoo *et al.* [144] have implemented the circuit in Fig. 20 with a 4-transmon circuit (Fig. 3a), measuring Q2, Q3 and identifying the four Bell states via quantum state tomography of Q1, Q4.

## 7.5. Distillation of entanglement

The purpose of entanglement distillation is to extract a maximally entangled state from a collection of less entangled states. This can be used as an entanglement resource, e.g. for repeaters in quantum communication [244]. The distillation concept applies to both pure and mixed states.

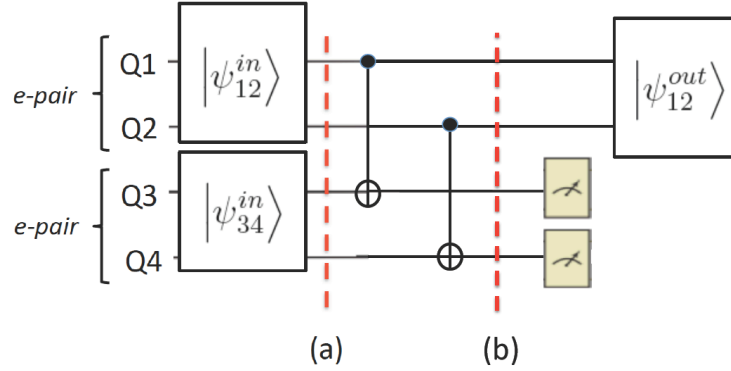


Figure 21: *Distillation of entanglement of two partially entangled pairs,  $\psi_{12}^{in}$  and  $\psi_{34}^{in}$ . The 4-qubit state at (a) is a product of two independent pairs. In contrast, the 4-qubit state  $\psi_{1234}$  at (b) is not factorisable at all, in general. Measurement of Q3,Q4 projects out a 2-qubit state, with two different outcomes:  $(Q3,Q4) = (0,0) \rightarrow \psi_{12}^{out1}$  and  $(Q3,Q4) = (1,1) \rightarrow \psi_{12}^{out2}$ . Both represent superpositions of Bell states. The instance of identical input pairs is very special,  $(0,0)$  producing a state with low concurrence  $C_1 < C_{in}$ , and  $(1,1)$  producing a Bell state state with  $C_2 = 1$ .*

A general two-qubit state can be written as  $\psi = a_0|00\rangle + a_1|01\rangle + a_2|10\rangle + a_3|11\rangle$ . A measure of entanglement is the Concurrence:  $C = 2|a_0a_3 - a_1a_2|$ . For a product state all coefficients are equal, and  $C = 0$ . For a Bell state, on the other hand,  $C = 1$ .

An example of a distillation quantum circuit is shown in Fig. 21. Two partially entangled and independent pairs of input states  $\psi_{12}$  and  $\psi_{34}$ :

$$|\psi_{12}^{in}\rangle = [\cos(\epsilon_{12}\frac{\pi}{4})|00\rangle + \sin(\epsilon_{12}\frac{\pi}{4})|11\rangle]; \quad C = \sin(\epsilon_{12}\frac{\pi}{2}) \quad (58)$$

$$|\psi_{34}^{in}\rangle = [\cos(\epsilon_{34}\frac{\pi}{4})|00\rangle + \sin(\epsilon_{34}\frac{\pi}{4})|11\rangle]; \quad C = \sin(\epsilon_{34}\frac{\pi}{2}) \quad (59)$$

are entangled by two CNOT gates, creating a 4-qubit entangled state  $\psi_{1234}$  at (b). Introducing  $\epsilon_{12} + \epsilon_{34} = 2\epsilon$  and  $\epsilon_{12} - \epsilon_{34} = \Delta\epsilon$  one obtains

$$\begin{aligned} |\psi_{1234}\rangle = & [\cos(\Delta\epsilon\frac{\pi}{4}) + \cos(\epsilon\frac{\pi}{2})]|0000\rangle + [\sin(\epsilon\frac{\pi}{2}) - \sin(\Delta\epsilon\frac{\pi}{4})]|0011\rangle \\ & + [\sin(\epsilon\frac{\pi}{2}) + \sin(\Delta\epsilon\frac{\pi}{4})]|1111\rangle + [\cos(\Delta\epsilon\frac{\pi}{4}) - \cos(\epsilon\frac{\pi}{2})]|1100\rangle \end{aligned} \quad (60)$$

Performing a Bell measurement of Q3 and Q4 results in  $(0,0)$  or  $(1,1)$  outcomes with equal probability, and projects the 4q-qubit state to one of two different entangled 2-qubit (Q1,Q2) Bell pairs (not normalised):

$$(0,0) \rightarrow |\psi_{12}^{out1}\rangle$$

$$= [\cos(\Delta\epsilon\frac{\pi}{4}) + \cos(\epsilon\frac{\pi}{2})]|00\rangle + [\cos(\Delta\epsilon\frac{\pi}{4}) - \cos(\epsilon\frac{\pi}{2})]|11\rangle \quad (61)$$

$$C_1 = |[\cos^2(\Delta\epsilon\frac{\pi}{4}) - \cos^2(\epsilon\frac{\pi}{2})]/[\cos^2(\Delta\epsilon\frac{\pi}{4}) + \cos^2(\epsilon\frac{\pi}{2})]| \quad (62)$$

$$(1, 1) \rightarrow |\psi_{12}^{out2}\rangle$$

$$= [\sin(\epsilon\frac{\pi}{2}) - \sin(\Delta\epsilon\frac{\pi}{4})]|00\rangle + [\sin(\epsilon\frac{\pi}{2}) + \sin(\Delta\epsilon\frac{\pi}{4})]|11\rangle \quad (63)$$

$$C_2 = |[\sin^2(\epsilon\frac{\pi}{2}) - \sin^2(\Delta\epsilon\frac{\pi}{4})]/[\sin^2(\epsilon\frac{\pi}{2}) + \sin^2(\Delta\epsilon\frac{\pi}{4})]| \quad (64)$$

In the case of identical input states ( $\Delta\epsilon = 0$ ), investigated experimentally by Oppinger *et al.* [145],

$$C_1 = |\sin^2(\epsilon\frac{\pi}{2})/[1 + \cos^2(\epsilon\frac{\pi}{2})]| \quad (65)$$

$$C_2 = 1, \quad \epsilon \neq 0 \quad (66)$$

Of the two resulting entangled pairs, the (0,0) outcome produces a less entangled  $\psi_{12}^{out1}$  output state than the input  $\psi_{12}$  state, while the (1,1) outcome produces a fully entangled  $\psi_{12}^{out2}$  Bell state with probability  $P_S = 0.5 \sin^2(\epsilon\frac{\pi}{2})$ , as demonstrated experimentally [145].

If the input states are not identical ( $\Delta\epsilon \neq 0$ ), there is a new dimension, and one must evaluate the concurrence as a functions of  $\epsilon_1$  and  $\epsilon_2$ ,  $C(\epsilon_1, \epsilon_2)$ .

## 8. Quantum state protection

### 8.1. Quantum control

*Quantum optimal control* is essentially a question of controlling qubit driving and time evolution via pulse shaping. The quantum system to be controlled is modeled by unperturbed and control Hamiltonians  $\hat{H}$  and  $\hat{H}_{ci}$  with  $u_i(t)$  the control fields (e.g. microwave driving fields) to be shaped:

$$\hat{H} = \hat{H} + \sum_i u_i(t) \hat{H}_{ci} \quad (67)$$

Pulse shaping [245–247] can be used to reduce single-qubit gate errors arising from the weak anharmonicity of transmon superconducting qubits [205, 248–250].

Motzoi et al. [251] developed optimal control methods for rapidly time-varying Hamiltonians, in the form of a numerical method to find optimal control pulses that account for the separation of timescales between the variation of the input control fields and the applied Hamiltonian. The simulation of the quantum evolution is accurate on the timescale of the fast variation in the applied Hamiltonian.

Egger and Wilhelm [252] have recently developed adaptive hybrid optimal quantum control for imprecisely characterized systems (Ad-HOC). The method combines open- and closed-loop optimal control by first performing a gradient search towards a near-optimal control pulse and then an experimental fidelity estimation with a gradient-Martinfree method. For typical settings in solid-state quantum information processing, Ad-HOC enhances gate fidelities by an order of magnitude, making optimal control theory applicable and useful.

### 8.2. Feedforward control

Feedforward control means reading out information from a qubit, or group of qubits, and sending the classical information at a later time to a device that controls another group of (distant) qubits. Teleportation is a typical example of strong (projective) measurement and digital feedforward control (Fig. 19) [143].

### 8.3. Feedback control

Feedback control differs from feedforward control in that the measured classical control information is fed back to the same group of qubits via a classical feedback loop.

*8.3.1. Digital feedback* control involves strong (projective) measurement on the device to be controlled, classical processing using fast electronics (FPGA), and finally communication of classical signals back to the device to operate digital quantum gates [258], e.g. to reset a qubit [125, 259], or to create deterministic entanglement by parity measurement and feedback [260].

*8.3.2. Analogue feedback* control involves weak (non-projective) measurement on the device to be controlled, classical processing using fast electronics (FPGA), and finally communication of classical signals back to the device to counteract the disturbance, e.g. in order to stabilise Rabi oscillations [261–263] or quantum trajectories [264–270].

*8.3.3. Measurement and back-action* is a continuous process with speed controlled by the interaction strength between the system and the measurement device. This means that the "collapse of the wave function", i.e. the separation into distinguishable projections, has a time scale, from weak (slow) to strong (fast) measurement [253]. There is a connection between information gain and back action, and the effects of back action can be undone under the right circumstances [254–257].

Groen et al. [257] performed a two-step indirect measurement of a transmon qubit with tunable measurement strength by partially entangling the qubit with an ancilla qubit (weak measurement), followed by a projective ancilla measurement using a dedicated resonator (strong, projective measurement). This revealed the back-action of the measurement on the qubit as a function of qubit-ancilla interaction strength and ancilla measurement basis. Nonclassical weak values were observed upon conditioning ancilla measurements on the outcome of a projective measurement of the qubit.

Monitoring a quantum state by weak measurements also makes it possible to "uncollapse" quantum states and achieve decoherence suppression by quantum measurement reversal [271–275]

#### *8.4. Error correction codes and stabilisers*

Quantum error correction (QEC) presents one of the greatest experimental challenges. QEC is quite well developed theoretically but experimentally it is just at the beginning. In this section we will describe a few simple examples of experimental applications, including pieces of the surface code on the way to the complete scheme [16, 19, 20, 276].

An error in a single qubit cannot be corrected - if an error changes the state of the qubit, a measurement of that state says nothing about the original state - the information is lost. Expanding the space of a qubit changes this situation because the information about the error can be stored for later correction - this is essentially the same as discussed earlier in terms of feedback undoing measurement back action.

Expanding the space means coding a qubit  $\alpha|0\rangle + \beta|1\rangle$  by representing it as a cluster of qubits - a logical qubit. For a given code, there are operators that commute with the code operators and have the same eigenstates - these are called stabilisers (see e.g. Ref. [277]). A measurement of a stabiliser operator then results in an eigenstate of the logical qubit, with no knowledge of the individual qubits.

A common measure of the size of the error is the Hamming distance, stating how many bits differ between the correct and corrupted codewords. Classically the simplest form of error correction is redundancy at a level corresponding to the Hamming distance. If one expands 0 and 1 into bit-string code words 00 and 11 with distinct parity +1,

defined by the bit sum modulo 2 checked by XOR gates, then a bit-flip error will lead to 01 or 10, and can be detected as a parity change to -1. Parity checks represent fundamental steps in both classical and quantum error detection schemes.

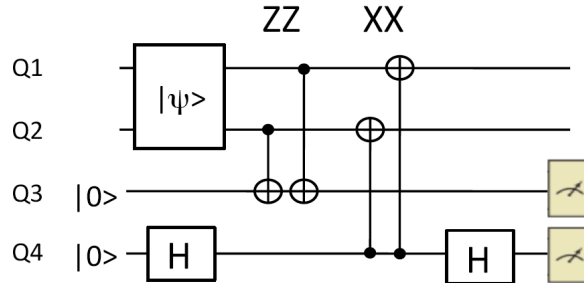


Figure 22: Quantum circuit for checking the ZZ (bit-flip) and XX (phase-flip) parities of a 2-qubit state  $|\psi\rangle$ . Since ZZ and XX commute, bit-flip and phase-flip parities can be checked independently. The Hadamard gates switch to the  $|+\rangle$  X-basis

In the quantum version in Fig. 22, the qubit  $|\psi\rangle = \alpha|0\rangle + \beta|1\rangle$  is coded as  $\alpha|00\rangle + \beta|11\rangle$ . One then adds a third and a fourth qubit for checking and storing the ZZ and XX parities of the codeword. The parity checks are then performed via CNOT (XOR) gates between each of the ancillas and the two qubits.

As a specific example, consider checking for bit-flips with the ZZ ( $\sigma_{z1}\sigma_{z2}$ ) operator in the  $|0\rangle, |1\rangle$  basis. The qubits+ancilla state is then  $(\alpha|00\rangle + \beta|11\rangle)|0\rangle = \alpha|000\rangle + \beta|110\rangle$ . If there is no bit flip, one obtains:  $CNOT_{23}CNOT_{13}(\alpha|000\rangle + \beta|110\rangle) = (\alpha|00\rangle + \beta|11\rangle)|0\rangle$ , where the ancilla stays in state  $|0\rangle$ , with parity +1. If there is a bit flip, leading to  $\alpha|01\rangle + \beta|10\rangle$ , the parity check results in:  $CNOT_{23}CNOT_{13}(\alpha|010\rangle + \beta|100\rangle) = (\alpha|01\rangle + \beta|10\rangle)|1\rangle$ , where the ancilla changes to state  $|1\rangle$ , with parity -1.

As another specific example, consider checking for phase-flips with the XX ( $\sigma_{x1}\sigma_{x2}$ ) operator in the  $|+\rangle, |-\rangle$  basis. Phase-flips are sign changes of the code word,  $\alpha|00\rangle - \beta|11\rangle$ , and look like bit-flips along the X-axis, corresponding to  $|+\rangle \rightarrow |-\rangle$ . The qubits+ancilla state is then  $(\alpha|00\rangle + \beta|11\rangle)|+\rangle = \alpha|00+\rangle + \beta|11+\rangle$ . If there is no phase flip, one obtains:  $CNOT_{42}CNOT_{41}(\alpha|00+\rangle + \beta|11+\rangle) = (\alpha|00\rangle + \beta|11\rangle)|+\rangle$ , where the ancilla stays in state  $|+\rangle$ , with parity +1. If there is a phase flip, leading to  $\alpha|00\rangle - \beta|11\rangle$ , the parity check results in:  $CNOT_{42}CNOT_{41}(\alpha|00+\rangle - \beta|11+\rangle) = (\alpha|00\rangle - \beta|11\rangle)|-\rangle$ , where the ancilla changes to state  $|-\rangle$ , with parity -1.

Since ZZ and XX commute,  $[ZZ, XX] = 0$ , bit-flip and phase-flip parities can be checked (and corrected) independently and the ZZ and XX parity eigenvalues characterise the state, (ZZ,XX): (+,+), (+,-), (-,+) and (-,-).

### 8.5. Three qubit code

To obtain a correctable code, classically the simplest case is to make use of redundancy via code words with three bits: 000 and 111, in which case a bit flip can be corrected by

a majority vote:  $010 \rightarrow 000$ , etc. Quantum mechanically the corresponding protected logic qubit becomes:

$$|\psi\rangle = \alpha|0\rangle + \beta|1\rangle \rightarrow \alpha|000\rangle + \beta|111\rangle \quad (68)$$

Experimental implementation of this coding has been done in ion traps [278–280], NV centra [281] and transmon circuits [19, 199]

A systematic scheme to correct bit flips in any of the three qubits requires separate ancillas for syndrome measurement, storage and correction, as illustrated in Fig. 23. This involves precisely the bit-flip ZZ parity-check procedure described in Fig. 22.

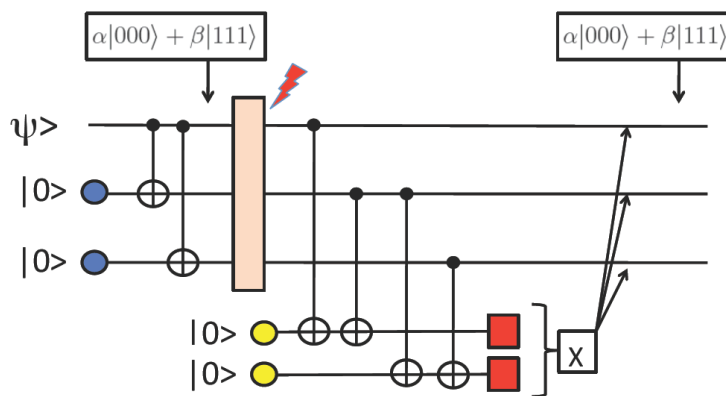


Figure 23: *Standard bit-flip QEC with two ancillas for detecting and storing the error syndrome, and correcting the error. In this way the code words are not perturbed by measurement and recoding not needed. The figure illustrates explicit error detection followed by feedforward control using e.g. FPGA electronics. The correction can also be implemented via Toffoli gates. In the case of phase flips one uses Hadamard gates to transform phase flips to bit flips, checks the parity, and then transforms back.*

Defining  $\hat{U}_1 = CNOT_{q1,a1}CNOT_{q2,a1}$  and  $\hat{U}_2 = CNOT_{q2,a2}CNOT_{q3,a2}$ , we want to calculate  $\hat{U}_2\hat{U}_1(\alpha|000\rangle + \beta|111\rangle)|00\rangle$ , and characterise the effects of bit flips via the ancilla syndrome.

Zero bit-flip error:

$$\hat{U}_2\hat{U}_1(\alpha|000\rangle + \beta|111\rangle)|00\rangle = (\alpha|000\rangle + \beta|111\rangle)|00\rangle \quad (69)$$

On measuring (00), do nothing.

Bit-flip error in qubit 1:

$$\hat{U}_2\hat{U}_1(\alpha|100\rangle + \beta|011\rangle)|00\rangle = (\alpha|100\rangle + \beta|011\rangle)|10\rangle \quad (70)$$

On measuring (10), X-flip qubit 1.

Bit-flip error in qubit 2:

$$\hat{U}_2\hat{U}_1(\alpha|010\rangle + \beta|101\rangle)|00\rangle = (\alpha|010\rangle + \beta|101\rangle)|11\rangle \quad (71)$$

On measuring (11), X-flip qubit 2.

Bit-flip error in qubit 3:

$$\hat{U}_2\hat{U}_1(\alpha|001\rangle + \beta|110\rangle)|00\rangle = (\alpha|001\rangle + \beta|110\rangle)|01\rangle \quad (72)$$

On measuring (01), X-flip qubit 3.

There are typically three ways to apply the correction:

1. By feed-forward application of X gates via fast electronics, flipping the faulty qubit;
2. By automatic correction via a set of Toffoli (CCNOT, controlled X) gates with suitable truth tables, flipping the faulty qubit. This corrects and restores the original coded qubit - there is then no need for re-coding, only the ancillas have to be reset.
3. To store the errors in classical memory, and correct at the end.

A single round of QEC for 3 qubits was implemented by Reed et al. [199] in a 3 transmon qubit circuit without ancillas, correcting for single bit- or phase-flips using a Toffoli gate. Recently the scheme in Fig. 23 was implemented by Riste et al. [19], detecting bit-flip errors in a logical qubit using stabilizer measurements. The experiment uses 3 qubits for encoding, 2 ancilla qubits for the syndrome, and fast feed-forward control for correction (Fig. 23).

Moreover, using their 9-qubit 1D chain, Kelly et al. [20] recently implemented the 3q repetition code with 3 QEC cycles, and extended the work to a 5q code. This work represents first steps toward the 2D-surface code, and will be discussed in some detail below.

Fast electronics makes it possible to perform qubit calibration during repetitive error detection [282]. Moreover, one does not have to apply corrections when errors are detected - it is enough to store the information about errors in classical memory and correct at the end [283, 284].

## 8.6. Surface codes

The surface (toric) QEC code was invented by Kitaev [?, 285] and is now at the focus of intense development and experimental implementations [283, 284, 286–289].

*8.6.1. Basic concepts and models* The surface code is connected with a specific geometrical arrangement (architecture) of qubits: 4 data qubits at the corners of a square with an ancilla qubit at the centre. The central aspect is to perform 4-qubit parity measurements on the data qubits using ZZZZ and XXXX stabiliser operators (Fig. 24) and to register the measured (classical) ancilla eigenvalue, showing whether there has been a bit-flip  $|0\rangle \rightarrow |1\rangle$  or a phase-flip  $|+\rangle \rightarrow |-\rangle$  in the 4q data cluster.

*8.6.2. 4-qubit parity measurements on a surface code plaquette* IBM has performed 4-qubit parity measurements (Fig. 24c) that demonstrate the detection of arbitrary single-qubit quantum errors on an effective 4-qubit plaquette (Fig. 24b) designed for the surface code using all-microwave control [276]. In particular, the qubit-qubit couplings are dynamically driven via the CR technique, and the pulse schemes include echo sequences to remove non-ideal-gate errors. Gates were characterised by randomised benchmarking

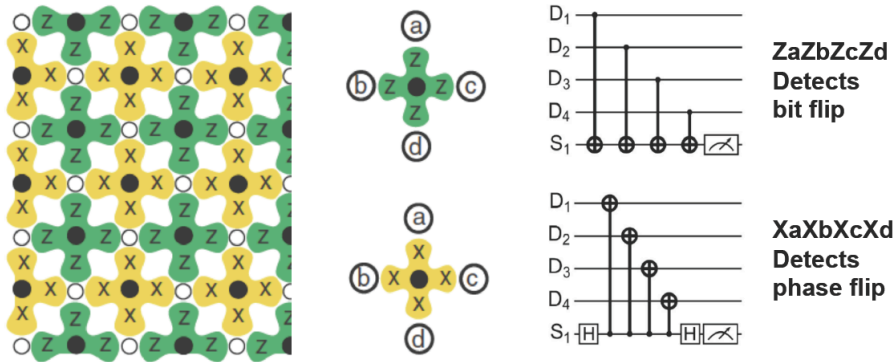


Figure 24: (a) Left: Part of a surface code qubit array layout [286]. (b) Middle: Basic 5 qubit plaquettes with 4 data qubits and a central ancilla qubit. (c) Right: Quantum circuits for 4q  $ZaZbZcZd$  and  $XaXbXcXd$  parity measurements. Note the order a-b-c-d forming an S-like trace. Adapted from [286].

(RB) and correct ZZZZ and XXXX parity assignments were obtained with 0.75-0.80 probability.

*8.6.3. Multi 2-qubit parity measurements on a surface code 1D chain* Martinis' group has performed a set of surface-code type of experiments on a linear 1D chain with 9 qubits [20,282] (Fig. 4), tracking errors as they occur by repeatedly performing projective quantum non-demolition parity measurements. This is a first step toward the 2D surface code scheme (Fig. 24), measuring ZZ (bit-flip) parities (Figs. 22, 23).

The first experiment used 5 qubits (Fig. 25a) with 3 data qubits and 2 measurement ancillas to implement the 3q repetition code (same circuit as in Fig. 23). The repetition code algorithm uses repeated entangling and measurement operations to detect bit-flips using the ZZ parity. Using the output from the measurement qubits during the repetition code for error detection, the initial state can be recovered by removing physical errors in software. Measurement qubits are initialised into the  $|0\rangle$  state and do not need to be reinitialised since measurement is QND.

Figure 25b shows a 9 qubit quantum circuit with 5 data qubits and 4 measurement ancillas, for three cycles of the repetition code, with examples of errors [20]. Errors propagate horizontally in time, and vertically through entangling gates. Different errors lead to different detection patterns: an error on a measurement qubit is detected in two subsequent rounds. Data qubit errors are detected on neighbouring measurement qubits in the same or next cycle. Data errors after the last round are detected by constructing the final set of ZZ eigenvalues from the data qubit measurements.

To study the ability to preserve quantum states, the data qubits were initialized into a GHZ state, and two rounds of the repetition code were applied. The result shows that the one-dimensional repetition code algorithm allows for preserving the quantum state in the case of no errors, and correcting bit-flip errors otherwise, purely through error detection and classical post-processing. This is similar to the full surface code,

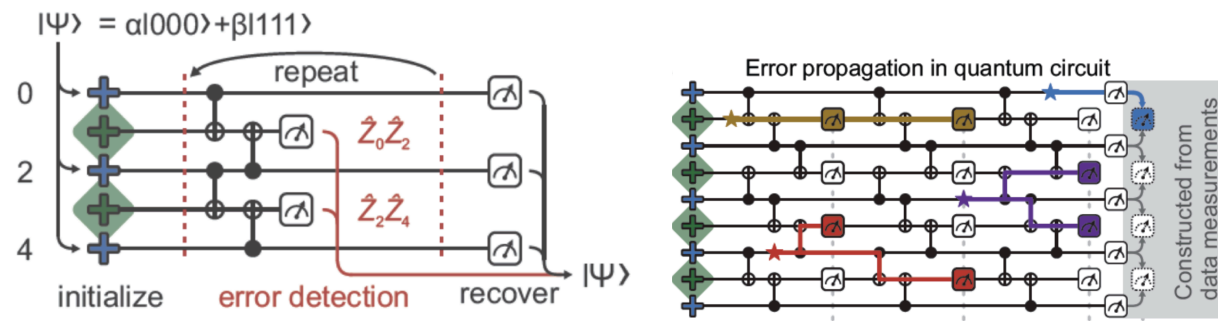


Figure 25: (a) Left: 3q repetition code  $\alpha|000\rangle + \beta|111\rangle$ : algorithm (same circuit as in Fig. 23). (b) Right: 5q repetition code  $\alpha|00000\rangle + \beta|11111\rangle$ : error propagation and identification. Adapted from [20]

avoiding the need for dynamic feedback with quantum gates.

Relative to a single physical qubit, the failure rate in retrieving an input state was reduced by a factor of 2.7 when using five qubits, and by a factor of 8.5 when using all nine qubits after eight cycles. Moreover, the preservation of the non-classical Greenberger-Horne-Zeilinger state was verified tomographically.

## 9. Quantum simulation of many-body systems

Quantum systems need quantum systems for efficient simulation [55]. Simulation of a large quantum system, say a molecule of medical interest, may be intractable on a classical digital computer due to lack of time and memory, but tractable on quantum computers and simulators in order to achieve necessary accuracy.

Ordinary classical digital computers are basically used for number crunching: encoding and running algorithms that process numbers for various purposes, like numerically solving equations, performing search, classifying data, and optimising approximate solutions. Classical digital computers are based on networks of logic gates and memory. The concept of digital quantum computation (QC) and simulation (QS) is similar: it involves circuit models with quantum gates to input, process and output digital quantum information [33, 36, 37, 290–295]. Both digital QC and QS map mathematical problems onto a quantum representation (Hilbert space), devises sequences of gate operations, and uses superposition and entanglement to compute and to achieve speedup.

In contrast, analogue QC and QS are not based on quantum gates, but on direct construction of the physical system Hamiltonian in hardware (HW). There are a number of ways to emulate interesting quantum Hamiltonians in quantum HW systems. In adiabatic QC (AQC) [57, 58] one adiabatically follows the development of the ground state when a perturbation is slowly switched on, switching the Hamiltonian from an initial model one to the final one, describing the transition to the desired interacting many-body system.

Finally, quantum annealing (QA) [296] is related to AQC in that one emulates a Hamiltonian in hardware. The difference is that one heats up and then cools the system, following its path toward the ground state via classical thermal and quantum tunneling transitions.

### 9.1. Basics of quantum simulation

Basically, a quantum simulator solves the time-dependent Schrödinger equation (TDSE) for a system described by a Hamiltonian  $\hat{H}$ ,

$$i\hbar\delta_t|\psi(t)\rangle = \hat{H}(t)|\psi(t)\rangle \quad (73)$$

via propagation of an initial state  $|\psi(t_0)\rangle$  using the time-evolution operator

$$|\psi(t)\rangle = \hat{U}(t, t_0)|\psi(t_0)\rangle = \hat{T} e^{-\frac{i}{\hbar} \int_{t_0}^t \hat{H}(t') dt'} |\psi(t_0)\rangle. \quad (74)$$

The initial state  $|\psi(t_0)\rangle$  represents an essential part of the problem. It can be a computational basis state or a superposition of configurations. If the configuration is not an eigenstate, the state will then evolve in time through state space and reflect the dynamics of the system Hamiltonian, and the Fourier spectrum will provide the energies of the eigenstates. A systematic way to construct the initial state  $|\psi(t_0)\rangle$  is to

start from a reference state and add states representing excitations from the reference state:

$$|\psi(t_0)\rangle = a_{ref}(t)|\psi_{ref}\rangle + \sum a_{ni}(t)c_p^+c_q|\psi_{ref}\rangle + \sum a_{mnji}(t)c_p^+c_q^+c_r c_s|\psi_{ref}\rangle + \dots \quad (75)$$

This represents a configuration interaction (CI) state; formal inclusion of all possible configurations defines the full CI (FCI) state. Simple approximations for  $|\psi(t_0)\rangle$  could be a product state, or a Hartree-Fock determinant. Advanced approximations can be constructed via coupled-cluster (CC) [297] or matrix product states (MPS) [298] constructions.

For a nice review and "hands-on" discussion of all the steps needed for simulating the time evolution of a  $H_2$  molecule and extracting the ground state energy, see Whitfield *et al.* [294].

### 9.2. Trotterisation

Since exponentials of a polynomial number of Pauli operators are known to be efficiently simulatable,  $e^{-i\hat{H}t}|\psi(0)\rangle$  can be implemented using a polynomial number of gates using a quantum computer. There are many different approaches that can be used to achieve this and most of them rely on Trotter decompositions involving discretisation of the time evolution [291, 293, 294].

Let us for simplicity consider a time-independent Hamiltonian, and set  $t_0 = 0$ . (In the following we also set  $\hbar = 1$ , with energy measured in units of frequency).

$$|\psi(t)\rangle = \hat{U}(t, 0)|\psi(0)\rangle = e^{-i\hat{H}t}|\psi(0)\rangle, \quad (76)$$

where

$$\hat{H} = \sum_{i=1,k} \hat{H}_i \quad (77)$$

Trotterisation (Lie-Trotter-Suzuki formula)

$$\begin{aligned} e^{-i\hat{H}t} &\approx [e^{-i(\hat{H}_1+\hat{H}_2+\dots+\hat{H}_k)t/m}]^m \\ &\approx [e^{-i\hat{H}_1t/m} e^{-i\hat{H}_2t/m} \dots e^{-i\hat{H}_kt/m}]^m \end{aligned} \quad (78)$$

makes it possible to express the time evolution operator as a sequence of operations of the individual terms  $\hat{H}_i$  of the Hamiltonian. These operations can be gate operations in a quantum circuit model, or the application of classical control fields in an analog quantum system, or combinations thereof. In practice one uses higher order Trotter formulas to minimize the errors [293, 300].

### 9.3. Phase estimation

The time evolution methods solve a dynamical simulation problems and do not directly solve the ground-state energy estimation problem. The phase estimation algorithm (PEA) (see e.g. [37, 292–294, 299]) provides the connection needed to relate the eigenvalue

estimation problem to the dynamical simulation problem. The left part of Fig. 26a describes the propagation of the quantum state  $\hat{U}|\psi\rangle = e^{-i\hat{H}t}|\psi\rangle$  in smaller and smaller steps (longer and longer times) to achieve the required accuracy. The phase information from the time evolution is stored in the ancillas, and the energy spectrum is finally analyzed by an inverse quantum Fourier transform (QFT) (right part of Fig. 26a).

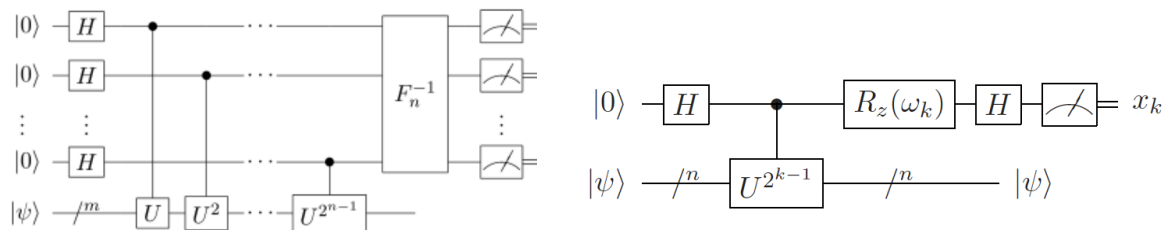


Figure 26: (a) *The Phase Estimation Algorithm (PEA)*. (b) *The  $k$ th iteration of the iterative PEA (IPEA)*. The feedback angle  $k$  depends on the previously measured bits [299].

The multi-qubit state  $|\psi\rangle$  itself in Fig. 26a can be efficiently implemented by a polynomial number of gates (Sect. 6.6), because the  $\hat{U}$ -operators consist of exponentials of polynomial numbers of Pauli operators in the Hamiltonian (cf. Fig. 14d). Calculation of the energy via the PEA is however not necessarily scaling polynomially: it employs Cntrl- $R_z(\theta)$  gates (cf. Fig. 14f), and the number depends on the accuracy required. For a large molecule, requiring many qubits and chemical precision, the number of gates will be very large, requiring long coherence times. This will be further discussed in Sect. 10.

The PEA in Fig. 26a requires as many ancillas as significant bits in the result. To save on the number of ancilla qubits, the PEA can be implemented through an iterative process using only a single ancilla qubit and classical feedback [294, 299], as illustrated in (Fig. 26b).

#### 9.4. Digital quantum simulation of spin models

In digital quantum simulation (DQS) one induces the time evolution of a qubit register in the quantum circuit model by applying a sequence of qubit gates according to a specific protocol. DQS has previously been implemented in an ion trap to perform universal digital quantum simulation of spin models [301], and now also on a transmon platforms [21, 302, 303] to simulate the dynamics of small spin systems.

*9.4.1. Two spin Ising and Heisenberg models* For a two-spin system, the canonical spin models are:

(i) The Ising model:

$$\hat{H}_I = J\sigma_{1z}\sigma_{2z} + B\sum\sigma_{iz} \tag{79}$$

(ii) The transverse field Ising model (TIM):

$$\hat{H}_{TIM} = J\sigma_{1x}\sigma_{2x} + B\sum\sigma_{iz} \quad (80)$$

(iii) The XY model:

$$\hat{H}_{XY} = J(\sigma_{1x}\sigma_{2x} + \sigma_{1y}\sigma_{2y}) + B\sum\sigma_{iz} \quad (81)$$

(iv) The XYZ anisotropic Heisenberg model:

$$\hat{H}_{XYZ} = J_x\sigma_{1x}\sigma_{2x} + J_y\sigma_{1y}\sigma_{2y} + J_z\sigma_{1z}\sigma_{2z} + B\sum\sigma_{iz} \quad (82)$$

The XY interaction  $\frac{1}{2}(\sigma_{1x}\sigma_{2x} + \sigma_{1y}\sigma_{2y}) = \sigma_{1+}\sigma_{2-} + \sigma_{1-}\sigma_{2+}$  is naturally implemented via the  $\sqrt{iSWAP}$  gate, tuning the qubits in and out of resonance, and can be used to construct a digital decomposition of the model-specific evolution and to extract its full dynamics.

Salathé et al. [303] performed digital quantum simulation of the XY and isotropic Heisenberg XYZ spin models with a four-transmon-qubit circuit quantum electrodynamics setup, using two qubits to represent the two spins. The isotropic model Hamiltonian can be written as

$$\hat{H}_{XYZ} = \frac{1}{2}(\hat{H}_{XY} + \hat{H}_{XZ} + \hat{H}_{YZ}) \quad (83)$$

and since the three terms commute, the time evolution operator takes the form of a simple product:  $U_{XYZ} = U_{XY}U_{XZ}U_{YZ}$ .

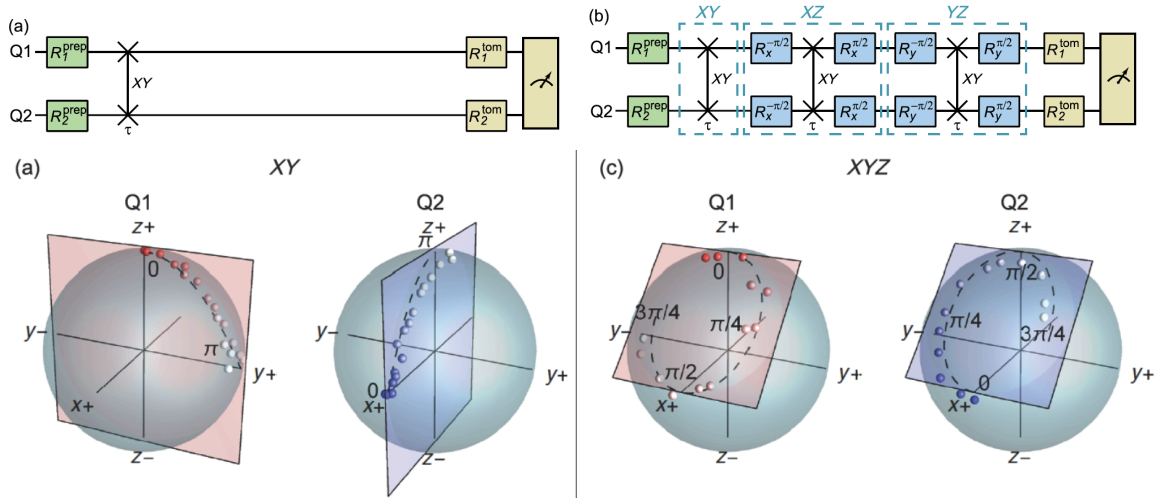


Figure 27: Upper panel: Circuit diagram to characterize the XY interaction on the qubits Q1 and Q2 symbolized by the vertical line which is activated for a time  $\tau$ . Digital quantum simulation of the two-spin Heisenberg (XYZ) interaction for time  $\tau$ . Lower panel: Experimentally determined coordinates of the Bloch vectors during exchange (XY) interaction represented by small red (Q1) and blue (Q2) points are compared to the ideal paths shown as dashed lines in the XY model. The ideal paths are in the YZ and XZ planes shown as blue and red planes intersecting the Bloch sphere. Adapted from [303].

Moreover, rotating the computational basis,

$$U_{XYZ} = U_{XY}U_{XZ}U_{YZ} \tag{84}$$

$$= U_{XY}R_y(-\pi/2)U_{XY}R_y(\pi/2)R_x(-\pi/2)U_{XY}R_x(\pi/2) \tag{85}$$

$$R_x(\pi/2) = \frac{1}{\sqrt{2}} \begin{pmatrix} 1 & -i \\ -i & 1 \end{pmatrix}, \quad R_y(\pi/2) = \frac{1}{\sqrt{2}} \begin{pmatrix} 1 & -1 \\ 1 & 1 \end{pmatrix} \tag{86}$$

makes it possible to apply the XZ and YZ interactions via the XY interaction.

The procedure is shown in Fig. 27, top panels, displaying the circuit diagrams to (a) characterize the XY interaction on the qubits Q1 and Q2 symbolized by the vertical line which is activated for a time  $\tau$ , and (b) digital quantum simulation of the two-spin Heisenberg (XYZ) interaction for time  $\tau$ . Fig. 27 (bottom, left) presents the non-stationary spin dynamics under the XY interaction for a characteristic initial two-qubit state  $|\psi(0)\rangle = |0\rangle(|0\rangle + |1\rangle)/2$  with spins pointing initially in the  $+z$  and  $+x$  directions. Since this is not an eigenstate of the Hamiltonian, the spins start to rotate due to the XY-interaction. Fig. 27 (right) presents the result of simulating the full Heisenberg model.

Salathé *et al.* [303] also performed digital quantum simulation of the transverse Ising model (TIM), Eq.(80). Here the XY and Z parts of the Hamiltonian do not commute, which means that one must implement a split-operator procedure (Trotterisation), as shown in Fig. 28, splitting the evolution over time  $\tau$  into  $n$  slices. In each Trotter time slice of length  $\tau/n$ , the  $R_x(\pm\pi)$  rotation operators change the sign of the second term in the XY interaction, adding up to the XX interaction, and  $R_z(\phi/n)$  implements the Z-part of the Hamiltonian.

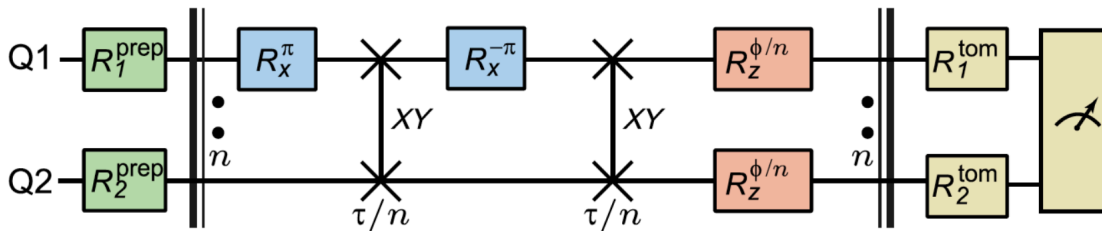


Figure 28: (c) Protocol to decompose and simulate Ising XY spin dynamics in a homogeneous transverse magnetic field. Adapted from [303].

Fig. 28 presents non-stationary spin dynamics under the XX and Z interactions for a characteristic initial two-qubit state  $|\psi(0)\rangle = |0\rangle(|0\rangle - i|1\rangle)/2$  with spins pointing initially in the  $+z$  and  $-y$  directions. The simulation uses  $n=3$  Trotter slices and demonstrates that after three iterations, the z-components of the spins oscillate as expected.

As explained before (Sect. 6.6), the approach uses only Clifford gates and is universal and efficient, employing only resources that are polynomial in the number of spins. An idea of the future challenges can be obtained from a recent investigation

of how to simulate the transverse Ising model (TIM) on a quantum computer including error correction with the surface code [304].

*9.4.2. Digitized adiabatic four spin transverse Ising model* An experiment with a 9-qubit superconducting circuit was recently carried out by Barends et al. [22]. They probed the adiabatic evolutions, and quantified the success of the algorithm for random spin problems, approximating the solutions to both frustrated Ising problems and problems with more complex interactions. The approach is compatible with small-scale systems as well as future error-corrected quantum computers.

The digital quantum simulation (DQS) involved the following two Hamiltonians:

$$\hat{H}_I = -B_{x,I} \sum_i \sigma_{ix} \quad (87)$$

describing noninteracting spins in an external field in the x-direction, and

$$\hat{H}_P = - \sum_i (B_{iz} \sigma_{iz} + B_{ix} \sigma_{ix}) - \sum_i (J_{zz}^{i,i+1} \sigma_{iz} \sigma_{i+1z} + J_{xx}^{i,i+1} \sigma_{ix} \sigma_{i+1x}) \quad (88)$$

describing a range of Ising-type spin Hamiltonians. For the analogue quantum simulation (AQS) part, these were combined:

$$\hat{H}(s) = (1 - s) \hat{H}_I + s \hat{H}_P \quad (89)$$

to allow one to perform DQS for a series of Hamiltonians from non-interacting spins (s=0) to a range of interacting spin models (s=1), and to follow the evolution of the density matrix.

Figure 29 shows an application where a four qubit system is stepwise evolved from an initial Hamiltonian  $H_I$ , where all spins are aligned along the x-axis, to a problem Hamiltonian  $H_P$  with equal ferromagnetic couplings between adjacent qubits, described by a 4-qubit GHZ state.

Barends et al. [22] also investigated digital evolutions of random stoquastic and non-stoquastic problems. Quantum stochastic calculus concerns generalisation of the Langevin equation to quantum systems. Because of the relation to stochastic processes one has adopted the term "stoquastic" to refer to quantum Hamiltonians where all off-diagonal matrix elements in the standard basis are real and non-positive [305]. Stoquastic Hamiltonians are very common in physics. Among spin-1/2 models, the well-studied ferromagnetic Heisenberg models and the quantum transverse Ising model [58] are stoquastic. Another example is a Heisenberg antiferromagnet on a cubic lattice.

Barends et al. chose to investigate a stoquastic frustrated Ising Hamiltonian having random local X and Z fields, and random zz couplings. Non-stoquastic problems have additional random xx couplings. The results show that the system can find the ground states of both stoquastic and non-stoquastic Hamiltonians with comparable performance.

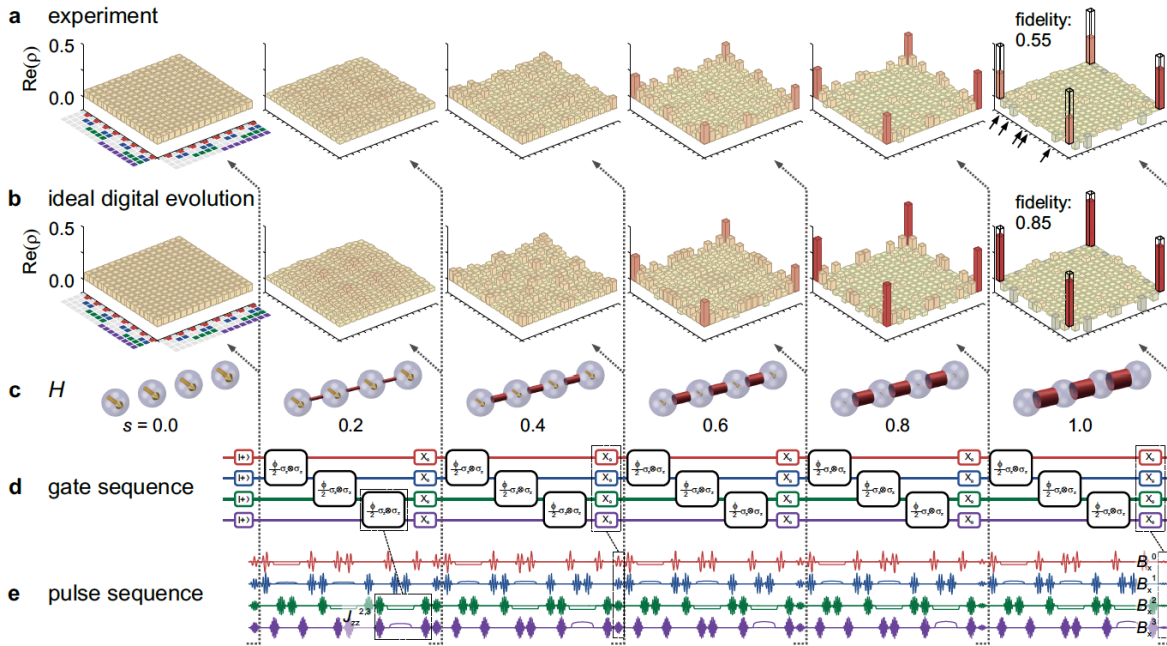


Figure 29: Quantum state tomography of the digital evolution into a Greenberger-Horne-Zeilinger state. A four qubit system is adiabatically evolved from an initial Hamiltonian where all spins are aligned along the  $X$  axis to a problem Hamiltonian with equal ferromagnetic couplings between adjacent qubits. The displayed five step algorithm is 2.1 microseconds long. Implementations of  $zz$  coupling and local  $X$ -fields are highlighted. Adapted from [22].

### 9.5. Digital quantum simulation of fermionic models

Computational Physics, Chemistry and Materials science deals with the structure and dynamics of electronic systems: atoms, molecules, solids, liquids, soft matter, etc. To describe these systems one needs the full machinery of quantum many-body theory involving fermionic and bosonic particles and excitations. So far we have been working with 2-level (spin) systems coupled to bosonic modes. However, to describe electronic systems, the fermionic anti-commutation rules have to be built in. One way to do this was invented a long time ago in the form of the the Jordan-Wigner (JW) transformation [306], working in the occupation-number representation and keeping track of parity under permutations via the the anti-commutation rules of a set of auxiliary Pauli  $\sigma$  operators embedded in the fermionic creation and annihilation operators. In this way the number of  $\sigma$  operators scales as  $O(n)$ , i.e. as the number of qubits.

Recently, Bravyi and Kitaev [307] derived an alternative (BK) transformation, using the qubits for storing parities rather than occupation numbers. This scheme also maps the fermionic operators on products of Pauli  $\sigma$  operators. One advantage, however, is that the number of  $\sigma$  operators scales as  $O(\log n)$ , which will be important for simulation of large systems that require large numbers of qubits.

These methods have been developed theoretically and simulated classically over the last 15 years [294, 308–313], but never explored experimentally, until now. The first experimental applications ever, with superconducting circuits, have recently been published, implementing digital simulation of the Fermi-Hubbard model [21] and the ground state binding curve of the hydrogen molecule,  $H_2$  [23] (see further Sect. 10.3).

For illustration of the approach to an elementary fermionic many-body system, consider a closed-shell atom or molecule, The general second-quantised Hamiltonian is given by:

$$\hat{H} = \sum_{pq} h_{pq} c_p^\dagger c_q + \frac{1}{2} \sum_{pqrs} h_{pqrs} c_p^\dagger c_q^\dagger c_r c_s \quad (90)$$

where the first term describes the single-particle kinetic+potential energy and the second term the 2-body Coulomb interaction. The indices refer to the set of basis orbitals (fermionic modes) used to expand the hamiltonian.

The simplest possible case is the ground state of a 2-electron system with a minimal basis of 2 states: a  $He$  atom with  $1s \uparrow 1s \downarrow$ , or a  $H_2$  molecule with  $1\sigma \uparrow 1\sigma \downarrow$ . The Hartree Hamiltonian is then given by:

$$\hat{H} = h_1 c_1^\dagger c_1 + h_2 c_2^\dagger c_2 + V_{12} c_1^\dagger c_1 c_2^\dagger c_2 \quad (91)$$

where the Hartree term can be written as  $V_{12} n_{1\uparrow} n_{2\downarrow}$ , on the form of a Hubbard onsite interaction (here is only one site).

The JW transformation becomes

$$c_1^\dagger = I \otimes \sigma^+ \quad (92)$$

$$c_2^\dagger = \sigma^+ \otimes \sigma_z \quad (93)$$

$$c_1 = I \otimes \sigma^- \quad (94)$$

$$c_2 = \sigma^- \otimes \sigma_z \quad (95)$$

Worked out in detail, one obtains [294]

$$c_1^\dagger c_1 = \frac{1}{2}(I - \sigma_{z1}) \quad (96)$$

$$c_2^\dagger c_2 = \frac{1}{2}(I - \sigma_{z2} \sigma_{z1}) \quad (97)$$

$$c_1^\dagger c_1 c_2^\dagger c_2 = \frac{1}{4}(I - \sigma_{z1} - \sigma_{z2} \sigma_{z1} + \sigma_{z2}) \quad (98)$$

The Hamiltonian then finally becomes [294]:

$$\hat{H} = h - h/2 (\sigma_{z1} + \sigma_{z2} \sigma_{z1}) + V/4 (1 - \sigma_{z1} + \sigma_{z2} - \sigma_{z2} \sigma_{z1}) \quad (99)$$

The evolution operator corresponding to the parts of the Hamiltonian with  $\sigma_z \otimes \sigma_z$  products,  $U = \exp[-i\frac{\theta}{2} \sigma_z \otimes \sigma_z]$  can be implemented by a quantum circuit of the form shown in Fig. 14e.

At the next level, the simplest possible case is still the ground state of a 2-electron He atom, but now with a slightly extended basis of 4 states, 1:  $1s \uparrow$ , 2:  $1s \downarrow$ , 3:  $2s \uparrow$  and 4:  $2s \downarrow$ . At this level one can begin to investigate effects of correlation on the

groundstate energy. Taking into account that in the ground state, only states 1 and 2 are occupied, the Hamiltonian can be written as:

$$\hat{H} = \hat{H}_1 + \hat{H}_2 \quad (100)$$

$$\hat{H}_1 = h_{11}c_1^\dagger c_1 + h_{22}c_2^\dagger c_2 \quad (101)$$

$$\hat{H}_2 = h_{1221}c_1^\dagger c_2^\dagger c_2 c_1 + h_{1243}(c_1^\dagger c_2^\dagger c_4 c_3 + c_3^\dagger c_4^\dagger c_2 c_1) \quad (102)$$

The interaction term can be rewritten as

$$\hat{H}_2 = V_{12}c_1^\dagger c_1 c_2^\dagger c_2 + V_{1324}(c_1^\dagger c_3 c_2^\dagger c_4 + c_3^\dagger c_1 c_4^\dagger c_2) \quad (103)$$

emphasizing the physical meaning of the terms: the first term describes the direct Coulomb interaction between the  $1s \uparrow$  and  $1s \downarrow$  electrons, while the second term describes the (radial) correlation energy generated by interacting virtual  $(1s \uparrow)^{-1}(2s \uparrow)$  and  $(1s \downarrow)^{-1}(2s \downarrow)$  electron-hole pair excitations.

The correlation term involves all four states, and therefore all four qubits. The result of applying the JW transformation then leads to the appearance of an interaction Hamiltonian of the form  $\sigma_\alpha \otimes \sigma_\beta \otimes \sigma_\gamma \otimes \sigma_\delta$ . A detailed analysis [294] shows that only the terms  $\sigma_x \sigma_x \sigma_y \sigma_y$ ,  $\sigma_y \sigma_y \sigma_x \sigma_x$ ,  $\sigma_y \sigma_x \sigma_x \sigma_y$ ,  $\sigma_x \sigma_y \sigma_y \sigma_x$  need to be considered. These can be generated by an evolution operator of the form  $U = \exp[-i\frac{\theta}{2}\sigma_z \otimes \sigma_z \otimes \sigma_z \otimes \sigma_z]$  together with suitable qubit rotations changing the computational basis. In particular, the  $\sigma_x \sigma_x \sigma_y \sigma_y$  term is implemented by a quantum circuit of the form shown in Fig. 30.

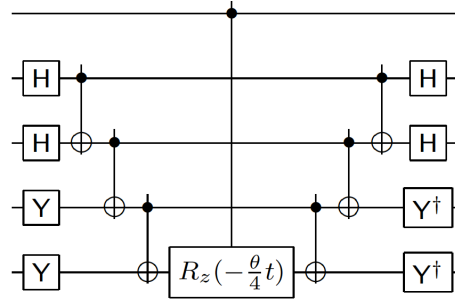


Figure 30: *Circuit implementing unitary propagation of the  $\sigma_x \otimes \sigma_x \otimes \sigma_y \otimes \sigma_y$  interaction term for the  $H_2$  (or  $He$ ) 4-state case, using the PEA to estimate the energy. The left sequence of CNOT gates detects the parity of the input state; this is followed by a PEA-controlled  $R_z$  rotation; the right sequence of CNOT gates "uncomputes" the state to make the evolution of the  $\sigma_z \otimes \sigma_z \otimes \sigma_z \otimes \sigma_z$  interaction term reversible. The single-qubit  $H$  and  $Y$  operations provide basis transformations to make the full circuit describe time evolution due to the  $\sigma_x \otimes \sigma_x \otimes \sigma_y \otimes \sigma_y$  interaction term. Adapted from [294].*

This method - the full approach with trotterisation and phase estimation - was recently applied by O'Malley *et al.* to the calculation the  $H_2$  binding energy curve, as discussed in Sect. 10

### 9.6. Analogue/adiabatic quantum simulation

In analogue quantum simulation (AQS) one induces the time evolution of a qubit register by application of a sequence of time-dependent external fields and internal interactions [33,314]. AQS has so far been implemented experimentally in ion traps [315–317], ultra-cold atoms in optical lattices [318–322] and photonics circuits [323–332], to perform simulation of various physical models involving spins, bosons and fermions.

With the advent of useful and powerful JJ-based qubit circuits, there is a recent surge of proposals involving superconducting qubits [118,333–346] as well experimental results [96,97,347–352] for superconducting circuits.

### 9.7. Digital-analogue quantum simulation

By digital-analogue quantum simulation we denote methods that control the time evolution (operator) by both (i) applying circuit-based digital gates (DQS) and (ii) evolving the Hamiltonian parameters in time (AQS). If the time scales are widely separated, e.g. the analogue evolution being adiabatic, the calculation becomes a number of complete DQS calculations for a series of adiabatic Hamiltonian time steps.

Recently a fermionic 4-mode problem was performed experimentally with a superconducting system by Barends et al. [21], implementing a scheme of Las Heras et al. [313]. The experiment involved time evolutions with constant interactions, with up to four fermionic modes encoded in four qubits, using the JordanWigner transformation. The time evolution involved in over 300 single-qubit and two-qubit gates, reaching global fidelities limited by gate errors in an intuitive error model. Barends et al. [21] also introduced time-dependence in the model Hamiltonian, by slowly ramping the hopping interaction  $V$  from zero to  $U$ , switching the system from localised to itinerant fermions, observing elements of a dynamic phase transition. The experiment, as well as that in [22], therefore may present a step on the path to creating an analogue-digital quantum simulator using discrete fermionic modes combined with discrete or continuous bosonic modes [353].

In the general case with no separation of time scales, the combined evolution needs to be implemented via the full evolution operator with time-dependent Hamiltonian, e.g. via alternating Trotter and Hamiltonian time steps. In the end combinations of analogue and digital simulation schemes may be the most powerful ones, driving or inducing selected terms in the Hamiltonian that allow sets of gates not possible in the undriven physical system.

## 10. Toward quantum chemistry simulation

Quantum chemistry is traditionally a testing ground for classical high-performance computing (HPC) [354] and currently at the focus of investigations of various advanced approximation methods in many-body physics [355–357]. The simulation of quantum chemistry is one of the most anticipated applications of quantum computing, but the scaling of known upper bounds on the complexity of these algorithms is very demanding. Hamiltonian problems with 2-body interactions have been shown to be QMA-hard [60], which means that it is fundamentally impossible to calculate the exact ground state electron structure of large molecules [61, 63–67]. This means that the quantum chemical problem of ground state energy search is non-polynomial (actually exponential) in time with respect to the system size. Consequently, like in the classical case, also quantum simulation of molecular electronic structure must build on advanced approximation schemes for full configuration interaction (FCI) to be tractable in high-accuracy calculations already for fairly small molecules.

Quantum simulation methods are now the targets of an emerging field of quantum HPC both theoretically [23, 146, 148–151, 293, 294, 300, 311, 358–374] and experimentally [23, 359, 370, 373, 375, 376]. Even if the number of gates "only" scales polynomially, the required number may still be prohibitive to reach chemical accuracy in near-future applications. However, applying the intuition of classical quantum chemistry to QS may reduce the computational complexity. A natural way forward is to depart from state-of-the-art classical approximate treatments of FCI and apply these to quantum algorithms [23, 300]. Also, it is very important to have realistic ideas of the computational effort needed for specific molecules, to be able to address cases that are tractable with present resources. Fortunately, the recent development has been quite dramatic [361]. Combined with the rapid development of superconducting multi-qubit systems, it now seems possible to go beyond toy models and implement larger-scale calculations on real hardware systems [23, 300, 359].

### 10.1. Hamiltonian ground-state energy estimation

The quantum phase estimation algorithm PEA efficiently finds the eigenvalue of a given eigenvector but requires fully coherent evolution. For large systems requiring many qubits and gate operations, the coherence time will eventually become too short. To alleviate this problem, Peruzzo et al. [359] introduced an alternative to the PEA that significantly reduces the requirements for coherent evolution. They have developed a reconfigurable quantum processing unit, which efficiently calculates the expectation value of a Hamiltonian, providing an exponential speedup over exact diagonalization, the only known exact method of solution to the problem on a traditional computer. The calculation is mainly classical but uses a quantum subroutine for exponential speedup of the critical step of quantum energy estimation. The power of the approach derives from the fact that quantum hardware can store a global quantum state with exponentially fewer resources than required by classical hardware, and as a result the QMA-hard

N-representability problem (constraining the two-electron reduced density matrix to represent an N-electron density matrix) [377] does not arise.

*10.1.1. Quantum energy estimation* The quantum energy estimation (QEE) algorithm computes the expectation value  $\langle \hat{H} \rangle = \langle \psi | \hat{H} | \psi \rangle$  of a given Hamiltonian  $\hat{H}$  with respect to a given state  $|\psi\rangle$ .

As discussed in Sect. 9, after JW or BK transformations [360] the second quantized Hamiltonian for electronic physical systems can be written in terms of Pauli operators as

$$\hat{H} = \sum_{i\alpha} h_{i\alpha} \sigma_{i\alpha} + \sum_{i\alpha, j\beta} h_{i\alpha, j\beta} \sigma_{i\alpha} \sigma_{j\beta} + \dots \quad (104)$$

with expectation value:

$$\langle \hat{H} \rangle = \sum_{i\alpha} h_{i\alpha} \langle \sigma_{i\alpha} \rangle + \sum_{i\alpha, j\beta} h_{i\alpha, j\beta} \langle \sigma_{i\alpha} \sigma_{j\beta} \rangle + \dots \quad (105)$$

The coefficients are determined using a classical quantum chemistry package.

The expectation value of a tensor product  $\langle \sigma_{i\alpha} \sigma_{j\beta} \sigma_{k\gamma} \dots \rangle$  of an arbitrary number of Pauli operators can be estimated by local measurement of each qubit. Such independent measurements can be performed in parallel, incurring a constant cost in time. The advantage of this approach is then that the coherence time to make a single measurement after preparing the state is  $O(1)$ . The disadvantage relative to the PEA is that the scaling in the total number of operations as a function of the desired precision is quadratically worse. The scaling will also reflect the number of state preparation repetitions required, whereas in PEA the number of state preparation steps is constant.

In the end, however, the QEE dramatically reduces the coherence time requirement, while maintaining an exponential advantage over the classical case by adding only a polynomial number of repetitions with respect to QPE [359].

*10.1.2. Quantum variational eigensolver* The quantum variational eigensolver (QVE) is based on the Ritz variational principle, finding the minimum of the expectation value of the Hamiltonian under variation of the trial state function: (i) prepare the trial state  $|\psi\rangle$ ; (ii) compute the Rayleigh-Ritz quotient  $\langle H_i \rangle = \langle \psi | \hat{H}_i | \psi \rangle / \langle \psi | \psi \rangle$  of all the terms in the Hamiltonian using the QEE as a subroutine; (iii) calculate  $\sum_i \langle H_i \rangle$ ; (iv) compare the resulting energy with the previous runs and feed back new parameters for the trial state. Note that the only step that is quantum is step (iii) - the other steps are prepared using a classical computer.

The issue now concerns state preparation. One example of a quantum state parameterized by a polynomial number of parameters for which there is no known efficient classical implementation is the unitary coupled cluster ansatz

$$|\psi\rangle = e^{T-T^\dagger} |\psi_{ref}\rangle \quad (106)$$

where  $|\psi_{ref}\rangle$  is some reference state, usually the Hartree Fock ground state, and  $T$  is the cluster operator for an  $N$  electron system, defined by operators

$$T = T_1 + T_2 + T_3 + \dots + T_N \quad (107)$$

producing 1, 2, 3, ...,  $N$  electron-hole pairs from the  $N$ -electron reference state. Explicitly for  $T_1$  and  $T_2$ :

$$T_1 = \sum_{pq} t_{pq} c_p^+ c_q \quad (108)$$

$$T_2 = \sum_{pqrs} t_{pqrs} c_p^+ c_q^+ c_r c_s \quad (109)$$

Obviously the series in Eqs. (108,109) generates in principle all possible configurations for FCI, producing all possible ground and excited state correlations.

In real molecules, often a limited number of these correlations produce the bulk of the interaction energy due to the Coulomb repulsion. The problem is that to achieve the accuracy needed for describing realistic molecular chemical energy surfaces and accurately predicting chemical reaction paths, a large number of small correlations are needed to build up to the final accurate result. This is QMA-hard, i.e. intractable for both classical and quantum computers. It is therefore a question of useful approximations.

In the case of the two-electron  $H_2$  and  $He-H^+$  molecules,  $N = 2$ . The cluster operators are then limited to  $T_1$  and  $T_2$  in Eq. (106) and it is possible to apply the full machinery with suitable approximations and to obtain chemical accuracy.

### 10.2. $H-H$ ground-state energy curve

We will now describe an experimental application of the QVE to the problem of the ground-state energy curve of the hydrogen molecule [23].

For a 2-electron system, the Hamiltonian reduces to

$$\hat{H} = \sum_{i\alpha} h_{i\alpha}(R) \sigma_{i\alpha} + \sum_{i\alpha, j\beta} h_{i\alpha, j\beta}(R) \sigma_{i\alpha} \sigma_{j\beta} \quad (110)$$

or equivalently

$$\hat{H} = g_0 \mathbf{1} + g_1 Z_0 + g_2 Z_1 + g_3 Z_0 Z_1 + g_4 X_0 X_1 + g_5 Y_0 Y_1 \quad (111)$$

where the set of parameters  $g_i = g_i(R)$  depends on the  $H-H$  distance and is obtained from the expectation values of the Hamiltonian terms evaluated on a classical computer using the basis (reference) states.

We discussed quantum state preparation in general in Sect. 9, and the coupled-cluster approach above. In QVE, the state  $|\psi(\theta)\rangle$  is parameterized by the action of a quantum circuit  $U(\theta)$  on an initial state  $|\psi_{ref}\rangle$ , i.e.  $|\psi(\theta)\rangle = U(\theta)|\psi_{ref}\rangle$ . Even if  $|\psi(\theta)\rangle$  is a simple product state and  $U(\theta)$  is a very shallow circuit,  $|\psi_{ref}\rangle$  can contain complex many-body correlations and span an exponential number of standard basis states.

The unitary coupled cluster approach states that the ground state of Eq. (106) can be expressed as

$$|\psi(\theta)\rangle = U(\theta)|\psi_{HF}\rangle = e^{-i\theta X_0 Y_1} |01\rangle \quad (112)$$

where  $|01\rangle$  is the Hartree-Fock (mean-field) state of molecular hydrogen in the representation of Eq. (106). The gate model circuit that performs this unitary mapping is shown in the software section of Fig. (31).

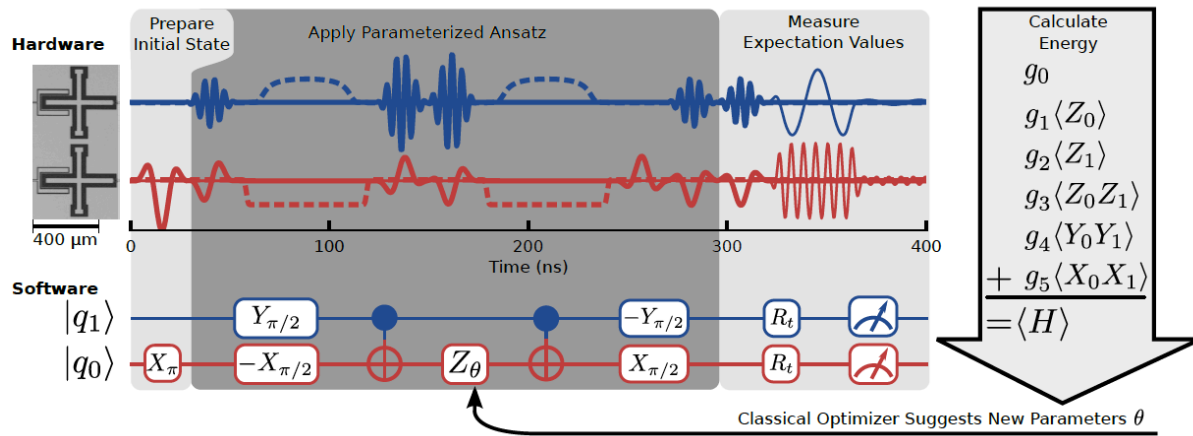


Figure 31: Schematic of the application of the quantum variational eigensolver (QVE) to the  $H_2$  ground state energy. The HW part (top panel) shows two Xmon transmon qubits and microwave pulse sequences to perform single-qubit rotations (thick lines), dc pulses for two-qubit entangling gates (dashed lines), and microwave spectroscopy tones for qubit measurements (thin lines). The SW quantum circuit diagram (bottom panel) shows preparation of the Hartree-Fock state, followed by application of the unitary coupled cluster ansatz in Eqs. 106,109 and efficient partial tomography ( $R_t$ ) to measure the expectation values in Eq. 112. Finally, the total energy is computed via the QEE protocol according to Eq. 112 and provided to a classical optimizer which suggests new parameters  $\theta$  for the time evolution operator  $U(\theta)$  (right panel). Adapted from [23].

The total energy bonding curve in Fig. (32) demonstrates chemical accuracy (better than  $10^{-3}$  hartree), which is a very important result. In contrast, the calculation using the full canonical protocol of Trotterisation plus quantum phase estimation (PEA) turns out much less accurate, amply demonstrating that the fully quantum approach is very demanding on coherence time.

### 10.3. $He-H^+$ ground-state energy curve

The QVE was originally applied to the helium-hydride cation  $He - H^+$  problem on a 2-qubit photonic processor by Peruzzo et al. [359]. Recently, Wang et al. [376] applied the IPEA to the  $He - H^+$  problem using a solid-state quantum register realised in a nitrogen-vacancy centre (NVC) in diamond, reporting an energy uncertainty (relative to

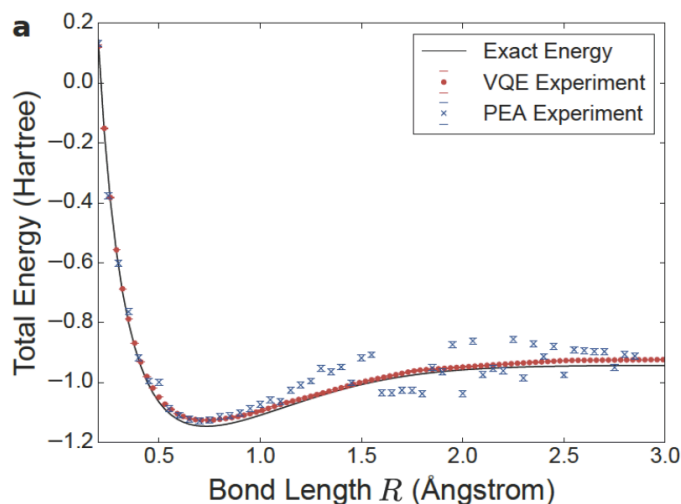


Figure 32: Total energy curve of molecular hydrogen as determined by both QVE and PEA. The QVE approach shows dissociation energy error of  $(8 \pm 5) \times 10^{-4}$  hartree (error bars on QVE data are smaller than markers). The PEA approach shows dissociation energy error of  $(1 \pm 1) \times 10^{-2}$  hartree. Adapted from [23].

the model basis) of the order of  $10^{-14}$  hartree, 10 orders of magnitude below the desired chemical precision. However, this remarkable precision only refers to the 13 iterations of the IPEA itself. The fundamental propagation of the quantum state using the time evolution operator was done on a classical computer. In a fully quantum approach Trotterisation will be necessary to create the state, which will put high demands on precision and coherence time. With present hardware systems, this will drastically reduce the accuracy, as is clear from the experimental results for  $H_2$  in Fig. 32 [23].

#### 10.4. Toward large-scale simulations

*10.4.1. From high-level language to hardware instructions* In order to assess the computational capability of even a small quantum systems for producing total-energy surfaces with chemical accuracy, it is necessary to develop simulation software all the way from high-level language programs down to hardware-specific instructions. Häner et al. [148] have recently developed a software methodology for compiling quantum programs that goes beyond the simulators that have been developed so far. The approach involves an embedded domain specific language by representing quantum types and operations through types and functions existing in a classical host language, underlining the roles of quantum computers as special purpose accelerators for existing classical codes. In the near term, a quantum software architecture will allow the control of small-scale quantum devices and enable the testing, design, and development of components on both the hardware and software side [148].

*10.4.2. Quantum computer emulation* Häner et al. [149] have introduced the concept of a quantum computer emulator as a component of a software framework for quantum computing. A QC emulator is an interface (HW or SW) that makes the user believe that she is operating a quantum computer even if the calculations are performed classically. This can enable a significant performance advantage by avoiding simulating essentially classical boolean logic by quantum gate operations. Häner et al. [149] describe various optimization approaches and present benchmarking results, establishing the superiority of quantum computer emulators in terms of performance. The results show [149] that emulating quantum programs allows to test and debug large quantum circuits at a cost that is substantially reduced when compared to the simulation approaches which have been taken so far. The advantage is already substantial for operations such as the quantum Fourier transforms, and grows to many orders of magnitude for arithmetic operations, since emulation avoids simulating ancilla qubits (needed for reversible arithmetic) at an exponential cost. Emulation will thus be a crucial tool for testing, debugging and evaluating the performance of quantum algorithms involving arithmetic operations.

*10.4.3. Electronic structure calculations - molecules* To describe the function of an enzyme from first principles is a computationally hard problem. While at present a quantitative understanding of chemical processes involving complex open-shell species remains beyond the capability of classical-computer simulations, the work of Reiher et al. [151] shows that quantum computers used as accelerators to classical computers could be used to elucidate this mechanism using a manageable amount of memory and time. In this context a quantum computer would be used to obtain, validate, or correct the energies of intermediates and transition states and thus give accurate activation energies for various transitions. In particular, Reiher et al. [151] show how a quantum computer can be employed to elucidate reaction mechanisms in complex chemical systems, using the open problem of biological nitrogen fixation in nitrogenase as an example. Detailed resource estimates show that, even when taking into account the substantial overhead of quantum error correction, and the need to compile into discrete gate sets, the necessary computations can be performed in reasonable time on small quantum computers. This demonstrates that quantum computers will realistically be able to tackle important problems in chemistry that are both scientifically and economically significant.

The required quantum computing resources are comparable to that needed for Shor's factoring algorithm for interesting numbers, both in terms of number of gates and physical qubits [151]. The complexity of these simulations is thus typical of that required for other targets for quantum computing, requiring robust qubits with long coherence time.

*10.4.4. Electronic structure of strongly correlated materials* Using a hybrid quantum-classical approach to correlated materials, Bauer et al. [150] show that by using a hybrid quantum-classical algorithm that incorporates the power of a small quantum computer

into a framework of classical embedding algorithms, the electronic structure of complex correlated materials can be efficiently tackled using a quantum computer. The quantum computer solves a small effective quantum impurity problem that is self-consistently determined via a feedback loop between the quantum and classical computation. Use of a quantum computer enables much larger and more accurate simulations than with any known classical algorithm, and will allow many open questions in quantum materials to be resolved once a small quantum computer with around one hundred logical qubits becomes available.

## 11. Adiabatic quantum optimisation

It is not known to what extent coherence and entanglement apply to AQC. (Except, since AQC has been shown to be equivalent to DQC [59], one would perhaps expect that coherence and entanglement are needed also for AQC to provide optimum processing speed).

### 11.1. Adiabatic quantum algorithms

Adiabatic quantum optimisation (AQO) is an adiabatic form of analog quantum computing/simulation [57–60, 70, 378–380]. AQO is in principle universal [59] and equivalent to the digital circuit model. AQO refers to zero temperature. In AQO one considers the time evolution  $|\psi(t)\rangle = \hat{U}(t, 0)|\psi(0)\rangle$  with a time-dependent Hamiltonian of the form:

$$\hat{H}(t) = [1 - s(t)]\hat{H}_0 + s(t)\hat{H}_T \quad (113)$$

The starting Hamiltonian  $H_0$  is given on a simple form, and the target Hamiltonian  $H_T$  is designed to encode the problem under consideration, often defined by an Ising type of Hamiltonian. One then searches for an optimal path on the ground state energy surface toward a global energy minimum representing a final solution  $|\psi(t_f)\rangle$  described by the target Hamiltonian  $H_T$  (Fig. 33).

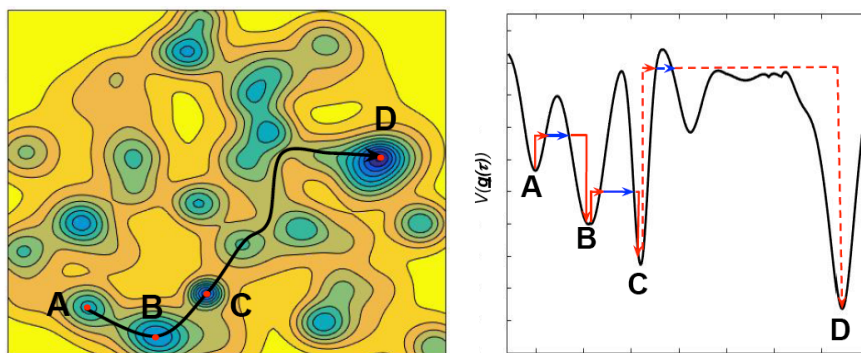


Figure 33: *Quantum adiabatic optimisation (AQO) and quantum annealing (QA).  $\hat{H}(t) = A(t)\hat{H}_0 + B(t)\hat{H}_T$ . Spin-glass (Ising) type of cost function defining the energy landscape  $H_T = \sum_{ij} a_{ij}x_i x_j + \sum_i b_i x_i$ . Adapted from Denchev et al. [89]*

The philosophy behind AQO is that a wide range of problems in science can be formulated as Ising models (see e.g. Refs. [381–388]), and therefore AQO could be a practical way to proceed toward addressing hard spin-glass type of problems with quantum computing. The vision is that gate-driven DQS will need extensive error correction and is, at best, a distant option, while AQO may be able to short-circuit that long path. However, there is seldom any free lunch - in the end calibration and embedding issues may limit the real power of AQO.

### 11.2. Quantum annealing

In Quantum Annealing (QA) the temperature of a system is lowered during the time-evolution of the Hamiltonian until the system gets trapped in an energy minimum, preferably a global minimum, but more typically a local one [87, 124, 296, 389, 390].

Quantum annealing can be looked upon in typically two ways:

- (i) As an extension of classical Simulated Annealing (SA) by including quantum tunneling in addition to thermal hopping over the barriers (Fig. 11.2) [378, 391] .
- (ii) As a version of Adiabatic QC/QS applied to real systems influenced by noise and imperfections [379] .

Traditionally, SA and QA has been performed with software running on classical machines, solving both classical and quantum problems, e.g. using quantum Monte Carlo (QMC), including descriptions of quantum tunneling [391]. Recently, however, the D-Wave machines (DW1-108 qubits; DW2-504 qubits; D-Wave 2X-1152 qubits) have been used to perform annealing in hardware. The mission is to perform QA (actually AQO!), and the goal has been to gain decisive speedup over classical machines because the hardware is intended to function as quantum circuits and to be able to profit from coherence and entanglement.

The D-Wave Systems machines are built top-down - scaling up is based on flux qubits and circuits with short coherence time [123, 124, 389]. As a result, the coherence and entanglement properties have to be investigated by performing various types of experiments on the machines and their components: Physics experiments on the hardware [123, 394], and "benchmarking" of the performance by running a range of QA schemes [87, 89, 296, 390, 392, 393, 395–399].

During the last three years, the topic has rapidly evolved, and by now a certain common understanding and consensus has been reached. Based on the discussion in some recent papers [89, 90, 400–406], the situation can be summed up in the following way:

- The behaviour of the D-Wave devices is consistent with quantum annealing
- No scaling advantage (quantum speedup) has so far been seen [406].
- QA is efficient in quickly finding good solutions as long as barriers are narrow, but ultimately gets stuck once broad barriers are encountered
- The Google D-Wave 2X results showing million-times speedup [89] are for native instances that perfectly fit the hardware graph of the device [90].
- For generic problems that do not map well onto the hardware of a QA, performance will suffer significantly [90, 406].
- Even more efficient classical optimization algorithms exist for these problems (mentioned in [89]), which outperform the current D-Wave 2X device for most problem instances [401, 403, 404].
- With improved engineering, especially faster annealing and readout, the time to perform a quantum annealing run can be reduced by a factor 100x over the current

generation devices [90].

- However, misspecification of the cost function due to calibration inaccuracies is a challenge that may hamper the performance of analog quantum annealers [90].
- Another challenge is the embedding of problems into the native hardware architecture with limited connectivity.
- There is the open question of quantum speedup in analog quantum annealing [406, 407].
- QA error correction has been demonstrated and may pave a path toward large scale noise-protected adiabatic quantum optimization devices [398, 399].
- Typically, classically computationally hard problems also seem to be hard problems for QA devices [406].
- Improved machine calibration, noise reduction, optimisation of the quantum annealing schedule, larger system sizes and tailored spin-glass problems may be needed for demonstrating quantum speedup.

## 12. Perspectives

### 12.1. Looking back

Once upon a time, 5 years ago, there was a major European flagship proposal to marry QIPC to classical high-performance computing (HPC). The effort failed, however, for a number of good reasons: (i) The classical HPC people had essentially no knowledge of what QIPC might be good for, and the QIPC side had no convincing arguments.; (ii) There was no clear and convincing focus on scalable quantum hardware and software; (iii) Solid-state circuits were still at an embryonic level, demonstrating some limited basic QIP functionality only at the 2-3 qubit level.

Since then, there has been dramatic progress in the way of superconducting devices and systems. It is now possible to build a variety of superconducting Josephson junction (JJ) multi(5-10)-qubit platforms able to seriously address proof-of-principles quantum simulations of significant interest for future Materials Science and Chemistry, as well as smaller-scale Physics problems (e.g. quantum magnetism) where classical computers already now cannot provide solutions. Moreover, D-Wave Systems now operates 1100 qubit systems for quantum annealing. One can expect these systems to develop toward better coherence. This means that there will be a range of systems and problems that can be investigated from both bottom-up and top-down points of view.

### 12.2. Looking around

The focus of the present review has so far been on superconducting devices and hybrid systems. It is now time to broaden the scope a bit and discuss the wider perspective including a number of emerging solid-state quantum technologies.

*Spins implanted in semiconductors* Originally, the solid-state approach to quantum computers was a silicon-based nuclear spin quantum computer [409]. This line of research has been very active ever since, with extensive efforts on technology for implanting spin impurities in semiconductors, in particular silicon. Presently there is great progress at the 1- and 2-qubit level [410–416] with reported qubit lifetimes up to 30 seconds [410] and robust 2-qubit gates [413]. Nevertheless, experience suggests that it may take quite some time to build multi-qubit systems. Possible routes may be on-chip coupling of implanted impurity spin arrays [417], or photonic coupling of individual spin qubits.

From a QIP point of view, however, the most advanced spin systems involve multi-qubit NV-centres in diamond [418,419], with demonstrations of quantum error correction (QEC) [281] and digital quantum simulation (DQS) [376]. There are also advanced plans for large-scale QIP in diamond [420].

*Interfaces and networks* In the future Quantum Internet [243,421] interfaces between stationary qubits and photons will be critically important. Such interfaces involve

the entanglement of qubits with single-photon emitters [422] and are typically based on semiconductor quantum dots [423, 424] or NV-centres [423, 425]. Important experimental steps toward large-scale quantum networks have recently been taken through demonstrations of loophole-free Bell tests [426, 427], quantum network memory [428], perfect state transfer of an entangled photonic qubit [429], and digital photonic QIP [430–432].

*Sensors* The future ultimate sensor may be a quantum computer at the tip of a scanning probe - "SPQ" - where e.g. the measured dephasing of the quantum device provides the information. Presently the quantum device is typically a diamond nanocrystal with an NV centre working as an advanced NMR probe with a built-in quantum pre-processor (see e.g. [433–437] and refs. therein).

### 12.3. Looking ahead

The field of experimental and applied quantum information processing with superconducting Josephson junction-based circuits and systems is now preparing for scaling up to levels of Quantum Supremacy. Within a few years there will be well-controlled coherent platforms with 20-30 qubits addressing a range of algorithms and benchmarking protocols, comparing favourably against the best classical systems and algorithms. And in view of the commitments of various groups around the world, in 5-7 years there will most likely be coherent functional 100 qubit devices claiming Quantum Supremacy.

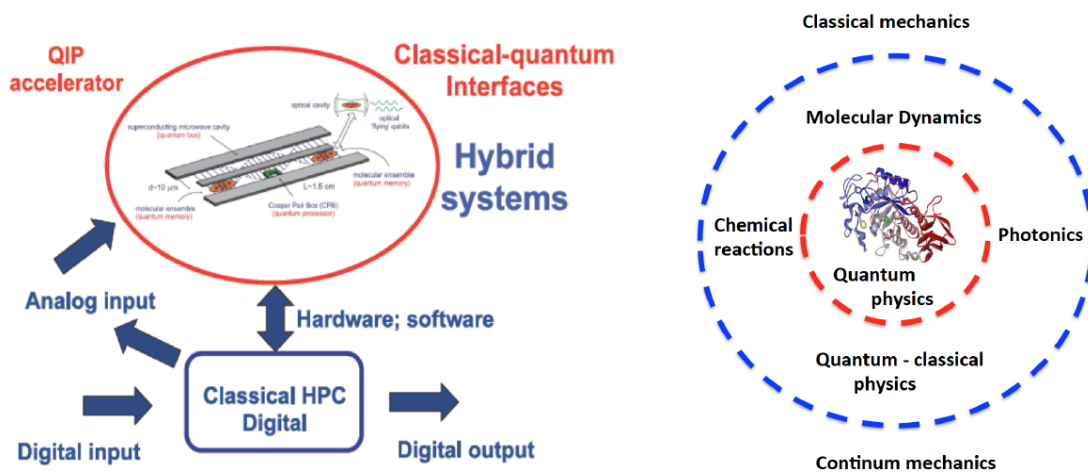


Figure 34: *Two pictures of embedding a quantum system in a classical environment: Left: A quantum accelerator embedded in a classical computer; Right: A physical quantum system embedded in a physical classical matrix.*

In parallel, there is intense work on scaling up *microfabricated ion traps* [438, 439], with applications to benchmarking [440], computing [441–443] and simulation.

[444, 445]. The NIST simulation [445] involves up to 219 ions (qubits) with global control, simulating spin-dynamics in a classically tractable 2D Ising model, laying the groundwork for the classically hard case of the transverse Ising model with variable range interactions.

On the really new side, after the initial experiments showing evidence for Majorana fermions in hybrid superconductor-semiconductor nanowire devices [446], *topological quantum computing* [447] is heading for experimental implementations [448, 449].

Quantum computing, emulation and simulation have finally become serious endeavours at a practical level, to present approximate solutions to hard problems with quantum speedup. Figure 34 presents a personal way to look at it in terms of multi-scale modelling [450], embedding quantum problems in a classical environment to make the full problem (more) tractable, only involving the quantum solver when the physics is manifestly quantum. This is the way Biology and Life works, so it looks like a good idea.

## References

- [1] J. Preskill, Quantum computing and the entanglement frontier, arXiv:1203.5813v3.
- [2] S. Boixo, S. V. Isakov, V. N. Smelyanskiy, R. Babbush, N. Ding, Z. Jiang, J. M. Martinis, and Hartmut Neven, Characterizing Quantum Supremacy in Near-Term Devices, arXiv:1608.00263v1.
- [3] P. W. Shor, Polynomial-Time Algorithms for Prime Factorization and Discrete Logarithms on a Quantum Computer, *SIAM J. Comput.* **26** (5): 1484-1509 (1997); arXiv:quant-ph/9508027v2.
- [4] P. Neumann, I. Jakobi, F. Dolde, C. Burk, R. Reuter, G. Waldherr, J. Honert, T. Wolf, A. Brunner, J. H. Shim, D. Suter, H. Sumiy, J. Isoya, and J. Wrachtrup, High-Precision Nanoscale Temperature Sensing Using Single Defects in Diamond, *Nano Lett.* **13**, 2738-2742 (2013).
- [5] A. Bienfait, J. J. Pla, Y. Kubo, M. Stern, X. Zhou, C. C. Lo, C. D. Weis, T. Schenkel, M. L. W. Thewalt, D. Vion, D. Esteve, B. Julsgaard, K. Mølmer, J. J. L. Morton and P. Bertet, Reaching the quantum limit of sensitivity in electron spin resonance, *Nature Nanotechnology* **11**, 253 (2016).
- [6] A. Bienfait, J. J. Pla, Y. Kubo, X. Zhou, M. Stern, C. C. Lo, C. D. Weis, T. Schenkel, D. Vion, D. Esteve, J. J. L. Morton and P. Bertet, Controlling spin relaxation with a cavity, *Nature* **531**, 74 (2016).
- [7] H. Eikmans, J.E. van Himbergen, H.S.J. van der Zant, K. de Boer and J.E. Mooij, Experiments and simulations on Josephson junction ladder arrays, *Physica B* **165&166**, 1569-1570 (1990).
- [8] Yu. Makhlin, G. Schön, and A. Shnirman, Josephson junction qubits with controlled couplings, *Nature* **398**, 305 (1999).
- [9] Yu. Makhlin, G. Schön, and A. Shnirman, Quantum State Engineering with Josephson-Junction Devices, *Rev. Mod. Phys.* **73**, 357 (2001).
- [10] Y. Nakamura, Yu. Pashkin and J.S. Tsai, Coherent control of macroscopic quantum states in a single-Cooperpair box, *Nature* **398**, 786 (1999).
- [11] A. Wallraff, D. I. Schuster, A. Blais, L. Frunzio, R.-S. Huang, J. Majer, S. Kumar, S. M. Girvin and R. J. Schoelkopf, Strong coupling of a single photon to a superconducting qubit using circuit quantum electrodynamics, *Nature (London)* **431**, 162 (2004).
- [12] A. Blais, R.-S. Huang, A. Wallraff, S. M. Girvin, and R. J. Schoelkopf, Cavity quantum electrodynamics for superconducting electrical circuits: An architecture for quantum computation, *Phys. Rev. A* **69**, 062320 (2004).
- [13] J. Koch, T.M. Yu, J.M. Gambetta, A.A. Houck, D.I Schuster, J. Majer, A. Blais, M.H. Devoret, S.M. Girvin, and R.J. Schoelkopf, Charge Insensitive Qubit Design from Optimizing the Cooper-Pair Box, *Phys. Rev. A* **76**, 042319 (2007).
- [14] H. Paik, D.I. Schuster, L.S. Bishop, G. Kirchmair, G. Catelani, A. P. Sears, B.R. Johnson, M.J. Reagor, L. Frunzio, L.I. Glazman, S.M. Girvin, M.H. Devoret, and R.J. Schoelkopf, Observation of High Coherence in Josephson Junction Qubits Measured in a Three-Dimensional Circuit QED Architecture, *Phys. Rev. Lett.* **107**, 240501 (2011).
- [15] J. M. Chow, J.M. Gambetta, E. Magesan, D.W. Abraham, A.W. Cross, B.R. Johnson, N.A. Masluk, C.A. Ryan, J.A. Smolin, S.J. Srinivasan and M. Steffen, Implementing a strand of a scalable fault-tolerant quantum computing fabric, *Nature Commun* **5**, 4015 (2014).
- [16] A. D. Corcoles, E. Magesan, S. J. Srinivasan, A. W. Cross, M. Steffen, J. M. Gambetta, and J.M. Chow, Detecting arbitrary quantum errors via stabilizer measurements on a sublattice of the surface code, *Nature Comm.* **6**: 6979 (2015).
- [17] R. Barends, J. Kelly, A. Megrant, A. Veitia, D. Sank, E. Jeffrey, T. C. White, J. Mutus, A. G. Fowler, B. Campbell, Y. Chen, Z. Chen, B. Chiaro, A. Dunsworth, C. Neill, P. O'Malley, P. Roushan, A. Vainsencher, J. Wenner, A. N. Korotkov, A. N. Cleland, John M. Martinis, Superconducting quantum circuits at the surface code threshold for fault tolerance, *Nature* **508**, 500-503 (2014).
- [18] O.-P. Saira, J. P. Groen, J. Cramer, M. Meretska, G. de Lange, and L. DiCarlo, Entanglement

- Genesis by Ancilla-Based Parity Measurement in 2D Circuit QED, *Phys. Rev. Lett.* **112**, 070502 (2014).
- [19] D. Riste, S. Poletto, M.-Z. Huang, A. Bruno, V. Vesterinen, O.-P. Saira, and L. DiCarlo, Detecting bit-flip errors in a logical qubit using stabilizer measurements, *Nature Comm.* **6**: 6983 (2015).
- [20] J. Kelly, R. Barends, A. G. Fowler, A. Megrant, E. Jeffrey, T. C. White, D. Sank, J. Y. Mutus, B. Campbell, Yu Chen, Z. Chen, B. Chiaro, A. Dunsworth, I.-C. Hoi, C. Neill, P. J. J. O'Malley, C. Quintana, P. Roushan, A. Vainsencher, J. Wenner, A. N. Cleland, and J. M. Martinis, State preservation by repetitive error detection in a superconducting quantum circuit, *Nature* **519**, 66 (2015).
- [21] R. Barends, L. Lamata, J. Kelly, L. Garca-lvarez, A. G. Fowler, A. Megrant, E. Jeffrey, T. C. White, D. Sank, J. Y. Mutus, B. Campbell, Yu Chen, Z. Chen, B. Chiaro, A. Dunsworth, I.-C. Hoi, C. Neill, P. J. J. O'Malley, C. Quintana, P. Roushan, A. Vainsencher, J. Wenner, E. Solano, and John M. Martinis, Digital quantum simulation of fermionic models with a superconducting circuit, *Nature Commun.* **6**, 7654 (2015).
- [22] R. Barends, A. Shabani, L. Lamata, J. Kelly, A. Mezzacapo, U. Las Heras, R. Babbush, A. G. Fowler, B. Campbell, Y. Chen, Z. Chen, B. Chiaro, A. Dunsworth, E. Jeffrey, E. Lucero, A. Megrant, J. Y. Mutus, M. Neeley, C. Neill, P. J. J. O'Malley, C. Quintana, P. Roushan, D. Sank, A. Vainsencher, J. Wenner, T. C. White, E. Solano, H. Neven, and John M. Martinis, Digitized adiabatic quantum computing with a superconducting circuit, *Nature* **534**, 222 (2016).
- [23] P. J. J. O'Malley, R. Babbush, I. D. Kivlichan, J. Romero, J. R. McClean, R. Barends, J. Kelly, P. Roushan, A. Tranter, N. Ding, B. Campbell, Y. Chen, Z. Chen, B. Chiaro, A. Dunsworth, A. G. Fowler, E. Jeffrey, A. Megrant, J. Y. Mutus, C. Neill, C. Quintana, D. Sank, A. Vainsencher, J. Wenner, T. C. White, P. V. Coveney, P. J. Love, H. Neven, A. Aspuru-Guzik, and J. M. Martinis, Scalable Quantum Simulation of Molecular Energies, *Phys. Rev. X* **6**, 031007 (2016).
- [24] S. Asaad, C. Dickel, S. Poletto, A. Bruno, N. K. Langford, M. A. Rol, D. Deurloo, and L. DiCarlo, Independent, extensible control of same-frequency superconducting qubits by selective broadcasting, *NPJ Quantum Information* **2**, 16029 (2016).
- [25] R. J. Schoelkopf and S. M. Girvin, Wiring up quantum systems, *Nature* **451**, 664 (2008).
- [26] J. Clarke and F.K. Wilhelm, Superconducting quantum bits, *Nature* **453**, 1033 (2008).
- [27] Nature Insight: Quantum coherence, *Nature* **453**, 1003-1049 (2008).
- [28] Thaddeus D. Ladd, Fedor Jelezko, Raymond Laflamme, Yasunobu Nakamura, Christopher Monroe, Jeremy L. O'Brien, Quantum Computing, *Nature* **464**, 45-53 (2010).
- [29] I. Siddiqi, Superconducting qubits: poised for computing?, *Supercond. Sci. Technol.* **24**, 091002 (2011).
- [30] Proceedings of the 2011 Les Houches Summer School on Quantum Machines, eds. M.H. Devoret, R.J. Schoelkopf and B. Huard (Oxford University Press, 2014).
- [31] M. H. Devoret and R. J. Schoelkopf, Superconducting Circuits for Quantum Information: An Outlook, *Science* **339**, 1169 (2013).
- [32] J. I. Cirac and P. Zoller, Goals and opportunities in quantum simulation, *Nature Phys.* **8**, 264-266 (2010).
- [33] K. L. Brown, W. J. Munro, V. M. Kendon, Using Quantum Computers for Quantum Simulation, *Entropy* **12**, 2268-2307 (2010).
- [34] J. T. Barreiro, M. Muller, P. Schindler, D. Nigg, T. Monz, M. Chwalla, M. Hennrich, C. F. Roos, P. Zoller and R. Blatt, An open-system quantum simulator with trapped ions, *Nature* **470**, 486-491 (2011).
- [35] R. Blatt and C. F. Roos, Quantum simulations with trapped ions, *Nature Phys.* **8**, 277 (2012).
- [36] I. M. Georgescu, S. Ashhab, and Franco Nori, Quantum simulation, *Rev. Mod. Phys.* **86**, 153 (2014).
- [37] M. A. Nielsen and I. L. Chuang, Quantum Computation and Quantum Information (Cambridge Univ. Press, Cambridge, 2nd Edition, 2010).
- [38] G. Wendin and V.S. Shumeiko, Quantum Bits with Josephson Junctions, *Low Temp. Phys.* **33**,

- 724 (2007).
- [39] S. M. Girvin, Circuit QED: Superconducting Qubits Coupled to Microwave Photons, in Proceedings of the 2011 Les Houches Summer School on Quantum Machines, eds. M.H. Devoret, R.J. Schoelkopf and B. Huard (Oxford University Press, 2014).
  - [40] J. Watrous, Quantum Computational Complexity, Encyclopedia of Complexity and System Science, Springer, 2009; arXiv: 0804.340.
  - [41] [https://complexityzoo.uwaterloo.ca/Complexity\\_Zoo](https://complexityzoo.uwaterloo.ca/Complexity_Zoo)
  - [42] A. Montanaro, Quantum algorithms: an overview, npj Quantum Information **2**, 15023 (2016).
  - [43] L. M. Adleman, Molecular computation of solutions to combinatorial problems, Science **266**, 1021 (1994).
  - [44] R. J. Lipton, DNA Solution of Hard Computational Problems, Science **268**, 542 (1995).
  - [45] H. Siegelmann, Computation beyond the Turing limit, Science **238**, 632-637 (1995).
  - [46] B. J. Copeland and O. Shagrir, Do accelerating Turing machines compute the uncomputable?, Minds and Machines **21**, 221 (2011).
  - [47] J. Cabessa, and H. T. Siegelmann, Evolving recurrent neural networks are super-Turing, International Joint Conference on Neural Networks (IJCNN), pp. 3200 - 3206 (2011).
  - [48] F. Manea, V. Mitrană, All NP-problems can be solved in polynomial time by accepting hybrid networks of evolutionary processors of constant size, Information Processing Letters **103**, 112 (2007).
  - [49] F. L. Traversa, C. Ramella, F. Bonani, and M. Di Ventra, Memcomputing NP-complete problems in polynomial time using polynomial resources and collective states, Science Advances **1**, e150003103 (2015).
  - [50] F. L. Traversa, and M. Di Ventra, Polynomial-time solution of prime factorization and NP-hard problems with digital memcomputing machines; arXiv:1512.05064.
  - [51] A. Vergis, K. Steiglitz, and B. Dickinson, The complexity of analog computation, Mathematics & Computers in Simulation **28**, 91-113 (1986).
  - [52] S. Aaronson, NP-complete Problems and Physical Reality, ACM SIGACT News, Complexity Theory Column **36**(1), 30-52 (2005).
  - [53] S. Aaronson, The Limits of Quantum Computers, Scientific American **298**, 62 (2008).
  - [54] S. Aaronson, Why Philosophers Should Care About Computational Complexity, In Computability: Gödel, Turing, Church, and beyond (eds. Copeland, B.; Posy, C.; Shagrir, O.) (2013).
  - [55] Richard P. Feynman, Simulating Physics with Computers, Int. J. Theor. Phys. **21**, 467 (1982).
  - [56] A. Barenco, C. H. Bennett, R. Cleve, D. P. DiVincenzo, N. Margolus, P. Shor, T. Sleator, J. A. Smolin, and H. Weinfurter, Elementary gates for quantum computation. Phys. Rev. A **52**, 3457 (1995).
  - [57] E. Farhi, J. Goldstone, S. Gutmann, and M. Sipser, Quantum computation by adiabatic evolution (2000); arXiv:quant-ph/0001106.
  - [58] E. Farhi, J. Goldstone, S. Gutmann, J. Lapan, A. Lundgren, and D. Preda, A Quantum Adiabatic Evolution Algorithm Applied to Random Instances of an NP-Complete Problem, Science **292**, 472 (2001).
  - [59] D. Aharonov, W. Van Dam, J. Kempe, Z. Landau, S. Lloyd, and O. Regev, Adiabatic Quantum Computation is Equivalent to Standard Quantum Computation, Proceedings 45th Annual IEEE Symposium on Foundations of Computer Science, 2004, pp. 42-51; arXiv:quant-ph/0405098.
  - [60] J. Kempe, A. Kitaev, O. Regev, The Complexity of the Local Hamiltonian Problem, SIAM J. Comput. **35**(5), 1070-1097 (2006).
  - [61] T. J. Osborne, Hamiltonian complexity, Rep. Prog. Phys. **75**, 022001 (2012).
  - [62] S. Gharibian, Y. Huang, Z. Landau, S. W. Shinz, Quantum Hamiltonian Complexity, Foundations and Trends in Theoretical Computer Science **10**(3), 159-282 (2015); arXiv:1401.3916v4.
  - [63] V. A. Rassolov and S. Garashchuk, Computational complexity in quantum chemistry, Chemical Physics Letters **464**, 262 (2008).
  - [64] N. Schuch and F. Verstraete, Computational complexity of interacting electrons and fundamental

- limitations of density functional theory, *Nature Physics* **5**, 732-735 (2009).
- [65] S. Aaronson, Computational complexity: Why quantum chemistry is hard, *News and Views: Nature Physics* **5**, 707-708 (2009).
- [66] J. D. Whitfield, P. J. Love, A. Aspuru-Guzik, Computational complexity in electronic structure, *Physical Chemistry Chemical Physics* **15**, 397-411 (2013).
- [67] J. D. Whitfield, M.-H. Yung, D. Tempel, S. Boxio, A. Aspuru-Guzik, Computational complexity of Time dependent Density Functional Theory, *New J. Phys.* **16**, 083035 (2014).
- [68] J. D. Whitfield and Z. Zimboras, On the NP-completeness of the Hartree-Fock method for translationally invariant systems, *J. Chem. Phys.* **141**, 234103 (2014).
- [69] D. Gosset and D. Nagaj, Quantum 3-SAT is QMA1-complete, 2013 IEEE 54TH annual symposium on Foundations of Computer Science (FOCS 2013), 756-765 (2013); arXiv:1302.0290v1.
- [70] E. Farhi, J. Goldstone, and S. Gutmann, A quantum approximate optimization algorithm (2014); arXiv:1411.4028.
- [71] G. Viglietta, Gaming is a hard job, but someone has to do it!, *Theory Comput. Syst.* **54**, 595 (2014); arXiv:1201.4995v5.
- [72] G. Aloupis, E. D. Demainey, A. Guo, and G. Viglietta, Classic Nintendo Games are (Computationally) Hard (2012). In: A. Ferro, F. Luccio, P. Widmayer, (eds.), FUN 2014, LNCS, vol. 8496, pp. 40-51; Springer, Heidelberg (2014); arXiv:1203.1895v3.
- [73] F. Verstraete, Worth the wait, *Nature Phys.* **11**, 524-525 (2015).
- [74] Z. Landau, U. Vazirani, and T. Vidick, A polynomial time algorithm for the ground state of one-dimensional gapped local Hamiltonians, *Nature Phys.* **11**, 566-569 (2015).
- [75] R. Jozsa and N. Linden, On the role of entanglement in quantum-computational speed-up, *Proc. R. Soc. Lond. A* **459**, 2011-2032 (2003).
- [76] R. Horodecki, P. Horodecki, M. Horodecki, and K. Horodecki, Quantum entanglement, *Rev. Mod. Phys.* **81**, 865 (2009).
- [77] N. Gisin, *Quantum Chance: Nonlocality, Teleportation and Other Quantum Marvels*, Copernicus/Springer, DOI: 10.1007/978-3-319-05473-5
- [78] Y. Huang, Computing quantum discord is NP-complete, *New Journal of Physics* **16**, 033027 (2014).
- [79] W. K. Wootters, Entanglement of formation and concurrence, *Quant. Inform. Comput.* **1**, 27-44 (2001).
- [80] J. Eisert, M. Cramer, and M. B. Plenio, Colloquium: Area laws for the entanglement entropy, *Rev. Mod. Phys.* **82**, 277 (2010).
- [81] C. Eltschka and J. Siewert, Quantifying entanglement resources, *J. Phys. A: Math. Theor.* **47**, 424005 (2014).
- [82] D. Girolami, A. M. Souza, V. Giovannetti, T. Tufarelli, J. G. Filgueiras, R. S. Sarthour, D. O. Soares-Pinto, I. S. Oliveira, and G. Adesso, Quantum Discord Determines the Interferometric Power of Quantum States, *Phys. Rev. Lett.* **112**, 210401 (2014).
- [83] Z. Xi, Y. Li, and H. Fan, Quantum coherence and correlations in quantum system, *Scientific Reports* **5**: 10922 (2015).
- [84] J. Ma, B. Yadin, D. Girolami, V. Vedral, and M. Gu, Converting Coherence to Quantum Correlations, *Phys. Rev. Lett.* **116**, 160407 (2016).
- [85] H. Ollivier and W. H. Zurek, Quantum Discord: A Measure of the Quantumness of Correlations, *Phys. Rev. Lett.* **88** 017901 (2002).
- [86] A. Dewes, R. Lauro, F. R. Ong, V. Schmitt, P. Milman, P. Bertet, D. Vion, and D. Esteve, Quantum speeding-up of computation demonstrated in a superconducting two-qubit processor, *Phys. Rev. B* **85**, 140503(R) (2012).
- [87] T. F. Rønnow, Z. Wang, J. Job, S. Boixo, S. V. Isakov, D. Wecker, J. M. Martinis, D. A. Lidar, and M. Troyer, Defining and detecting quantum speedup, *Science* **334**, 420 (2014).
- [88] D S. Steiger, T. F. Rnnow, and M. Troyer, Heavy tails in the distribution of time-to-solution for classical and quantum annealing, *Phys. Rev. Lett.* **115**, 230501 (2015).
- [89] V. S. Denchev, S. Boixo, S. V. Isakov, N. Ding, R. Babbush, V. Smelyanskiy, J. Martinis, and H.

- Neven, What is the Computational Value of Finite Range Tunneling?, *Phys. Rev. X* **6**, 031015 (2016).
- [90] I. Zintchenko, E. Brown, and M. Troyer, Recent developments in quantum annealing, December 7, 2015 <http://www.scottaaronson.com/troyer.pdf>
- [91] D.P. DiVincenzo, Topics in Quantum Computers. In: Mesoscopic Electron Transport, L. Kowenhoven, G. Schoen and L. Sohn (eds.), NATO ASI Series E, Kluwer Ac. Publ., Dordrecht, 1996; arXiv:cond-mat/9612126v2
- [92] D.P. DiVincenzo, The physical implementation of quantum computation, *Fortschritte der Physik* **48**, 771 (2000).
- [93] John M. Martinis, S. Nam, J. Aumentado, C. Urbina, Rabi Oscillations in a Large Josephson-Junction Qubit. *Phys. Rev. Lett.* **89**, 117901 (2002).
- [94] M. Ansmann, H. Wang, R. C. Bialczak, M. Hofheinz, E. Lucero, M. Neeley, A. D. O’Connell, D. Sank, M. Weides, J. Wenner, A. N. Cleland, J. M. Martinis, Violation of Bell’s inequality in Josephson phase qubits, *Nature* **461**, 504 (2009).
- [95] R. Barends, J. Kelly, A. Veitia, A. Megrant, A. G. Fowler, B. Campbell, Y. Chen, Z. Chen, B. Chiaro, A. Dunsworth, I.-C. Hoi, E. Jeffrey, C. Neill, P. J. J. O’Malley, J. Mutus, C. Quintana, P. Roushan, D. Sank, J. Wenner, T. C. White, A. N. Korotkov, A. N. Cleland, John M. Martinis, Rolling quantum dice with a superconducting qubit, *PRA* **90**, 030303(R) (2014).
- [96] Y. Chen, P. Roushan, D. Sank, C. Neill, Erik Lucero, Matteo Mariantoni, R. Barends, B. Chiaro, J. Kelly, A. Megrant, J. Y. Mutus, P. J. J. O’Malley, A. Vainsencher, J. Wenner, T. C. White, Yi Yin, A. N. Cleland, John M. Martinis, Emulating weak localization using a solid-state quantum circuits, *Nature Commun.* **5**, 5184 (2014).
- [97] P. Roushan, C. Neill, Yu Chen, M. Kolodrubetz, C. Quintana, N. Leung, M. Fang, R. Barends, B. Campbell, Z. Chen, B. Chiaro, A. Dunsworth, E. Jeffrey, J. Kelly, A. Megrant, J. Mutus, P. O’Malley, D. Sank, A. Vainsencher, J. Wenner, T. White, A. Polkovnikov, A. N. Cleland, J. M. Martinis, Observation of topological transitions in interacting quantum circuits, *Nature* **515**, 241 (2014).
- [98] M. Mariantoni, H. Wang, T. Yamamoto, M. Neeley, R. C. Bialczak, Y. Chen, M. Lenander, E. Lucero, A. D. O’Connell, D. Sank, M. Weides, J. Wenner, Y. Yin, J. Zhao, A. N. Korotkov, A. N. Cleland, and J. M. Martinis, Implementing the Quantum von Neumann Architecture with Superconducting Circuits, *Science* **334**, 61 (2011).
- [99] E. Lucero, R. Barends, Y. Chen, J. Kelly, M. Mariantoni, A. Megrant, P. O’Malley, D. Sank, A. Vainsencher, J. Wenner, T. White, Y. Yin, A. N. Cleland, J. M. Martinis, Computing prime factors with a Josephson phase qubit quantum processor, *Nature Phys.* **8**, 719-723 (2012).
- [100] D. Vion, A. Aassime, A. Cottet, P. Joyez, H. Pothier, C. Urbina, D. Esteve, M. H. Devoret, Manipulating the Quantum State of an Electrical Circuit, *Science* **296**, 886 (2002).
- [101] A. Cottet, Ph.D. thesis, Université Paris VI, 2002.
- [102] E. Collin, G. Ithier, A. Aassime, P. Joyez, D. Vion, and D. Esteve, NMR-like Control of a Quantum Bit Superconducting Circuit, *Phys. Rev. Lett.* **93**, 157005 (2004).
- [103] R. Barends, J. Kelly, A. Megrant, D. Sank, E. Jeffrey, Y. Chen, Y. Yin, B. Chiaro, J. Mutus, C. Neill, P. O’Malley, P. Roushan, J. Wenner, T. C. White, A. N. Cleland, and John M. Martinis, Coherent Josephson Qubit Suitable for Scalable Quantum Integrated Circuits, *Phys. Rev. Lett.* **111**, 080502 (2013).
- [104] J. M. Martinis and A. Megrant, UCSB final report for the CSQ program: Review of decoherence and materials physics for superconducting qubits, arXiv:1410.5793v1.
- [105] Y. Chen, C. Neill, P. Roushan, N. Leung, M. Fang, R. Barends, J. Kelly, B. Campbell, Z. Chen, B. Chiaro, A. Dunsworth, E. Jeffrey, A. Megrant, J. Y. Mutus, P. J. J. O’Malley, C. M. Quintana, D. Sank, A. Vainsencher, J. Wenner, T. C. White, Michael R. Geller, A. N. Cleland, J. M. Martinis, Qubit architecture with high coherence and fast tunable coupling, *Phys. Rev. Lett.* **113**, 220502 (2014).
- [106] T. W. Larsen, K. D. Petersson, F. Kuemmeth, T. S. Jespersen, P. Krogstrup, J. Nygard, C.

- M. Marcus, A Semiconductor Nanowire-Based Superconducting Qubit, *Phys. Rev. Lett.* **115**, 127001 (2015).
- [107] L. Casparis, T. W. Larsen, M. S. Olsen, F. Kuemmeth, P. Krogstrup, J. Nygrd, K. D. Petersson, C. M. Marcus, Gatemon Benchmarking and Two-Qubit Operation, *Phys. Rev. Lett.* **116**, 150505 (2016).
- [108] V. E. Manucharyan, J. Koch, L. I. Glazman, M. H. Devoret, Fluxonium: Single Cooper-Pair Circuit Free of Charge Offsets, *Science* **326**, 113 (2009).
- [109] I. M. Pop, K. Geerlings, G. Catelani, R. J. Schoelkopf, L. I. Glazman and M. H. Devoret, Coherent suppression of electromagnetic dissipation due to superconducting quasiparticles, *Nature* **508**, 369 (2014).
- [110] J. E. Mooij, T. P. Orlando, L. Levitov, L. Tian, C. H. van der Wal, and S. Lloyd, *Science* **285**, 1036 (1999).
- [111] C.H. van der Wal, A. C. J. ter Haar, F. K. Wilhelm, R. N. Schouten, C. J. P. M. Harmans, T. P. Orlando, S Lloyd, and J. E. Mooij, *Science* **290**, 773 (2000).
- [112] I. Chiorescu, Y. Nakamura, C. J. P. M. Harmans, and J. E. Mooij, Coherent Quantum Dynamics of a Superconducting Flux Qubit, *Science* **299**, 1869 (2003).
- [113] T. Niemczyk, F. Deppe, H. Huebl, E. P. Menzel, F. Hocke, M. J. Schwarz, J. J. Garcia-Ripoll, D. Zueco, T. Hmmer, E. Solano, A. Marx, R. Gross. Circuit quantum electrodynamics in the ultrastrong-coupling regime, *Nature Phys.* **6**, 772-776 (2010).
- [114] E. P. Menzel, R. Di Candia, F. Deppe, P. Eder, L. Zhong, M. Ihmig, M. Haeberlein, A. Baust, E. Hoffmann, D. Ballester, K. Inomata, T. Yamamoto, Y. Nakamura, E. Solano, A. Marx, R. Gross. Path Entanglement of Continuous-Variable Quantum Microwaves, *Phys. Rev. Lett.* **109**, 250502 (2012).
- [115] L. Zhong, E. P. Menzel, R. Di Candia, P. Eder, M. Ihmig, A. Baust, M. Haeberlein, E. Hoffmann, K. Inomata, T. Yamamoto, Y. Nakamura, E. Solano, F. Deppe, A. Marx, R. Gross. Squeezing with a flux-driven Josephson parametric amplifier. *New. J. of Phys.* **15**, 125013 (2013).
- [116] M. Haeberlein, F. Deppe, A. Kurcz, J. Goetz, A. Baust, P. Eder, K. Fedorov, M. Fischer, E. P. Menzel, M. J. Schwarz, F. Wulschner, E. Xie, L. Zhong, E. Solano, A. Marx, J.-J. Garcia-Ripoll, and R. Gross, Spin-boson model with an engineered reservoir in circuit quantum electrodynamics, arXiv: 1506.09114v1.
- [117] M. Jerger, S. Poletto, P. Macha, U. Hübner, E. Ilichev, and A. V. Ustinov, Frequency division multiplexing readout and simultaneous manipulation of an array of flux qubits, *Appl. Phys. Lett.* **101**, 042604 (2012)
- [118] P. Macha, G. Oelsner, J.-M. Reiner, M. Marthaler, S. Andr, G. Schön, U. Hübner, H.-G. Meyer, E. Ilichev and A. V. Ustinov, Implementation of a quantum metamaterial using superconducting qubits, *Nature Commun.* **5**, 5146 (2014).
- [119] K. Kakuyanagi, Y. Matsuzaki, C. Deprez, H. Toida, K. Semba, H. Yamaguchi, W. J. Munro and S. Saito, Observation of collective coupling between an engineered ensemble of macroscopic artificial atoms and a superconducting resonator, (2016); arXiv:1606.04222 .
- [120] M. Stern, G. Catelani, Y. Kubo, C. Grezes, A. Bienfait, D. Vion, D. Esteve, and P. Bertet, Flux-qubits with long coherence times for hybrid quantum circuits, *Phys. Rev. Lett.* **113**, 123601 (2014).
- [121] M. Steffen, S. Kumar, D. P. DiVincenzo, J. R. Rozen, G. A. Keefe, M. B. Rothwell, and M. B. Ketchen, High-Coherence Hybrid Superconducting Qubit, *Phys. Rev. Lett.* **105**, 100502 (2010).
- [122] F. Yan, S. Gustavsson, A. Kamal, J. Birenbaum, A.P. Sears, D. Hover, T.J. Gudmundsen, J.L. Yoder, T.P. Orlando, J. Clarke, A.J. Kerman, and W.D. Oliver, The Flux Qubit Revisited, arXiv:1508.06299
- [123] R. Harris, M. W. Johnson, T. Lanting, A. J. Berkley, J. Johansson, P. Bunyk, E. Tolkacheva, E. Ladizinsky, N. Ladizinsky, T. Oh, F. Cioata, I. Perminov, P. Spear, C. Enderud, C. Rich, S. Uchaikin, M. C. Thom, E. M. Chapple, J. Wang, B. Wilson, M. H. S. Amin, N. Dickson, K. Karimi, B. Macready, C. J. S. Truncik, and G. Rose, Experimental investigation of an eight-qubit

- unit cell in a superconducting optimization processor, *Phys. Rev. B* **82**, 024511 (2010).
- [124] P. I. Bunyk, E. Hoskinson, M. W. Johnson, E. Tolkacheva, F. Altomare, A. J. Berkley, R. Harris, J. P. Hilton, T. Lanting, J. Whittaker, Architectural considerations in the design of a superconducting quantum annealing processor, *IEEE Transactions on Applied Superconductivity* **24**(4), 1700110 (2014).
- [125] D. Riste, J. G. van Leeuwen, H.-S. Ku, K.W. Lehnert, and L. DiCarlo, Initialization by Measurement of a Superconducting Quantum Bit Circuit, *Phys. Rev. Lett.* **109**, 050507 (2012).
- [126] J. E. Johnson, C. Macklin, D. H. Slichter, R. Vijay, E.B. Weingarten, J. Clarke, and I. Siddiqi, Heralded State Preparation in a Superconducting Qubit, *Phys. Rev. Lett.* **109**, 050506 (2012).
- [127] C.C. Bultink, M.A. Rol, X. Fu, B.C.S. Dikken, J.C. de Sterke, R.F.L. Vermeulen, R.N. Schouten, A. Bruno, K.L.M. Bertels, and L. DiCarlo, Active resonator reset in the non-linear regime of circuit QED to improve multi-round quantum parity checks, *Phys. Rev. Applied* **6**, 034008 (2016).
- [128] D.T. McClure, H. Paik, L.S. Bishop, M. Steffen, J.M. Chow, J.M. Gambetta, Rapid Driven Reset of a Qubit Readout Resonator, *Phys. Rev. Appl.* **5**, 011001 (2016).
- [129] R. Vijay, M. H. Devoret, and I. Siddiqi, The Josephson bifurcation amplifier, *Rev. Sci. Instrum.* **80**, 111101 (2009).
- [130] M. A. Castellanos-Beltran and K. W. Lehnert, Widely tunable parametric amplifier based on a superconducting quantum interference device array resonator, *Appl. Phys. Lett.* **91**, 083509 (2007).
- [131] N. Roch, E. Flurin, F. Nguyen, P. Morfin, P. Campagne-Ibarcq, M. H. Devoret, and B. Huard, Widely Tunable, Nondegenerate Three-Wave Mixing Microwave Device Operating near the Quantum Limit, *Phys. Rev. Lett.* **108**, 147701 (2012).
- [132] C. Eichler, Y. Salathe, J. Mlynek, S. Schmidt, and A. Wallraff, Quantum-Limited Amplification and Entanglement in Coupled Nonlinear Resonators, *Phys. Rev. Lett.* **113**, 110502 (2014).
- [133] K. O'Brien, C. Macklin, I. Siddiqi, and X. Zhang, Resonantly phase-matched Josephson junction traveling wave parametric amplifier, *Phys. Rev. Lett.* **113**, 157001 (2014).
- [134] X. Zhou, V. Schmitt, P. Bertet, D. Vion, W. Wustmann, V. Shumeiko, and D. Esteve, High-gain weakly non-linear flux-modulated Josephson parametric amplifier using a SQUID array, *Phys. Rev. B* **89**, 214517 (2014).
- [135] V. Schmitt, X. Zhou, K. Juliusson, B. Royer, A. Blais, P. Bertet, D. Vion, and D. Esteve, Multiplexed readout of transmon qubits with Josephson bifurcation amplifiers, *Phys. Rev. A* **90**, 062333 (2014).
- [136] L. Sun, A. Petrenko, Z. Leghtas, B. Vlastakis, G. Kirchmair, K. M. Sliva, A. Narla, M. Hatridge, S. Shankar, J. Blumoff, L. Frunzio, M. Mirrahimi, M. H. Devoret, and R. Schoelkopf, Tracking Photon Jumps with Repeated Quantum Non-Demolition Parity Measurements, *Nature* **511** 444-448 (2014).
- [137] E. Jeffrey, D. Sank, J.Y. Mutus, T.C. White, J. Kelly, R. Barends, Y. Chen, Z. Chen, B. Chiaro, A. Dunsworth, A. Megrant, P.J.J. O'Malley, C. Neill, P. Roushan, A. Vainsencher, J. Wenner, A.N. Cleland, J. M. Martinis, Fast accurate state measurement with superconducting qubits, *Phys. Rev. Lett.* **112**, 190504 (2014).
- [138] Philip Krantz, Andreas Bengtsson, Michael Simoen, Simon Gustavsson, Vitaly Shumeiko, W.D. Oliver, C.M. Wilson, Per Delsing and Jonas Bylander, Single-shot read-out of a superconducting qubit using a Josephson parametric oscillator, *Nature Commun.* **7**: 11417 (2016).
- [139] Daniel Sank, Zijun Chen, Mostafa Khezri, J. Kelly, R. Barends, Y. Chen, A. Fowler, E. Jeffrey, E. Lucero, A. Megrant, J. Mutus, M. Neeley, P. Roushan, A. Vainsencher, T. White, B. Campbell, B. Chiaro, A. Dunsworth, C. Neill, P. J. J. O'Malley, C. Quintana, J. Wenner, A. N. Korotkov, and J. M. Martinis, Measurement-induced state transitions in a superconducting qubit: Beyond the rotating wave approximation (2016); arXiv:1606.05721v1.
- [140] D. Riste, C.C. Bultink, M.J. Tiggelman, R.N. Schouten, K.W. Lehnert, and L. DiCarlo, Millisecond charge-parity fluctuations and induced decoherence in a superconducting qubit. *Nature Commun.* **4**: 1913 (2013).

- [141] A. Bruno, G. de Lange, S. Asaad, K. van der Enden, N. K. Langford, and L. DiCarlo, Reducing intrinsic loss in superconducting resonators by surface treatment and deep etching of silicon substrates. *Applied Physics Letters* **106**, 182601 (2015).
- [142] L. DiCarlo, J.M. Chow, J.M. Gambetta, L.S. Bishop, B.R. Johnson, D.I. Schuster, J. Majer, A. Blais, L. Frunzio, S.M. Girvin, and R.J. Schoelkopf, Demonstration of two-qubit algorithms using a superconducting quantum processor, *Nature* **460**, 240 (2009).
- [143] L. Steffen, Y. Salathe, M. Oppliger, P. Kurpiers, M. Baur, C. Lang, C. Eichler, G. Puebla-Hellmann, A. Fedorov and A. Wallraff, Deterministic quantum teleportation with feed-forward in a solid state system, *Nature* **500**, 319 (2013).
- [144] J. Heinsoo, et al., Entanglement swapping, In preparation (2016).
- [145] M. Oppliger, J. Heinsoo, Y. Salath, A. Potocnik, G. S. Paraoanu, M. Mondal, and A. Wallraff, Entanglement distillation in circuit quantum electrodynamics (2016); in preparation.
- [146] LIQUi| >: A Software Design Architecture and Domain-Specific Language for Quantum Computing, D. Wecker and K. M. Svore, arXiv:1402.4467v1.
- [147] B. Valiron, N. J. Ross, P. Selinger, D. S. Alexander, J. M. Smith, Programming the Quantum Future, *Communications of the ACM* **58**(8), 52-61 (2015).
- [148] T. Häner, D. S. Steiger, K. Svore, and M. Troyer, A Software Methodology for Compiling Quantum Programs. arXiv:1604.01401v2.
- [149] T. Häner, D. S. Steiger, M. Smelyanskiy, and M. Troyer, High Performance Emulation of Quantum Circuits, arXiv:1604.06460v1.
- [150] B. Bauer, D. Wecker, A. J. Millis, M. B. Hastings, and Matthias Troyer, Hybrid quantum-classical approach to correlated materials, arXiv:1510.03859v1.
- [151] M. Reiher, N. Wiebe, K. M. Svore, D. Wecker, and M. Troyer, Elucidating Reaction Mechanisms on Quantum Computers, arXiv:1605.03590v2
- [152] S. Bravyi and D. Gosset, Improved Classical Simulation of Quantum Circuits Dominated by Clifford Gates, *Phys. Rev. Lett.* **116**, 250501 (2016).
- [153] E.T. Jaynes, F.W. Cummings, Comparison of quantum and semiclassical radiation theories with application to the beam maser, *Proc. IEEE* **51**(1), 89-109 (1963).
- [154] C. Gerry and P. Knight, *Introductory Quantum Optics*, Cambridge University Press, 2005.
- [155] Michael R. Geller, Emmanuel Donate, Yu Chen, Charles Neill, Pedram Roushan, John M. Martinis, Tunable coupler for superconducting Xmon qubits: Perturbative nonlinear model. *Phys. Rev. A* **92**, 012320 (2015).
- [156] M. Wallquist, V. S. Shumeiko, and G. Wendin, Selective coupling of superconducting charge qubits mediated by a tunable stripline cavity, *Phys. Rev. B* **74**, 224505 (2006).
- [157] D. Kafri, C. Quintana, Y. Chen, A. Shabani, J. M. Martinis, and H. Neven, Tunable inductive coupling of superconducting qubits in the strongly nonlinear regime (2016); arXiv:1606.08382v1.
- [158] J. Lantz, M. Wallquist, V. S. Shumeiko, and G. Wendin, Josephson junction qubit network with current-controlled interaction, *Phys. Rev. B* **70**, 140507(R) (2004).
- [159] M Wallquist, J Lantz, V S Shumeiko and G Wendin, Superconducting qubit network with controllable nearest-neighbour coupling, *New J. Phys.* **7**, 178 (2005).
- [160] Markus Aspelmeyer, Tobias J. Kippenberg, and Florian Marquardt, Cavity optomechanics, *Rev. Mod. Phys.* **86**, 1391 (2014).
- [161] G. Kurizki, P. Bertet, Y. Kubo, K. Mølmer, D. Petrosyan, P. Rabl, and J. Schmiedmayer, Quantum technologies with hybrid systems, *PNAS* **112**, 3866 (2015).
- [162] Y. Kubo, F. R. Ong, P. Bertet, D. Vion, V. Jacques, D. Zheng, A. Drau, J.-F. Roch, A. Auffeves, F. Jelezko, J. Wrachtrup, M.F. Barthe, P. Bergonzo, D. Esteve, Strong Coupling of a Spin Ensemble to a Superconducting Resonator, *Phys. Rev. Lett.* **105**, 140502 (2010).
- [163] D. I. Schuster, A. P. Sears, E. Ginossar, L. DiCarlo, L. Frunzio, J. J. L. Morton, H. Wu, G. A. D. Briggs, B. B. Buckley, D. D. Awschalom, and R. J. Schoelkopf, High-Cooperativity Coupling of Electron-Spin Ensembles to Superconducting Cavities, *Phys. Rev. Lett.* **105**, 140501 (2010).
- [164] R. Amsüss, Ch. Koller, T. Nöbauer, S. Putz, S. Rotter, K. Sandner, S. Schneider, M. Schramböck,

- G. Steinhauser, H. Ritsch, J. Schmiedmayer, and J. Majer, Cavity QED with Magnetically Coupled Collective Spin States, *Phys. Rev. Lett.* **107**, 060502 (2011).
- [165] P. Bushev, A. K. Feofanov, H. Rotzinger, I. Protopopov, J. H. Cole, C. M. Wilson, G. Fischer, A. Lukashenko, A. V. Ustinov, Rare earth spin ensemble magnetically coupled to a superconducting resonator, *Phys. Rev. B* **84**, 060501(R) (2011).
- [166] Y. Kubo, I. Diniz, A. Dewes, V. Jacques, A. Drau, J.-F. Roch, A. Auffeves, D. Vion, D. Esteve, and P. Bertet, Storage and retrieval of a microwave field in a spin ensemble, *Phys. Rev. A* **85**, 012333 (2012).
- [167] C. Grezes, B. Julsgaard, Y. Kubo, M. Stern, T. Umeda, J. Isoya, H. Smuiya, H. Abe, S. Onoda, T. Ohshima, V. Jacques, J. Esteve, D. Vion, D. Esteve, K. Moelmer, and P. Bertet, Multi-mode storage and retrieval of microwave fields in a spin ensemble, *Phys. Rev. X* **4**, 021049 (2014).
- [168] Y. Kubo, C. Grezes, A. Dewes, T. Umeda, J. Isoya, H. Sumiya, N. Morishita, H. Abe, S. Onoda, T. Ohshima, V. Jacques, A. Drau, J.-F. Roch, I. Diniz, A. Auffeves, D. Vion, D. Esteve, and P. Bertet, Hybrid Quantum Circuit with a Superconducting Qubit Coupled to a Spin Ensemble, *Phys. Rev. Lett.* **107**, 220501 (2011).
- [169] X. Zhu, S. Saito, A. Kemp, K. Kakuyanagi, S.-i. Karimoto, H. Nakano, W. J. Munro, Y. Tokura, M. S. Everitt, K. Nemoto, M. Kasu, N. Mizuochi and K. Semba, Coherent coupling of a superconducting flux qubit to an electron spin ensemble in diamond, *Nature* **478**, 221 (2011).
- [170] A. D. OConnell, M. Hofheinz, M. Ansmann, R.C. Bialczak, M. Lenander, E. Lucero, M. Neeley, D. Sank, H. Wang, M. Weides, J. Wenner, J. M. Martinis and A. N. Cleland, Quantum ground state and single-phonon control of a mechanical resonator, *Nature* **464**, 697 (2010).
- [171] F. Lecocq, J. D. Teufel, J. Aumentado and R.W. Simmonds, Resolving the vacuum fluctuations of an optomechanical system using an artificial atom, *Nature Phys.* **11** 635 (2015).
- [172] J.-M. Pirkkalainen, S. U. Cho, Jian Li, G. S. Paraoanu, P. J. Hakonen and M. A. Sillanpää, Hybrid circuit cavity quantum electrodynamics with a micromechanical resonator, *Nature* **494**, 211 (2013).
- [173] M. V. Gustafsson, T. Aref, A. F. Kockum, M. K. Ekström, G. Johansson, and P. Delsing, Propagating phonons coupled to an artificial atom, *Science* **346**, 207-211 (2014).
- [174] A. Frisk Kockum, P. Delsing, and G. Johansson, Designing frequency-dependent relaxation rates and Lamb shifts for a giant artificial atom, *Phys. Rev. A* **90**, 013837 (2014).
- [175] J. Bochmann, A. Vainsencher, D. D. Awschalom and A. N. Cleland, Nanomechanical coupling between microwave and optical photons, *Nature Phys.* **9**, 712 (2013).
- [176] R. W. Andrews, R. W. Peterson, T. P. Purdy, K. Cicak, R. W. Simmonds, C. A. Regal and K. W. Lehnert, Bidirectional and efficient conversion between microwave and optical light, *Nature Phys.* **10**, 321 (2014).
- [177] J.-M. Pirkkalainen, S.U. Cho, F. Massel, J. Tuorila, T.T. Heikkilä, P.J. Hakonen and M.A. Sillanpää, Cavity optomechanics mediated by a quantum two-level system, *Nature Commun.* **6**: 6981 (2015).
- [178] T. Bagci, A. Simonsen, S. Schmid, L. G. Villanueva, E. Zeuthen, J. Appel, J. M. Taylor, A. Srensen, K. Usami, A. Schliesser, and E. S. Polzik, Optical detection of radio waves through a nanomechanical transducer. *Nature* **507**, 81 (2014).
- [179] O. Cernotik and K. Hammerer, Measurement-induced long-distance entanglement of superconducting qubits using optomechanical transducers, *Phys. Rev. A* **94**, 012340 (2016).
- [180] V.S. Shumeiko, Quantum acousto-optic transducer for superconducting qubits, *Phys. Rev. A* **93**, 023838 (2016).
- [181] C. Rigetti and M. H. Devoret, Fully Microwave-Tunable Universal Gates in Superconducting Qubits with Linear Couplings and Fixed Transition Frequencies, *Phys. Rev. B.* **81**, 134507 (2010)
- [182] J. M. Chow, A. D. Corcoles, J. M. Gambetta, C. Rigetti, B. R. Johnson, John A. Smolin, J. R. Rozen, G. A. Keefe, M. B. Rothwell, M. B. Ketchen, and M. Steffen, A simple all-microwave entangling gate for fixed-frequency superconducting qubits, *Phys. Rev. Lett.* **107**, 080502 (2011).

- [183] A. Corcoles, J. M. Gambetta, J. M. Chow, J. A. Smolin, M. Ware, J.D. Strand, B.L. T. Plourde, and M. Steffen. Process verification of two-qubit quantum gates by randomized benchmarking, *Phys. Rev. A* **87**, 030301(R) (2013).
- [184] S. Sheldon, E. Magesan, J. M. Chow, and J. M. Gambetta, Procedure for systematically tuning up crosstalk in the cross resonance gate, *Phys. Rev. A* **93**, 060302(R) (2016).
- [185] J M Chow, J M Gambetta, A W Cross, S T Merkel, C Rigetti and M Steffen, Microwave-activated conditional-phase gate for superconducting qubits, *New J. Phys.* **15**, 115012 (2013).
- [186] M. Sandberg, C. M. Wilson, F. Persson, T. Bauch, G. Johansson, V. Shumeiko, T. Duty and P. Delsing, Tuning the field in a microwave resonator faster than the photon lifetime, *Appl. Phys. Lett.* **92**, 203501 (2008).
- [187] A. Palacios-Laloy, F. Nguyen, F. Mallet, P. Bertet, D. Vion and D. Esteve, Tunable resonators for quantum circuits. *J. Low Temp. Phys.* **151**, 1034 (2008).
- [188] M. Wallquist, V. S. Shumeiko and G. Wendin , Selective coupling of superconducting charge qubits mediated by a tunable stripline cavity, *Phys. Rev. B* **74**, 224506 (2006).
- [189] M Sandberg, F Persson, I C Hoi, C M Wilson and P Delsing, Exploring circuit quantum electrodynamics using a widely tunable superconducting resonator, *Phys. Scr.* **T137** 014018 (2009).
- [190] A. W. Cross and J. M. Gambetta, Optimized pulse shapes for a resonator-induced phase gate, *Phys. Rev. A* **91**, 032325 (2015).
- [191] D. C. McKay, Stefan Filipp, Antonio Mezzacapo, Easwar Magesan, Jerry M. Chow, Jay M. Gambetta, A universal gate for fixed-frequency qubits via a tunable bus, arXiv:1604.03076v2.
- [192] H. Paik, A. Mezzacapo, M. O. Sandberg, D. T. McClure, B. Abdo, A. D. Corcoles, O. E. Dial, D. F. Bogorin, B. L. T. Plourde, M. Steffen, A. W. Cross, J. M. Gambetta, and J. M. Chow, Experimental demonstration of a resonator-induced phase gate in a multi-qubit circuit QED system, arXiv:1606.00685v1.
- [193] C. K. Andersen and K. Mølmer, Multi-frequency modes in superconducting resonators: Bridging frequency gaps in off- resonant couplings, *Phys. Rev. A* **91**, 023828 (2015).
- [194] S. Felicetti, M. Sanz, L. Lamata, G. Romero, G. Johansson, P. Delsing, and E. Solano, Dynamical Casimir Effect Entangles Artificial Atoms, *Phys. Rev. Lett.* **113**, 093602 (2014).
- [195] T. Monz, P. Schindler, J. Barreiro, M. Chwalla, D. Nigg, W. A. Coish, M. Harlander, W. Hnsel, M. Hennrich, and R. Blatt, 14-Qubit Entanglement: Creation and Coherence, *Phys. Rev. Lett.* **106**, 130506 (2011).
- [196] K. Mølmer and A. Sorensen, Multiparticle Entanglement of Hot Trapped Ions, *Phys. Rev. Lett.* **82**, 1835 (1999).
- [197] K. Mølmer and A. Sorensen, Quantum Computation with Ions in Thermal Motion, *Phys. Rev. Lett.* **82**, 1971 (1999).
- [198] A. Sorensen and K. Mølmer, Entanglement and quantum computation with ions in thermal motion, *Phys. Rev. A* **62**, 022311 (2000).
- [199] M.D. Reed, L. DiCarlo, S. Nigg, L. Sun, L. Frunzio, S.M. Girvin, and R.J. Schoelkopf, Realization of three-qubit quantum error correction with superconducting circuits, *Nature* **482**, 382 (2012).
- [200] A. Fedorov, L. Steffen, M. Baur, M. P. da Silva, and A. Wallraff, Implementation of a Toffoli gate with superconducting circuits, *Nature* **481**, 170 (2012).
- [201] E. Zahedinejad, J. Ghosh, and B. C. Sanders, High-Fidelity Single-Shot Toffoli Gate via Quantum Control, *Phys. Rev. Lett.* **114**, 200502 (2015).
- [202] E. Zahedinejad, J. Ghosh, and B. C. Sanders, Designing high-fidelity single-shot three-qubit gates: A machine learning approach, arXiv: 1511.08862v1.
- [203] B. Giles and P. Selinger, Exact synthesis of multiqubit Clifford+ T circuits, *Phys. Rev. A* **87**, 032332 (2013).
- [204] O. Di Matteo and M. Mosca, Parallelizing quantum circuit synthesis, arXiv:1606.07413v1
- [205] R. Bianchetti, S. Filipp, M. Baur, J. M. Fink, C. Lang, L. Steffen, M. Boissonneault, A. Blais, and A. Wallraff, Control and Tomography of a Three Level Superconducting Artificial Atom,

- Phys. Rev. Lett. **105**, 223601 (2010).
- [206] I. L. Chuang and M. A. Nielsen, Prescription for experimental determination of the dynamics of a quantum black box, *J. Mod. Opt.* **44**, 2455-2467 (1997).
- [207] M. Mohseni, A. T. Rezakhani, and D. A. Lidar, Quantum-process tomography: Resource analysis of different strategies, *Phys. Rev. A* **77**, 032322 (2008).
- [208] J. Yuen-Zhou, J. J. Krich, I. Kassal, A. S. Johnson, and A. Aspuru-Guzik, *Ultrafast Spectroscopy: Quantum Information and Wavepackets*, IOP Publishing Ltd 2014; DOI 10.1088/978-0-750-31062-8
- [209] M. Christandl and R. Renner, Reliable Quantum State Tomography, *Phys. Rev. Lett.* **109**, 120403 (2012).
- [210] T. Yamamoto, M. Neeley, E. Lucero, R. C. Bialczak, J. Kelly, M. Lenander, M. Mariantoni, A. D. O'Connell, D. Sank, H. Wang, M. Weides, J. Wenner, Y. Yin, A. N. Cleland, J. M. Martinis, Quantum process tomography of two-qubit controlled-Z and controlled-NOT gates using superconducting phase qubits, *Phys. Rev. B* **82**, 184515 (2010).
- [211] M. Baur, A. Fedorov, L. Steffen, S. Filipp, M. P. da Silva, and A. Wallraff, Benchmarking a Quantum Teleportation Protocol in Superconducting Circuits Using Tomography and an Entanglement Witness, *Phys. Rev. Lett.* **108**, 040502 (2012).
- [212] Universal Quantum Gate Set Approaching Fault-Tolerant Thresholds with Superconducting Qubits, J. M. Chow, J. M. Gambetta, A. D. Corcoles, S. T. Merkel, J. A. Smolin, C. Rigetti, S. Poletto, G. A. Keefe, M. B. Rothwell, J. R. Rozen, M. B. Ketchen, and M. Steffen, *Phys. Rev. Lett.* **109**, 060501 (2012).
- [213] E. Knill, D. Liebfreid, R. Reichle, J. Britton, R. B. Blakestad, J. D. Jost, C. Langer, R. Ozeri, S. Seidelin, and D. J. Wineland, Randomized Benchmarking of Quantum Gates, *Phys. Rev. A* **77**, 012307 (2008).
- [214] J. J. Wallman and S. T. Flammia, Randomized Benchmarking with Confidence, *New J. Phys.* **16**, 103032 (2014).
- [215] H. Ball, T. M. Stace, S. T. Flammia, and M. J. Biercuk, Effect of noise correlations on randomized benchmarking, *Phys. Rev. A* **93**, 022303 (2016).
- [216] R. L. Kosut, Quantum Process Tomography via  $\ell_1$ -norm Minimization, arXiv:0812.4323v2.
- [217] D. Gross, Y.-K. Liu, S. T. Flammia, S. Becker, and J. Eisert, Quantum State Tomography via Compressed Sensing, *Phys. Rev. Lett.* **105**, 150401 (2010).
- [218] A. Shabani, R. L. Kosut, M. Mohseni, H. Rabitz, M. A. Broome, M. P. Almeida, A. Fedrizzi and A. G. White, Efficient measurement of quantum dynamics via compressive sensing, *Phys. Rev. Lett.* **106**, 100401 (2011).
- [219] S. T. Flammia, D. Gross, Y.-K. Liu, and J. Eisert, Quantum tomography via compressed sensing: error bounds, sample complexity and efficient estimators, *New J. Phys.* **14**, 095022 (2012).
- [220] A. V. Rodionov, A. Veitia, R. Barends, J. Kelly, D. Sank, J. Wenner, J. M. Martinis, R. L. Kosut, and A. N. Korotkov, Compressed sensing quantum process tomography for superconducting quantum gates, *Phys. Rev. B* **90**, 144504 (2014).
- [221] F. Huszar and N. M. T. Houlby, Adaptive Bayesian Quantum Tomography, *Phys. Rev. A* **85**, 052120 (2012).
- [222] K. S. Kravtsov, S. S. Straupe, I. V. Radchenko, N. M. T. Houlby, F. Huszar, and S. P. Kulik, Experimental adaptive Bayesian tomography, *Phys. Rev. A* **87**, 062122 (2013).
- [223] D. H. Mahler, L. A. Rozema, A. Darabi, C. Ferrie, R. Blume-Kohout, and A. M. Steinberg, Adaptive Quantum State Tomography Improves Accuracy Quadratically, *Phys. Rev. Lett.* **111**, 183601 (2013).
- [224] J. M. Chow, J. M. Gambetta, L. Tornberg, Jens Koch, Lev S. Bishop, A. A. Houck, B. R. Johnson, L. Frunzio, S. M. Girvin, and R. J. Schoelkopf, Randomized benchmarking and process tomography for gate errors in a solid-state qubit, *Phys. Rev. Lett.* **102**, 090502 (2009).
- [225] E. Magesan, J. M. Gambetta, and J. Emerson, Scalable and Robust Randomized Benchmarking of Quantum Processes, *Phys. Rev. Lett.* **106**, 180504 (2011).

- [226] S. Kimmel, M. P. da Silva, C. A. Ryan, B. R. Johnson, and T. Ohki, Robust Extraction of Tomographic Information via Randomized Benchmarking, *Phys. Rev. X* **4**, 011050 (2014).
- [227] C.A. Ryan, B.R. Johnson, J. M. Gambetta, J. M. Chow, M.P. da Silva, O. E. Dial, T. A. Ohki, Tomography via Correlation of Noisy Measurement Records, *Phys. Rev. A* **91**, 022118 (2015).
- [228] B. R. Johnson, M. P. da Silva, C. A. Ryan, S. Kimmel, Jerry M. Chow, and Thomas A. Ohki, Demonstration of Robust Quantum Gate Tomography via Randomized Benchmarking, *New J. Phys.* **17**, 113019 (2015).
- [229] A. W. Cross, E. Magesan, L. S Bishop, J. A. Smolin, J. M. Gambetta, Scalable randomised benchmarking of non-Clifford gates, *NPJ Quantum Information* **2**: 16012 (2016).
- [230] E. Magesan, Jay M. Gambetta, B. R. Johnson, C. A. Ryan, J. M. Chow, S. T. Merkel, M. P. da Silva, G. A. Keefe, M. B. Rothwell, T. A. Ohki, M. B. Ketchen, and M. Steffen, Efficient Measurement of Quantum Gate Error by Interleaved Randomized Benchmarking, *Phys. Rev. Lett.* **109**, 080505 (2012).
- [231] S. Sheldon, L. S. Bishop, S. Filipp, M. Steffen, J. M. Chow, and J. M. Gambetta, Characterizing errors on qubit operations via iterative randomized benchmarking, *Phys. Rev. A* **93**, 012301 (2016).
- [232] T. Chasseur, D. M. Reich, C. P. Koch, and F. K. Wilhelm, Hybrid benchmarking of arbitrary quantum gates, *arXiv:1606.03927v2*.
- [233] O. Moussa, M. P. da Silva, C. A. Ryan, R. Laflamme, Practical experimental certification of computational quantum gates via twirling, *Phys. Rev. Lett.* **109**, 070504 (2012).
- [234] D. Lu, H. Li, D.-A. Trottier, J. Li, A. Brodutch, A. P. Krismanich, A. Ghavami, G. I. Dmitrienko, G. Long, J. Baugh, and Raymond Laflamme, Experimental Estimation of Average Fidelity of a Clifford Gate on a 7-Qubit Quantum Processor, *Phys. Rev. Lett.* **114**, 140505 (2015).
- [235] E. Farhi and A. W. Harrow, Quantum Supremacy through the Quantum Approximate Optimization Algorithm, *arXiv:1602.07674v1*
- [236] D. F. Kerridge, Inaccuracy and inference, *J. Roy. Statist. Soc. Sec. B* **23**, 184-194 (1961).
- [237] G. E. Crooks, On Measures of Entropy and Information, *Tech. Note.* 009 v4 beta; <http://threeplusone.com/info>
- [238] J. A. Mlynek, A. A. Abdumalikov, J. M. Fink, L. Steffen, M. Baur, C. Lang, A. F. van Loo, and A. Wallraff, Demonstrating W-type Entanglement of Dicke-States in Resonant Cavity Quantum Electrodynamics, *Phys. Rev. A* **86**, 053838 (2012).
- [239] M. Riebe, H. Hffner, C. F. Roos, W. Hnsel, J. Benhelm, G. P. T. Lancaster, T. W. Krber, C. Becher, F. Schmidt-Kaler, D. F. V. James and R. Blatt, Deterministic quantum teleportation with atoms, *Nature* **429**, 734 (2004).
- [240] M. D. Barrett, J. Chiaverini, T. Schaetz, J. Britton, W. M. Itano, J. D. Jost, E. Knill, C. Langer, D. Leibfried, R. Ozeri and D. J. Wineland, Deterministic quantum teleportation of atomic qubits. *Nature* **429**, 737 (2004).
- [241] W. Pfaff, B. J. Hensen, H. Bernien, S. B. van Dam, M. S. Blok, T. H. Taminiau. M. J. Tiggelman, R. N. Schouten, D. J. Twitchen, R. Hanson, Unconditional quantum teleportation between distant solid-state quantum bits, *Science* **345**, 532 (2014).
- [242] M. Zukowski, A. Zeilinger, M. A. Horne, and A. K. Ekert, "Event-Ready-Detectors" Bell Experiment via Entanglement Swapping, *Phys. Rev. Lett.* **71**, 4287 (1993).
- [243] T. Herbst, T. Scheidl, M. Fink, J. Handsteiner, B. Wittmann, R. Ursin, and A. Zeilinger, Teleportation of entanglement over 143 km, *PNAS* **112**, 14202 (2015).
- [244] S. Waeldchen, J. Gertis, E. T. Campbell, and J. Eisert, Renormalizing Entanglement Distillation, *Phys. Rev. Lett.* **116**, 020502 (2016).
- [245] F. Motzoi, J. M. Gambetta, P. Rebentrost, and F. K. Wilhelm, Simple Pulses for Elimination of Leakage in Weakly Nonlinear Qubits, *Phys. Rev. Lett.* **103**, 110501 (2009).
- [246] J. M. Chow, L. DiCarlo, J. M. Gambetta, F. Motzoi, L. Frunzio, S. M. Girvin, R. J. Schoelkopf, Implementing optimal control pulse shaping for improved single-qubit gates, *Phys. Rev. A* **82**, 040305 (2010).

- [247] J. M. Gambetta, F. Motzoi, S. T. Merkel, and F. K. Wilhelm, Analytic control methods for high-fidelity unitary operations in a weakly nonlinear oscillator, *Phys. Rev. A* **83**, 012308 (2011).
- [248] Z. Chen, J. Kelly, C. Quintana, R. Barends, B. Campbell, Y. Chen, B. Chiaro, A. Dunsworth, A. G. Fowler, E. Lucero, E. Jeffrey, A. Megrant, J. Mutus, M. Neeley, C. Neill, P. J. J. O'Malley, P. Roushan, D. Sank, A. Vainsencher, J. Wenner, T. C. White, A. N. Korotkov, and J. M. Martinis, Measuring and Suppressing Quantum State Leakage in a Superconducting Qubit, *Phys. Rev. Lett.* **116**, 020501 (2016).
- [249] V. Vesterinen, O.-P. Saira, A. Bruno, and L. DiCarlo, Mitigating information leakage in a crowded spectrum of weakly anharmonic qubits; arXiv:1405.0450.
- [250] J. Kelly, R. Barends, B. Campbell, Y. Chen, Z. Chen, B. Chiaro, A. Dunsworth, A. G. Fowler, I. Hoi, E. Jeffrey, A. Megrant, J. Mutus, C. Neill, P.J.J. OMalley, C. Quintana, P. Roushan, D. Sank, A. Vainsencher, J. Wenner, T. C. White, A. N. Cleland, John M. Martinis, Optimal quantum control using randomized benchmarking, *Phys. Rev. Lett.* **112**, 240504 (2014).
- [251] F. Motzoi, J. M. Gambetta, S. T. Merkel, and F. K. Wilhelm, Optimal control methods for rapidly time-varying Hamiltonians, *Phys. Rev. A* **84**, 022307 (2011).
- [252] D. J. Egger and F. K. Wilhelm, Adaptive Hybrid Optimal Quantum Control for Imprecisely Characterized Systems, *Phys. Rev. Lett.* **112**, 240503 (2014).
- [253] G. G. Gillett, R. B. Dalton, B. P. Lanyon, M. P. Almeida, M. Barbieri, G. J. Pryde, J. L. O'Brien, K. J. Resch, S. D. Bartlett, and A. G. White, Experimental Feedback Control of Quantum Systems Using Weak Measurements, *Phys. Rev. Lett.* **104**, 080503 (2010).
- [254] L. Tornberg and G. Johansson, High-fidelity feedback-assisted parity measurement in circuit QED, *Phys. Rev. A* **82**, 012329 (2010).
- [255] Lars Tornberg, S. Barzanjeh, D. P. DiVincenzo, Stochastic-master-equation analysis of optimized three-qubit nondemolition parity measurements, *Phys. Rev. A* **89**,11 (2014).
- [256] A. Frisk Kockum, L. Tornberg, and G. Johansson, Undoing measurement-induced dephasing in circuit QED, *Phys. Rev. A* **85**, 052318 (2012).
- [257] J.P. Groen, D. Riste, L. Tornberg, J. Cramer, P.C. de Groot, T. Picot, G. Johansson, and L. DiCarlo, Partial-measurement back-action and non-classical weak values in a superconducting circuit, *Phys. Rev. Lett.* **111**,090506 (2013).
- [258] D. Riste and L. DiCarlo, Digital Feedback in Superconducting Quantum Circuits, in "Superconducting Devices in Quantum Optics", R. H. Hadfield, G. Johansson (Eds.), Springer, 2016; ISBN: 9783319240916. arXiv:1508.01385v1.
- [259] D. Riste, C.C. Bultink, K.W. Lehnert, and L. DiCarlo, Feedback control of a solid-state qubit using high-fidelity projective measurement, *Phys. Rev. Lett.* **109**, 240502 (2012).
- [260] D. Riste, M. Dukalski, C.A. Watson, G. de Lange, M.J. Tiggeleman, Ya.M. Blanter, K.W. Lehnert, R.N. Schouten, and L. DiCarlo, Deterministic entanglement of superconducting qubits by parity measurement and feedback. *Nature* **502**, 350 (2013).
- [261] R. Ruskov and A. N. Korotkov, Quantum feedback control of a solid-state qubit, *Phys. Rev. B* **66**, 041401 (2002).
- [262] A. N. Korotkov, Simple quantum feedback of a solid-state qubit, *Phys. Rev. B* **71**, 2013(R) (2005).
- [263] R. Vijay, C. Macklin, D. H. Slichter, S. J. Weber, K. W. Murch, R. Naik, A. N. Korotkov, I. Siddiqi, Stabilizing Rabi oscillations in a superconducting qubit using quantum feedback, *Nature* **490**, 77-80 (2012).
- [264] K. W. Murch, S. J. Weber, C. Macklin, I. Siddiqi, Observing single quantum trajectories of a superconducting qubit, *Nature* **502**, 211 (2013).
- [265] P. Campagne-Ibarcq, E. Flurin, N. Roch, D. Darson, P. Morfin, M. Mirrahimi, M. H. Devoret, F. Mallet, and B. Huard, Persistent Control of a Superconducting Qubit by Stroboscopic Measurement Feedback, *Phys. Rev. X* **3**, 021008 (2013).
- [266] S. J. Weber, A. Chantasri, J. Dressel, A. N. Jordan, K. W. Murch, I. Siddiqi, Mapping the optimal route between two quantum states, *Nature* **511**, 570-573 (2014).
- [267] G. de Lange, D. Rist, M. J. Tiggeleman, C. Eichler, L. Tornberg, G. Johansson, A. Wallraff, R.

- N. Schouten, and L. DiCarlo, Reversing quantum trajectories with analog feedback. *Phys. Rev. Lett.* **112**, 080501 (2014).
- [268] N. Roch, M. E. Schwartz, F. Motzoi, C. Macklin, R. Vijay, A. W. Eddins, A. N. Korotkov, K. B. Whaley, M. Sarovar, and I. Siddiqi, Observation of Measurement-Induced Entanglement and Quantum Trajectories of Remote Superconducting Qubits, *Phys. Rev. Lett.* **112**, 170501 (2014).
- [269] D. Tan, Kater Murch, Steven Webe, Irfan Siddiqi, Klaus Moelmer, Prediction and retrodiction for a continuously monitored superconducting qubit, *Phys. Rev. Lett.* **114**, 090403 (2015).
- [270] Shang-Yu Huang, Hsi-Sheng Goan, Xin-Qi Li, and G. J. Milburn, Generation and stabilization of a three-qubit entangled state in circuit QED via quantum feedback control. *Phys. Rev. A* **88**, 062311 (2013).
- [271] N. Katz, M. Neeley, M. Ansmann, Radoslaw C. Bialczak, M. Hofheinz, E. Lucero, A. O'Connell, H. Wang, A. N. Cleland, J. M. Martinis, and A. N. Korotkov, Reversal of the Weak Measurement of a Quantum State in a Superconducting Phase Qubit, *Phys. Rev. Lett.* **101**, 200401 (2008).
- [272] A. N. Korotkov and K. Keane, Decoherence suppression by quantum measurement reversal, *Phys. Rev. A* **81**, 040103(R) (2010).
- [273] J. A. Sherman, M. J. Curtis, D. J. Szwer, D. T.C. Allcock, G. Imreh, D. M. Lucas, and A. M. Steane, Experimental Recovery of a Qubit from Partial Collapse, *Phys. Rev. Lett.* **111**, 180501 (2013).
- [274] K. Keane and A. N. Korotkov, Simplified quantum error detection and correction for superconducting qubits. *Phys. Rev. A* **86**, 012333 (2012).
- [275] Y. P. Zhong, Z. L. Wang, J. M. Martinis, A. N. Cleland, A. N. Korotkov and H. Wang, Reducing the impact of intrinsic dissipation in a superconducting circuit by quantum error detection, *Nature Commun.* **5**: 3135, (2014).
- [276] M. Takita, A. D. Corcoles, E. Magesan, B. Abdo, M. Brink, A. Cross, J. M. Chow, and J. M. Gambetta, Demonstration of weight-four parity measurements in the surface code architecture, arXiv:1605.01351v2.
- [277] J. Martinis, Qubit metrology for building a fault-tolerant quantum computer, *NPJ Quantum Information* **1**, 15005 (2015).
- [278] P. Schindler, J. T. Barreiro, T. Monz, V. Nebendahl, D. Nigg, M. Chwalla, M. Hennrich, and R. Blatt, Experimental Repetitive Quantum Error Correction, *Science* **332**, 1059-1061 (2011).
- [279] Philipp Schindler, Thomas Monz, Daniel Nigg, Julio T. Barreiro, Esteban A. Martinez, Matthias F. Brandl, Michael Chwalla, Markus Hennrich, and Rainer Blatt, Undoing a Quantum Measurement, *Phys. Rev. Lett.* **110**, 070403 (2013).
- [280] J. Chiaverini, D. Leibfried, T. Schaetz, M. D. Barrett, R. B. Blakestad, J. Britton, W.M. Itano, J. D. Jost, E. Knill, C. Langer, R. Ozeri and D. J. Wineland, Realization of quantum error correction, *Nature* **432**, 602 (2004).
- [281] G. Waldherr, Y. Wang, S. Zaiser, M. Jamali, T. Schulte-Herbruggen, H. Abe, T. Ohshima, J. Isoya, J. F. Du, P. Neumann and J. Wrachtrup, Quantum error correction in a solid-state hybrid spin register, *Nature* **506**, 204 (2014).
- [282] J. Kelly, R. Barends, A. G. Fowler, A. Megrant, E. Jeffrey, T. C. White, D. Sank, J. Y. Mutus, B. Campbell, Yu Chen, Z. Chen, B. Chiaro, A. Dunsworth, E. Lucero, M. Neeley, C. Neill, P. J. J. O'Malley, C. Quintana, P. Roushan, A. Vainsencher, J. Wenner, and John M. Martinis, Scalable in-situ qubit calibration during repetitive error detection; arXiv:1603.03082v1
- [283] A. G. Fowler and J. M. Martinis, Quantifying the effects of local many-qubit errors and non-local two-qubit errors on topological codes, *Phys. Rev. A* **89**, 032316 (2014).
- [284] Austin G. Fowler, D. Sank, J. Kelly, R. Barends, John M. Martinis, Scalable extraction of error models from the output of error detection circuits; arXiv:1405.1454.
- [285] A. Y. Kitaev, Quantum Error Correction with Imperfect Gates, Proceedings of the 3rd International Conference of Quantum Communication and Measurement, Ed. O. Hirota, A. S. Holevo, and C. M. Caves (New York, Plenum, 1997).
- [286] A.G. Fowler, M. Mariantoni, J.M. Martinis, and A.N. Cleland, Surface codes: Towards practical

- large-scale quantum computation, *Phys. Rev. A* **86**, 032324 (2012).
- [287] Y. Tomita and K. M. Svore, Low-distance Surface Codes under Realistic Quantum Noise, *Phys. Rev. A* **90**, 062320 (2014).
- [288] B. M. Terhal, Quantum error correction for quantum memories, *Rev. Mod. Phys.* **87**, 307 (2015).
- [289] J. Ghosh and A. Fowler, A Leakage-Resilient Approach to Fault-Tolerant Quantum Computing with Superconducting Elements, *Phys. Rev. A* **91**, 020302(R) (2015).
- [290] S. Lloyd, Universal Quantum Simulators, *Science* **273**, 1073 (1996).
- [291] D.S. Abrams and S. Lloyd: Simulation of many-body fermi systems on a universal quantum computer, *Phys. Rev. Lett.* **79**, 2586 (1997).
- [292] D.S. Abrams and S. Lloyd: Quantum algorithms providing exponential speed increase for finding eigenvalues and eigenvectors, *Phys. Rev. Lett.* **83**, 5162 (1999).
- [293] A. Aspuru-Guzik, A.D. Dutoi, P.J. Love, and M. Head-Gordon, Simulated quantum computation of molecular energies, *Science* **309**, 1704 (2005).
- [294] J. D. Whitfield, J. Biamonte and A. Aspuru-Guzik, Simulation of electronic structure Hamiltonians using quantum computers, *Molecular Physics* **109**, 735-750 (2011).
- [295] R. P. Muller and R. Blume-Kohout, The Promise of Quantum Simulation, *ACS Nano* **9**, 7738 (2015).
- [296] S. Boixo, T. F. Rønnow, S. V. Isakov, Z. Wang, D. Wecker, D. A. Lidar, J. M. Martinis, and M. Troyer, Evidence for quantum annealing with more than one hundred qubits, *Nature Phys.* **10**, 218-224 (2014).
- [297] R. J. Bartlett and M. Musiał, Coupled-cluster theory in quantum chemistry, *Rev. Mod. Phys.* **79**, 291 (2007).
- [298] F. Verstraete, J.I. Cirac, and V. Murg, Matrix Product States, Projected Entangled Pair States, and variational renormalization group methods for quantum spin systems, *Adv. Phys.* **57**, 143 (2008).
- [299] M. Dobsicek, G. Johansson, V.S. Shumeiko, G. Wendin, Arbitrary accuracy iterative phase estimation algorithm as a two qubit benchmark, *Physical Review A* **76**, 030306 (2007).
- [300] R. Babbush, J. McClean, D. Wecker, A. Aspuru-Guzik and N. Wiebe, Chemical Basis of Trotter-Suzuki Errors in Quantum Chemistry Simulation, *Phys. Rev. A* **91**, 022311 (2015).
- [301] B. P. Lanyon, C. Hempel, D. Nigg, M. Mller, R. Gerritsma, F. Zhringer, P. Schindler, J. T. Barreiro, M. Rambach, G. Kirchmair, M. Hennrich, P. Zoller, R. Blatt, C. F. Roos, Universal Digital Quantum Simulation with Trapped Ions, *Science* **334**, 57 (2011).
- [302] U. Las Heras, A. Mezzacapo, L. Lamata, S. Filipp, A. Wallraff, and E. Solano, Digital Quantum Simulation of Spin Systems in Superconducting Circuits, *Phys. Rev. Lett.* **112**, 200501 (2014).
- [303] Y. Salathe, M. Mondal, M. Oppliger, J. Heinsoo, P. Kurpiers, A. Potocnik, A. Mezzacapo, U. Las Heras, L. Lamata, E. Solano, S. Filipp, and A. Wallraff, Digital quantum simulation of spin models, with circuit quantum electrodynamics, *Phys. Rev. X* **5**, 021027 (2015).
- [304] H. You, M. R. Geller, and P. C. Stancil, Simulating the transverse Ising model on a quantum computer: Error correction with the surface code, *Phys. Rev. A* **87**, 032341 (2013).
- [305] Sergey Bravyi, David P. DiVincenzo, Roberto Oliveira, Barbara M. Terhal, The Complexity of Stoquastic Local Hamiltonian Problems, *Quantum Information and Computation* **8**, 361 (2008).
- [306] P. Jordan and E. Wigner, Über das Paulische Äquivalenzverbot, *Z. Phys.* **47**, 631 (1928).
- [307] S. B. Bravyi, A.Yu. Kitaev, *Annals of Physics* **298**, 210-226 (2002).
- [308] G. Ortiz, J. E. Gubernatis, E. Knill, and R. Laflamme, Quantum algorithms for fermionic simulations, *Phys. Rev. A* **64**, 022319 (2001) (erratum; *Phys. Rev. A* **65**, 029902 (2002)).
- [309] R. Somma, G. Ortiz, J. Gubernatis, E. Knill, and R. Laflamme, Simulating physical phenomena by quantum networks, *Phys. Rev. A* **65**, 042323 (2002).
- [310] L. Lamata, J. Casanova, R. Gerritsma, C. F. Roos, J. J. Garcia-Ripoll, and E. Solano, Relativistic quantum mechanics with trapped ions, *Journal: New J. Phys.* **13**, 095003 (2011).
- [311] J. T. Seeley, M. J. Richard and P. J. Love, The Bravyi-Kitaev transformation for quantum computation of electronic structure, *J. Chem. Phys.* **137**, 224109 (2012).

- [312] L. García-Álvarez, J. Casanova, A. Mezzacapo, I. L. Egusquiza, L. Lamata, G. Romero, and E. Solano, Fermion-Fermion Scattering in Quantum Field Theory with Superconducting Circuits, *Phys. Rev. Lett.* **114**, 070502 (2015).
- [313] U. Las Heras, L. García-Álvarez, A. Mezzacapo, E. Solano and L. Lamata, Fermionic models with superconducting circuits, *EPJ Quantum Technology* **2**:8 (2015).
- [314] V. M. Kendon, K. Nemoto and W. J. Munro, Quantum analogue computing, *Phil. Trans. R. Soc. A* **368**, 3609 (2010).
- [315] R. Gerritsma, G. Kirchmair, F. Zähringer, E. Solano, R. Blatt and C. F. Roos, Quantum simulation of the Dirac equation, *Nature* **463**, 68 (2010).
- [316] J. W. Britton et al., Engineered two-dimensional Ising interactions in a trapped-ion quantum simulator with hundreds of spins, *Nature* **484**, 489 (2012).
- [317] R. Islam et al., Emergence and frustration of magnetism with variable-range interactions in a quantum simulator, *Science* **340**, 583 (2013).
- [318] I. Bloch, J. Dalibard and S. Nascimbène, Quantum simulations with ultracold quantum gases, *Nature Phys.* **8**, 267 (2012).
- [319] U. Schneider et al., Fermionic transport and out-of-equilibrium dynamics in a homogeneous Hubbard model with ultracold atoms, *Nature Phys.* **8**, 213 (2012).
- [320] T. Fukuhara et al., Microscopic observation of magnon bound states and their dynamics, *Nature* **502**, 76 (2013).
- [321] M. Aidelsburger et al., Realization of the Hofstadter Hamiltonian with Ultracold Atoms in Optical Lattices, *Phys. Rev. Lett.* **111**, 185301 (2013).
- [322] H. Miyake et al., Realizing the Harper Hamiltonian with Laser-Assisted Tunneling in Optical Lattices, *Phys. Rev. Lett.* **111**, 185302 (2013).
- [323] A. Aspuru-Guzik and P. Walther, Photonic quantum simulators, *Nature Phys.* **8**, 285 (2012)
- [324] P. Shadbolt, J. C. F. Matthews, A. Laing, and J. L. O'Brien, Testing foundations of quantum mechanics with photons, *Nature Phys.* **10**, 278-286 (2014).
- [325] A. P. Lund, A. Laing, S. Rahimi-Keshari, T. Rudolph, J.L. O'Brien, and T.C. Ralph, Boson Sampling from a Gaussian State, *Phys. Rev. Lett.* **113**, 100502 (2014).
- [326] N. Spagnolo, C. Vitelli, M. Bentivegna, D. J. Brod, A. Crespi, F. Flamini, S. Giacomini, G. Milani, R. Ramponi, P. Mataloni, R. Osellame, E. F. Galvao and F. Sciarrino, Experimental validation of photonic boson sampling, *Nature Photonics* **8**, 615 (2014).
- [327] M. Bentivegna, N. Spagnolo, C. Vitelli, F. Flamini, N. Viggianiello, L. Latmira, P. Mataloni, D. J. Brod, E. F. Galvao, A. Crespi, R. Ramponi, R. Osellame and F. Sciarrino, Experimental scattershot boson sampling, *Science Advances* **1**, e1400255 (2015).
- [328] M. Bentivegna, N. Spagnolo and F. Sciarrino, Is my boson sampler working?, *New J. Phys.* **18**, 041001 (2016).
- [329] F. Caruso, A. Crespi, A. G. Ciriolo, F. Sciarrino and R. Osellame. Fast escape of a quantum walker from an integrated photonic maze, *Nature Commun.* **7**: 11682 (2016).
- [330] A. Crespi, R. Osellame, R. Ramponi, M. Bentivegna, F. Flamini, N. Spagnolo, N. Viggianiello, L. Innocenti, P. Mataloni, and F. Sciarrino, "Suppression law of quantum states in a 3-D photonic fast Fourier transform chip", *Nature Commun.* **7**: 10469 (2016).
- [331] X. Qiang, T. Loke A. Montanaro, K. Aungkunsiri, X. Zhou, J. L. O'Brien, J. B. Wang and J. C. F. Matthews, Efficient quantum walk on a quantum processor, *Nature Commun.* **7**:11511(2016).
- [332] T. Inagaki, K. Inaba, R. Hamerly, K. Inoue, Y. Yamamoto, and H. Takesue, Large-scale Ising spin network based on degenerate optical parametric oscillators, *Nature Photonics* **10**, 415 (2016).
- [333] Andrew A. Houck, Hakan E. Türeci and Jens Koch, On-chip quantum simulation with superconducting circuits, *Nature Phys.* **8**, 292-299 (2012).
- [334] Sebastian Schmidt and Jens Koch, Circuit QED lattices, Towards quantum simulation with superconducting circuits, *Ann. Phys. (Berlin)* **525**(6), 395-412 (2013).
- [335] Sean Barrett, Klemens Hammerer, Sarah Harrison, Tracy E. Northup, and Tobias J. Osborne, Simulating Quantum Fields with Cavity QED, *Phys. Rev. Lett.* **110**, 090501 (2013).

- [336] Uwe-Jens Wiese, Towards quantum simulating QCD, *Nuclear Physics A* **931**, 246-256 (2014).
- [337] M. Dalmonte, S.I. Mirzaei, P. R. Muppalla, D. Marcos, P. Zoller, G. Kirchmair, Realizing Dipolar Spin Models with Arrays of Superconducting Qubits, *Phys. Rev. B* **92**, 174507 (2015).
- [338] Yuanwei Zhang, Lixian Yu, J. -Q Liang, Gang Chen, Suotang Jia and Franco Nori, Quantum phases in circuit QED with a superconducting qubit array, *Sci. Rep.* **4**: 4083 (2014).
- [339] S. Ashhab, Simulating systems of itinerant spin-carrying particles using arrays of superconducting qubits and resonators, *New J. Phys.* **16**, 113006 (2014).
- [340] A. Mezzacapo, U. Las Heras, J. S. Pedernales, L. DiCarlo, E. Solano, and L. Lamata, Digital quantum Rabi and Dicke models in superconducting circuits *Sci. Rep.*, **4**: 7482 (2014).
- [341] F. Mei, V. M. Stojanovic, I. Siddiqi, and L. Tian, Analog superconducting quantum simulator for Holstein polarons, *Phys. Rev. B* **88**, 224502 (2013).
- [342] V. M. Stojanovic, M. Vanevic, E. Demler, and L. Tian, Transmon-based simulator of nonlocal electron-phonon coupling: A platform for observing sharp small-polaron transitions, *Phys. Rev. B* **89**, 144508 (2014).
- [343] S. Zippilli, M. Grajcar, E. Il'ichev, and F. Illuminati, Simulating long-distance entanglement in quantum spin chains by superconducting flux qubits, *Phys. Rev. A* **91**, 022315 (2015).
- [344] S. Mostame, P. Rebentrost, D. I. Tsomokos and A. Aspuru-Guzik, Quantum simulator of an open quantum system using superconducting qubits: exciton transport in photosynthetic complexes, *New J. Phys.* **14** 105013 (2012).
- [345] D. J. Egger, F. K. Wilhelm, Multimode circuit QED with hybrid metamaterial transmission lines, *Phys. Rev. Lett.* **111**, 163601 (2013)
- [346] M. R. Geller, J. M. Martinis, A. T. Sornborger, P. C. Stancil, E. J. Pritchett, and A. Galiutdinov, Universal quantum simulation with pre-threshold superconducting qubits: Single-excitation subspace method, *Phys. Rev. A* **91**, 062309 (2015).
- [347] C. Eichler, J. Mlynek, J. Butscher, P. Kurpiers, K. Hammerer, T. Osborne, and A. Wallraff, Exploring Interacting Quantum Many-Body Systems by Experimentally Creating Continuous Matrix Product States in Superconducting Circuits, *Phys. Rev. X* **5**, 041044 (2015).
- [348] J. Li, M. P. Silveri, K. S. Kumar, J.-M. Pirkkalainen, A. Vepsäläinen, W. C. Chien, J. Tuorila, M. A. Sillanpää, P. J. Hakonen, E. V. Thuneberg, and G. S. Paraoanu, Motional averaging in a superconducting qubit, *Nature Commun.* **4**, 1420 (2013).
- [349] C. Neill, P. Roushan, M. Fang, Y. Chen, M. Kolodrubetz, Z. Chen, A. Megrant, R. Barends, B. Campbell, B. Chiaro, A. Dunsworth, E. Jeffrey, J. Kelly, J. Mutus, P. J. J. O'Malley, C. Quintana, D. Sank, A. Vainsencher, J. Wenner, T. C. White, A. Polkovnikov, J. M. Martinis, Ergodic dynamics and thermalization in an isolated quantum system, *Nature Physics* (2016); doi:10.1038/nphys3830; arXiv:1601.00600.
- [350] P. Roushan, C. Neill, A. Megrant, Y. Chen, R. Babbush, R. Barends, B. Campbell, Z. Chen, B. Chiaro, A. Dunsworth, A. Fowler, E. Jeffrey, J. Kelly, E. Lucero, J. Mutus, P. J.J. O'Malley, M. Neeley, C. Quintana, D. Sank, A. Vainsencher, J. Wenner, T. White, E. Kapit, H. Neven, and J. Martinis Chiral groundstate currents of interacting photons in a synthetic magnetic field (2016); arXiv:1606.00077v2.
- [351] S. Hacoen-Gourgy, V. Ramasesh, C. De Grandi, I. Siddiqi, and S. M. Girvin, Cooling and Autonomous Feedback in a Bose-Hubbard chain, *Phys. Rev. Lett.* **115**, 240501 (2015).
- [352] G. Kirchmair, B. Vlastakis, Z. Leghtas, S. E. Nigg, H. Paik, E. Ginossar, M. Mirrahimi, L. Frunzio, S. M. Girvin and J. Schoelkopf, Observation of quantum state collapse and revival due to the single-photon Kerr effect, *Nature* **495**, 205 (2013).
- [353] L. Garcá-Álvarez, U. Las Heras, A. Mezzacapo, M. Sanz, E. Solano, and L. Lamata, Quantum chemistry and charge transport in biomolecules with superconducting circuits, *Sci. Rep.* **6**: 27836 (2016).
- [354] J.A. Pople, Nobel Lecture: Quantum chemical models, *Rev. Mod. Phys.* **71**, 1267 (1999).
- [355] F. Verstraete and J. I. Cirac, Continuous Matrix Product States for Quantum Fields, *Phys. Rev. Lett.* **104**, 190405 (2010).

- [356] V. Khoromskaia and B. N. Khoromskij, Tensor numerical methods in quantum chemistry: from HartreeFock to excitation energies, *Phys. Chem. Chem. Phys.* **17**(47), 31491-31509 (2015).
- [357] S. Szalay, M. Pfeiffer, V. Murg, G. Barcza, F. Verstraete, R. Schneider and O. Legeza, Tensor product methods and entanglement optimization for ab initio quantum chemistry, *Int. J. Quant. Chem.* **115**, 1342 (2015).
- [358] D. Poulin, M.B. Hastings, D. Wecker, N. Wiebe, A. C. Doherty, and M. Troyer, The Trotter Step Size Required for Accurate Quantum Simulation of Quantum Chemistry, *Quantum Information and Computation* **15**, No. 5&6, 361 (2015).
- [359] A. Peruzzo, J. McClean, P. Shadbolt, M-H Yung, X-Q Zhou, P.J. Love, A. Aspuru-Guzik, and J.L. O'Brien, A variational eigenvalue solver on a photonic quantum processor, *Nature Comm.* **5**: 4213 (2014).
- [360] A. Tranter, S. Sofia, J. Seeley, M. Kaicher, J. McClean, R. Babbush, P. V. Coveney, F. Mintert, F. Wilhelm, and P. J. Love, *Int. J. Quantum Chemistry* **115**, 1431 (2015).
- [361] L. Mueck, Quantum reform, *Nature Chemistry* **7**, 361 (2015).
- [362] P. Love, Back to the Future: A roadmap for quantum simulation from vintage quantum chemistry, *Advances in Chemical Physics* **154**, 39 (2014).
- [363] Borzu Toloui and Peter Love, Quantum Algorithms for Quantum Chemistry based on the sparsity of the CI-matrix, arXiv:1312.2579v2
- [364] Ryan Babbush, Peter J. Love and Alan Aspuru-Guzik, Adiabatic Quantum Simulation of Quantum Chemistry, *Scientific Reports* **4**: 6603 (2014).
- [365] M.-H. Yung, J. Casanova, A. Mezzacapo, J. McClean, L. Lamata, A. Aspuru-Guzik, and E. Solano, From transistor to trapped-ion computers for quantum chemistry, *Sci. Rep.* **4**: 3589 (2014).
- [366] M. B. Hastings, D. Wecker, B. Bauer, and M. Troyer, Improving Quantum Algorithms for Quantum Chemistry, *Quant. Inf. Comput* **15**, 1 (2015).
- [367] J. R. McClean, R. Babbush, P. J. Love, and A. Aspuru-Guzik, Exploiting Locality in Quantum Computation for Quantum Chemistry, *J. Phys. Chem. Lett.* **5**(24), 4368-4380 (2014).
- [368] C. Zalka, Simulating quantum systems on a quantum computer. *Proc. R. Soc. Lond. A* **454**, 313-322 (1998).
- [369] I. Kassal, S. P. Jordan, P. J. Love, M. Mohseni, and A. Aspuru-Guzik, Polynomial-time quantum algorithm for the simulation of chemical dynamics, *PNAS* **105**, 18681 (2008).
- [370] D. Lu, N. Xu, R. Xu, H. Chen, J. Gong, X. Peng, and J. Du, Simulation of chemical isomerization reaction dynamics on a NMR quantum simulator, *Phys. Rev. Lett.* **107**, 020501 (2011).
- [371] E. J. Pritchett, C. Benjamin, A. Galiutdinov, M. R. Geller, I. A. T. Sornborger, P. C. Stancil and J. M. Martinis, Quantum Simulation of Molecular Collisions with Superconducting Qubits, (2010); arXiv:1008.0701.
- [372] A. T. Sornborger, Quantum simulation of tunneling in small systems, *Sci. Rep.* **2**: 597 (2012).
- [373] B. P. Lanyon, J. D. Whitfield, G. G. Gillett, M. E. Goggin, M. P. Almeida, I. Kassal, J. D. Biamonte, M. Mohseni, B. J. Powell, M. Barbieri, A. Aspuru-Guzik and A. G. White, Towards quantum chemistry on a quantum computer, *Nature Chem.* **2**, 106 (2010).
- [374] K. Sugisaki, S. Yamamoto, S. Nakazawa, K. Toyota, K. Sato, D. Shiomi, and T. Takui, Quantum Chemistry on Quantum Computers: A Polynomial-Time Quantum Algorithm for Constructing the Wave Functions of Open-Shell Molecules, *J. Phys. Chem. A* **2016**, 6459-6466 (2016).
- [375] J. Du, N. Xu, X. Peng, P. Wang, S. Wu, and D. Lu, NMR Implementation of a Molecular Hydrogen Quantum Simulation with Adiabatic State Preparation, *Phys. Rev. Lett.* **104**, 030502 (2010).
- [376] Y. Wang, F. Dolde, J. Biamonte, R. Babbush, V. Bergholm, S. Yang, I. Jakobi, P. Neumann, A. Aspuru-Guzik, J.D. Whitfield, and J. Wrachtrup, Quantum simulation of helium hydride cation in a solid-state spin register, *ACS Nano* **9**, 7769 (2015).
- [377] Y.-K. Liu, M. Christandl, F. Verstraete, N-representability is QMA-complete, *Phys. Rev. Lett.* **98**, 110503 (2007).

- [378] A. Das and B. K. Chakrabarti, Quantum Annealing and Analog Quantum Computation, *Rev. Mod. Phys.* **80**, 1061 (2008).
- [379] V. Bapst, L. Foini, F. Krzakala, G. Semerjian, and F. Zamponi, The Quantum Adiabatic Algorithm applied to random optimization problems: the quantum spin glass perspective, *Physics Reports* **523**, 127 (2013).
- [380] J. Biamonte, V. Bergholm, J. Fitzsimons, and A. Aspuru-Guzik, Adiabatic quantum simulators, *AIP Advances* **1**, 022126 (2011)
- [381] A. Lucas, Ising formulations of many NP problems, *Frontiers in Physics* **2**, 5 (2014); arXiv:1302.5843.
- [382] M. H. Amin, E. Andriyash, J. Rolfe, B. Kulchytskyy, and R. Melko, Quantum Boltzmann Machine, arXiv:1601.02036.
- [383] N. S. Dattani and N. Bryans, Quantum factorization of 56153 with only 4 qubits, arXiv:1411.6758v3.
- [384] I. Hen, Period finding with adiabatic quantum computation, *Europhys. Lett.* **105**, 50005 (2014).
- [385] I. Hen, Fourier-transforming with quantum annealers, *Front. Phys.* **2**, 44 (2014).
- [386] A. Perdomo-Ortiz, N. Dickson, M. Drew-Brook, G. Rose and Alan Aspuru-Guzik, Finding low-energy conformations of lattice protein models by quantum annealing, *Sci. Rep.* **2**: 571 (2012).
- [387] Z. Bian, F. Chudak, W. G. Macready, L. Clark, and F. Gaitan, Experimental determination of Ramsey numbers with quantum annealing, *Phys. Rev. Lett.* **111**, 130505 (2013).
- [388] F. Gaitan and L. Clark, Graph isomorphism and adiabatic quantum computing, *Phys. Rev. A* **89**, 022342 (2014).
- [389] M. W. Johnson, M. H. S. Amin, S. Gildert, T. Lanting, F. Hamze, N. Dickson, R. Harris, A. J. Berkley, J. Johansson, P. Bunyk, E. M. Chapple, C. Enderud, J. P. Hilton, K. Karimi, E. Ladizinsky, N. Ladizinsky, T. Oh, I. Perminov, C. Rich, M. C. Thom, E. Tolkacheva, C. J. S. Truncik, S. Uchaikin, J. Wang, B. Wilson and G. Rose, Quantum annealing with manufactured spins, *Nature* **473**, 194 (2011).
- [390] S. Boixo, T. Albash, F. Spedalieri, N. Chancellor, D.A. Lidar, Experimental Signature of Programmable Quantum Annealing, *Nature Commun.* **4**: 2067 (2013).
- [391] H. Nishimori, J. Tsuda, and S. Knysh, Comparative Study of the Performance of Quantum Annealing and Simulated Annealing, *Phys. Rev. E* **91**, 012104 (2015).
- [392] P. J. D. Crowley, T. Duric, W. Vinci, P. A. Warburton, and A. G. Green, Quantum and classical dynamics in adiabatic computation, *Phys. Rev. A* **90**, 042317 (2014).
- [393] N. G. Dickson, M. W. Johnson, M. H. Amin, R. Harris, F. Altomare, J. Berkley, P. Bunyk, J. Cai, E. M. Chapple, P. Chavez, F. Cioata, T. Cirip, P. deBuen, M. Drew-Brook, C. Enderud, S. Gildert, F. Hamze, J. P. Hilton, E. Hoskinson, K. Karimiet, E. Ladizinsky, N. Ladizinsky, T. Lanting, T. Mahon, R. Neufeld, T. Oh, I. Perminov, C. Petroff, A. Przybysz, C. Rich, P. Spear, A. Tcaciuc, M. C. Thom, E. Tolkacheva, S. Uchaikin, J. Wang, A. B. Wilson, Z. Merali, and G. Rose, Thermally assisted quantum annealing of a 16-qubit problem, *Nature Commun.* **4**: 1903 (2013).
- [394] T. Lanting, A. J. Przybysz, A. Yu. Smirnov, F. M. Spedalieri, M. H. Amin, A. J. Berkley, R. Harris, F. Altomare, S. Boixoy, P. Bunyk, N. Dickson, C. Enderud, J. P. Hilton, E. Hoskinson, M. W. Johnson, E. Ladizinsky, N. Ladizinsky, R. Neufeld, T. Oh, I. Perminov, C. Rich, M. C. Thom, E. Tolkacheva, S. Uchaikin, A. B. Wilson, and G. Rose, Entanglement in a Quantum Annealing Processor, *Phys. Rev. X* **4**, 021041 (2014).
- [395] S. Boixo, V. N. Smelyanskiy, A. Shabani, S. V. Isakov, M. Dykman, V. S. Denchev, M. Amin, A. Smirnov, M. Mohseni, and H. Neven, Computational Role of Multiqubit Tunneling in a Quantum Annealer, *Nature Commun.* **7**: 10327 (2016).
- [396] T. Albash, T. Ronnow, M. Troyer, D.A. Lidar, Reexamining classical and quantum models for the D-Wave One processor, *The European Physics Journal, Special Topics* **224**, 111 (special issue on quantum annealing) (2015).
- [397] T. Albash, W. Vinci, A. Mishra, P.A. Warburton, and D.A. Lidar, Consistency tests of classical

- and quantum models for a quantum annealer, *Phys. Rev. A* **91**, 042314 (2015).
- [398] K.P. Pudenz, T. Albash, and D.A. Lidar, Error Corrected Quantum Annealing with Hundreds of Qubits, *Nature Commun.* **5**, 3243 (2014).
- [399] K. Pudenz, T. Albash, and D. Lidar, Quantum Annealing Correction for Random Ising Problems, *Phys. Rev. A* **91**, 042302 (2015).
- [400] J. King, S. Yarkoni, M. M. Nevisi, J. P. Hilton, and C. C. McGeoch, Benchmarking a quantum annealing processor with the time-to-target metric, arXiv:1508.05087v1.
- [401] S. V. Isakov, I. N. Zintchenko, T. F. Rnnow, and M. Troyer, Optimised Simulated Annealing for Ising Spin Glasses, *Comput. Phys. Commun.* **192**, 265 (2015).
- [402] V. Martin-Mayor and I. Hen, Unraveling Quantum Annealers using Classical Hardness, *Sci. Rep.* **5**: 15324 (2015).
- [403] A. Selby, Efficient subgraph-based sampling of Ising-type models with frustration, (2014); arXiv:1409.3934.
- [404] <http://www.scottaaronson.com/blog/?p=2555>; comment #204
- [405] <http://www.scottaaronson.com/blog/?p=2555>
- [406] H. G. Katzgraber, F. Hamze, Z. Zhu, A. J. Ochoa, and H. Munoz-Bauza, Seeking Quantum Speedup Through Spin Glasses: The Good, the Bad, and the Ugly, *Phys. Rev. X* **5**, 031026 (2015).
- [407] I. Hen, J. Job, T. Albash, T. F. Ronnow, M. Troyer, and D. Lidar, Probing for quantum speedup in spin glass problems with planted solutions, *Phys. Rev. A* **92**, 042325 (2015)
- [408] Y. Cao, R. Babbush, J. Biamonte, and S. Kais, Towards Experimentally Realizable Hamiltonian Gadgets, *Phys. Rev. A* **91**, 012315 (2015).
- [409] B. E. Kane, A silicon-based nuclear spin quantum computer, *Nature* **393**, 133 (1998).
- [410] J.T. Muhonen, J.P. Dehollain, A. Laucht, F.E. Hudson, T. Sekiguchi, K.M. Itoh, D.N. Jamieson, J.C. McCallum, A.S. Dzurak, A. Morello, Storing quantum information for 30 seconds in a nanoelectronic device, *Nature Nanotechnology* **9**, 986-991 (2014).
- [411] M. Veldhorst, J. C. C. Hwang, C. H. Yang, A. W. Leenstra, B. de Ronde, J. P. Dehollain, J. T. Muhonen, F. E. Hudson, K. M. Itoh, A. Morello, and A. S. Dzurak, An addressable quantum dot qubit with fault-tolerant control-fidelity, *Nature Nanotechnology* **9**, 981-985 (2014).
- [412] J. P. Dehollain, J. T. Muhonen, K. Y. Tan, A. Saraiva, D. N. Jamieson, A. S. Dzurak and A. Morello, Single-shot readout and relaxation of singlet and triplet states in exchange-coupled P31 electron spins in silicon, *Physical Review Letters* **112**, 236801 (2014).
- [413] R. Kalra, A. Laucht, C.D. Hill and A. Morello, Robust two-qubit gates for donors in silicon controlled by hyperfine interactions, *Physical Review X* **4**, 021044 (2014).
- [414] A. Morello, Quantum spintronics: Single spins in silicon carbide, *Nature Mater.* **14**, 135 (2014).
- [415] D. J. Christle, A. L. Falk, P. Andrich, P. V. Klimov, J. U. Hassan, N. T. Son, E. Jánzén, T. Ohshima and D. D. Awschalom, Isolated electron spins in silicon carbide with millisecond coherence times, *Nature Mater.* **14**, 160-163 (2015).
- [416] M. Widmann, S.-Y. Lee, T. Rendler, N. T. Son, H. Fedder, S. Paik, L.-P. Yang, N. Zhao, S. Yang, I. Booker, A. Denisenko, M. Jamali, S. A. Momenzadeh, I. Gerhardt, T. Ohshima, A. Gali, E. Jánzén and J. Wrachtrup, Coherent control of single spins in silicon carbide at room temperature, *Nature Mater.* **14**, 164-168 (2015).
- [417] M. Singh, J. L. Pacheco, D. Perry, E. Garratt, G. Ten Eyck, N. C. Bishop, J. R. Wendt, R. P. Manginell, J. Dominguez, T. Pluym, D. R. Luhman, E. Bielejec, M. P. Lilly, and M. S. Carroll, Electrostatically defined silicon quantum dots with counted antimony donor implants, *Applied Physics Letters* **108**, 062101 (2016).
- [418] L. Childress and R. Hanson, Diamond NV centers for quantum computing and quantum networks, *MRS Bulletin* **38**, 134 (2013).
- [419] Marcus W. Doherty, Neil B. Manson, Paul Delaney, Fedor Jelezko, Joerg Wrachtrup, Lloyd C.L. Hollenberg, The nitrogen-vacancy colour centre in diamond, *Physics Reports* **528**, 1 (2013).
- [420] K. Nemoto, M. Trupke, S. J. Devitt, A. M. Stephens, B. Scharfenberger, K. Buczak, T. Nöbauer,

- M. S. Everitt, J. Schmiedmayer, and William J. Munro, Photonic Architecture for Scalable Quantum Information Processing in Diamond, *Phys. Rev. X* **4**, 031022 (2014).
- [421] H. J. Kimble, The quantum internet, *Nature* **453**, 1023 (2008).
- [422] N. Matsuda and H. Takesue, Generation and manipulation of entangled photons on silicon chips, *Nanophotonics* **5**(3), 440-455 (2016).
- [423] W. B. Gao, A. Imamoglu, H. Bernien and R. Hanson, Coherent manipulation, measurement and entanglement of individual solid-state spins using optical fields, *Nature Photonics* **9**, 363 (2015).
- [424] I. E. Zadeh, A. W. Elshaari, K. D. Jöns, A. Fognini, D. Dalacu, P. J. Poole, M. E. Reimer, and V. Zwiller, Deterministic Integration of Single Photon Sources in Silicon Based Photonic Circuits, *Nano Lett.* **16**, 2289 (2016).
- [425] K. Nemoto, M. Trupke, S. J. Devitt, B. Scharfenberger, K. Buczak, J. Schmiedmayer and W. J. Munro, Photonic Quantum Networks formed from NV-centers, *Sci. Rep.* **6** : 26284 (2016).
- [426] B. Hensen, H. Bernien, A. E. Drau, A. Reiserer, N. Kalb, M.S. Blok, J. Ruitenberg, R. F. L. Vermeulen, R. N. Schouten, C. Abelln, W. Amaya, V. Pruneri, M. W. Mitchell, M. Markham, D. J. Twitchen, D. Elkouss, S. Wehner, T. H. Taminiau, R. Hanson, Loophole-free Bell inequality violation using electron spins separated by 1.3 kilometres, *Nature* **526**, 682 (2015).
- [427] B. Hensen, N. Kalb, M.S. Blok, A. Drau, A. Reiserer, R.F.L. Vermeulen, R.N. Schouten, M. Markham, D.J. Twitchen, K. Goodenough, D. Elkouss, S. Wehner, T.H. Taminiau, R. Hanson, Loophole-free Bell test using electron spins in diamond: second experiment and additional analysis, *Sci. Rep.* **6**: 30289 (2016).
- [428] A. Reiserer, N. Kalb, M. S. Blok, K. J. M. van Bemmelen, D. J. Twitchen, M. Markham, T. H. Taminiau, and R. Hanson, Robust quantum-network memory using decoherence-protected subspaces of nuclear spins, *Phys. Rev. X* **6**, 021040 (2016).
- [429] R. J. Chapman, M. Santandrea, Z. Huang, G. Corrielli, A. Crespi, M.-H. Yung, R. Osellame and A. Peruzzo, Experimental perfect state transfer of an entangled photonic qubit, *Nature Commun.* **7**: 11339 (2016).
- [430] S. Barz, I. Kassal, M. Ringbauer, Y. O. Lipp, B. Dakic, A. Aspuru-Guzik and P. Walther, A two-qubit photonic quantum processor and its application to solving systems of linear equations, *Sci. Rep.* **4**: 6115 (2014).
- [431] S. Barz, R. Vasconcelos, C. Greganti, M. Zwerger, W. Dür, H. J. Briegel, and P. Walther, Demonstrating elements of measurement-based quantum error correction, *Phys. Rev. A* **90**, 042302 (2014).
- [432] C. Greganti, M.-C. Roehsner, S. Barz, T. Morimae and P. Walther Demonstration of measurement-only blind quantum computing, *New J. Phys.* **18**, 013020 (2016).
- [433] M. Chipaux, A. Tallaire, J. Achard, S. Pezzagna, J. Meijer, V. Jacques, J.-F. Roch, T. Debuisschert. Magnetic imaging with an ensemble of Nitrogen Vacancy centers in diamond, *Eur. Phys. J. D* **69**, 166 (2015).
- [434] S. Kaufmann, D. A. Simpson, L. T. Hall, V. Perunicic, P. Senn, S. Steinert, L. P. McGuinness, B. C. Johnson, T. Ohshima, F. Caruso, J. Wrachtrup, R. E. Scholten, P. Mulvaney, and L. Hollenber, Detection of atomic spin labels in a lipid bilayer using a single-spin nanodiamond probe, *PNAS* **110**, 10894 (2013).
- [435] L. P. McGuinness, Y. Yan, A. Stacey, D. A. Simpson, L. T. Hall, D. Maclaurin, S. Praver, P. Mulvaney, J. Wrachtrup, F. Caruso, R. E. Scholten, and L. C. L. Hollenberg, Quantum measurement and orientation tracking of fluorescent nanodiamonds inside living cells, *Nature Nanotechnology* **6**, 358 (2014).
- [436] T. Staudacher, N. Raatz, S. Pezzagna, J. Meijer, F. Reinhard, C.A. Meriles and J. Wrachtrup, Probing molecular dynamics at the nanoscale via an individual paramagnetic centre, *Nature Commun.* **6**: 8527 (2015).
- [437] I. Lovchinsky, A. O. Sushkov, E. Urbach, N. P. de Leon, S. Choi, K. De Greve, R. Evans, R. Gertner, E. Bersin, C. Miller, L. McGuinness, F. Jelezko, R. L. Walsworth, H. Park, M. D. Lukin, Nuclear magnetic resonance detection and spectroscopy of single proteins using quantum logic,

- Science **351**, 836 (2016).
- [438] D.-I. Cho, S. Hong, M. Lee and T. Kim, A review of silicon microfabricated ion traps for quantum information processing, *Micro and Nano Systems Letters* **3**: 2 (2015).
- [439] M.F. Brandl, M.W. van Mourik, L. Postler, A. Nolf, K. Lakhmanskiy, R.R. Paiva, S. Mller, N. Daniilidis, H. Hffner, V. Kaushal, T. Ruster, C. Warschburger, H. Kaufmann, U.G. Poschinger, F. Schmidt-Kaler, P. Schindler, T. Monz, R. Blatt, Cryogenic setup for trapped ion quantum computing; arXiv:1607.04980.
- [440] C. A. Riofrio, D. Gross, S. T. Flammia, T. Monz, D. Nigg, R. Blatt, J. Eisert, Experimental quantum compressed sensing for a seven-qubit system; arXiv:1608.02263.
- [441] T. Monz, D. Nigg, E. A. Martinez, M. F. Brandl, P. Schindler, R. Rines, S. X. Wang, I. L. Chuang, and R. Blatt, Realization of a scalable Shor algorithm, *Science* **351**, 1068 (2016).
- [442] S. Debnath, N. M. Linke, C. Figgatt, K. A. Landsman, K. Wright and C. Monroe, Demonstration of a small programmable quantum computer with atomic qubits, *Nature* **536**, 63 (2016).
- [443] E. A. Martinez, T. Monz, D. Nigg, P. Schindler, and R. Blatt, Compiling quantum algorithms for architectures with multi-qubit gates, *New J. Phys.* **18**, 063029 (2016).
- [444] E. A. Martinez, C. A. Muschik, P. Schindler, D. Nigg, A. Erhard, M. Heyl, P. Hauke, M. Dalmonte, T. Monz, P. Zoller, R. Blatt, Real-time dynamics of lattice gauge theories with a few-qubit quantum computer, *Nature* **534**, 516 (2016).
- [445] J. G. Bohnet, B. C. Sawyer, J. W. Britton, M. L. Wall, A. M. Rey, M. Foss-Feig, and J. J. Bollinger, Quantum spin dynamics and entanglement generation with hundreds of trapped ions, *Science* **352**, 1297 (2016).
- [446] V. Mourik, K. Zuo, S. M. Frolov, S. R. Plissard, E. P. A. M. Bakkers, and L. P. Kouwenhoven, Signatures of Majorana fermions in hybrid superconductor-semiconductor nanowire devices, *Science* **336**, 1003 (2012).
- [447] S. Das Sarma, M. Freedman, C. Nayak, Majorana Zero Modes and Topological Quantum Computation, *NJ Quantum Information* **1**, 15001 (2015)
- [448] David Aasen, Michael Hell, Ryan V. Mishmash, Andrew Higginbotham, Jeroen Danon, Martin Leijnse, Thomas S. Jespersen, Joshua A. Folk, Charles M. Marcus, Karsten Flensberg, and Jason Alicea, Milestones toward Majorana-based quantum computing; arXiv: 1511.05153v2.
- [449] D. J. Clarke, J. D. Sau, and S. Das Sarma, A Practical Phase Gate for Producing Bell Violations in Majorana Wires, *Phys. Rev. X* **6**, 021005 (2016).
- [450] A. Warshel, Multiscale Modeling of Biological Functions: From Enzymes to Molecular Machines, *Angwandte Chemie* **53**, 10020 (2014).